Università del Piemonte Orientale

"Amedeo Avogadro"

Department of Pharmaceutical Sciences

Ph.D. Program in Chemistry & Biology

XXXII cycle 2016-2019

Chemistry of APIs: Synthesis and Solid-State Properties

Mauro Barbero

Supervised by: Prof Giovanni B. Giovenzana

Ph.D. Program Co-Ordinator: Prof. Luigi Panza

Università del Piemonte Orientale

"Amedeo Avogadro"

Department of Pharmaceutical Sciences

Ph.D. Program in Chemistry & Biology

XXXII cycle 2016-2019

Chemistry of APIs: Synthesis and Solid-State Properties

SSD: CHIM/03

Chemical methodologies for new molecules and nanomaterials

Mauro Barbero

Supervised by: Prof Giovanni B. Giovenzana

Ph.D. Program Co-Ordinator: Prof. Luigi Panza

DECLARATION AND AUTHORISATION TO ANTIPLAGIARISM DETECTION

The undersigned ....MAURO BARBERO............student of the Chemistry & Biology

Ph.D course (XXXIICycle)

declares:

- to be aware that the University has adopted a web-based service to detect plagiarism through a software system called "Turnit.in",

- his/her Ph.D. thesis was submitted to Turnit.in scan and reasonably it resulted an original document, which correctly cites the literature;

acknowledges:

- his/her Ph.D. thesis can be verified by his/her Ph.D. tutor and/or Ph.D Coordinator in order to confirm its originality.

Date: ...15/11/2019............. Signature: ....

XY/tcs
Percorso del file

Table of Contents

Chapter 1: Introduction

1.1. Introduction

APIs (Active Pharmaceutical Ingredients) are the biological active compounds of pharmaceutical formulations. APIs are molecules able to induce a biological effect, playing a very important role for the world public health and, for this reason, they are employed for the prevention or eradication of some pathologies and diseases.

Different types of APIs are available on the market, starting from older synthetic to newer biotechnological and bio-fermentation drugs. As a result, the global market of these compounds reaches $182.2 billion in 2019 but future predictions are projecting the market over $300 billion by 2025[1,2]. These important data are closely related to all facilities in the world dedicated to the synthesis or preparation of all starting materials and intermediates needed for the production of APIs.

Thanks to the continuous worldwide request of these compounds, pharmaceutical companies are involved in the development of new and innovative drugs for the treatment of on chronic, cardiovascular and cancer diseases[2], and many other pathologies.

The above cited three classes have an important impact on the drug market but nowadays, the development of news HP-APIs (High Potent-APIs) facilities, related to the high-potent drugs production, the recent production of biopharmaceutical compounds and the continuous growth of the market of generics, are leading the big pharma into new important market area, and, for these reasons, pharmaceutical companies are investing significant technological and economical resources for the development of new and competitive synthetic processes.

APIs can be produced by three different industries:
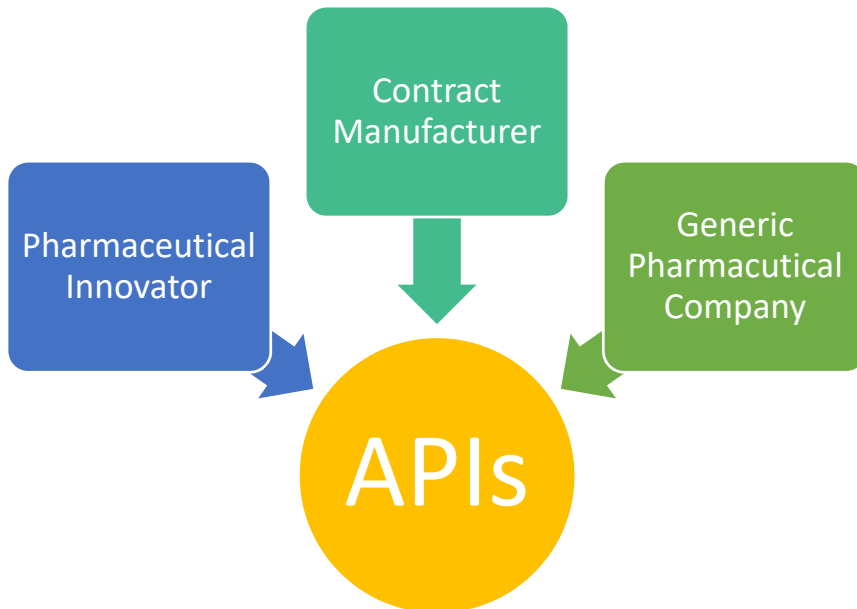
Pharmaceutical Innovators are focused on introducing new APIs on the market. Once the APIs is launched on the market, its production may be outsourced to contract manufacturers, the latter being in charge for the production of batches of specific APIs. When intellectual property (IP) on an API expires, it becomes a "generic API" and other companies enter in this market to develop cheaper alternative production processes of the API. Nevertheless, the quality of the APIs must not to be inferior of the original branded compound. During the synthesis, all pending patented processes must be bypassed with the main goal identified in finding a cheaper production cost while maintaining the quality of the final product.

The manufacturing of APIs is strictly supervised by specific government agencies, different for each country but with the aim to control the quality standard of GMP rules (Good Manufacturing Practices). For example, AIFA (Agenzia Italiana del Farmaco), FDA (Food and Drug Administration)

and EMA (European Medicine Agency) are the government agency operating in Italy, U.S and Europe, respectively.

APIs must meet different quality requirements such as:

- structural identification (NMR, HPLC retention time, single-crystal X-ray or powder X-ray),
- purity assessment (HPLC purity, residual solvents by GC, water content, presence of heavy metals, etc),
- appearance (colour and morphology),
- physico-chemical properties (pH, melting point),
- solid-state properties (crystal form, eventual polymorphs, solvates).

All these parameters are well discussed in the ICH guide-lines[3]. ICH (International Council for Harmonization of Technical Requirements for Pharmaceuticals for Human Use) defines a series of tests and procedure that pharma company must follow for the correct production and characterisation of the product. Generally, ICH are divided in four categories:

- Quality guidelines
- Safety guidelines
- Efficacy guidelines
- Multidisciplinary guidelines

For example, Q3C(R6) guideline refers to possible residual solvents in the final API, with corresponding limit (PDE: Permitted Daily Exposure), or Q1A – Q1F guidelines refer to the stability of API. A very important ICH guidelines is Q3D(R1) that refers to the possible amount of elements like Cu, Pb, Pd, Pt, Sn, Rh and many others, setting a very low limit[3].

After all these considerations regarding the quality and characteristics of the APIs, the main goal of a pharmaceutical company is related to the effective production of active compounds.

APIs manufacturing requires a robust synthetic process in order to minimize or reduce the possible problems during the production, especially when reaching industrial scale.

Moreover, particular attention is focused on the factors influencing the total cost of the final API, including the price of the starting materials, the number of synthetic steps, yield, production costs, catalysts (if present) and many others.

For these reasons, the pharmaceutical industries employ a lot of scientific and technological resources with the aims to reduce the production costs, increase the total yield in order to increase the total profit.

In order to develop a robust synthetic process, a huge number of resources are employed by pharma industry devoted to the identification of the best reaction conditions. To this purpose, a general scheme of process is followed (Scheme 1.1):
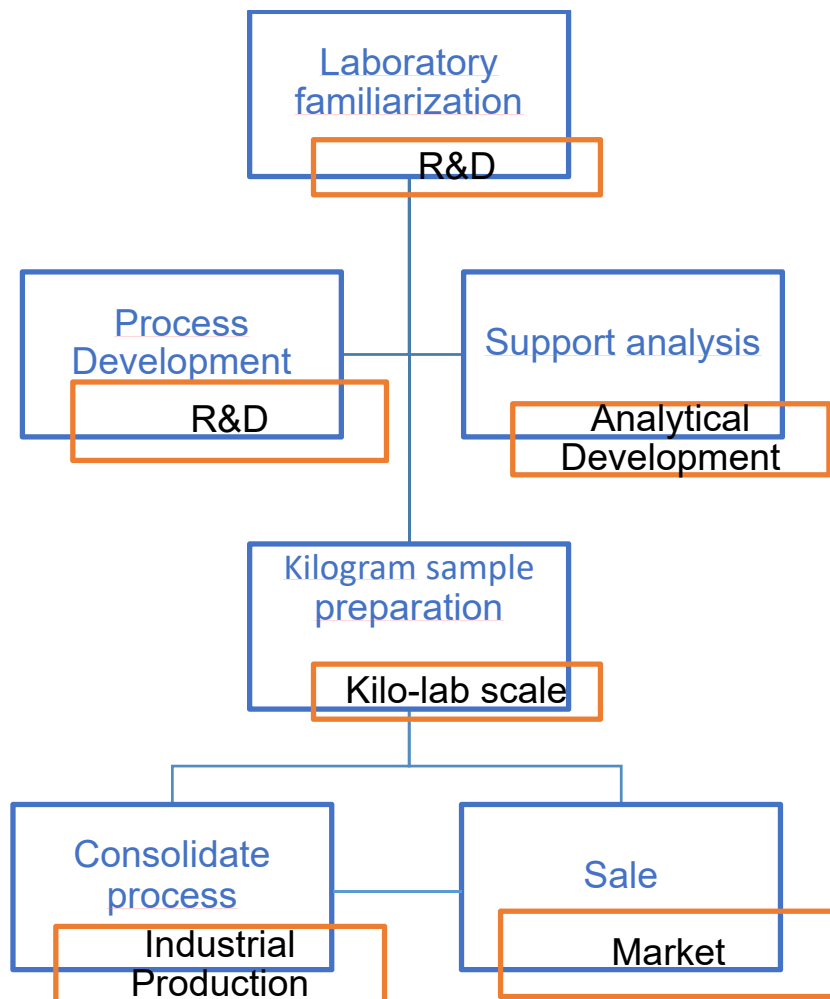
Scheme 1.1: General scheme of process development

The first step is the R&D laboratory, in which the desired API is designed and synthesized *ab initio* or following literature procedures taken from patents or articles. In this phase, the attention is paid to avoid inappropriate synthetic procedures such as the use of hazardous reagents or combination of them and dangerous operative conditions.

After this screening, the main activities are focused on R&D process development.

During this step, all issues related to the synthetic route such as production costs, starting materials and yield, must be solved in order to develop a robust and cheap process. After these identifications, the synthetic process can be produced in different scales following kilogram or bulk scale reaching the final sales stage.

The main goal of the pharmaceutical industry is to decrease the cost related to an API production. Different areas are closely related to each other and affect positively or negatively the total cost. This relationship is showed in Scheme 1.2.
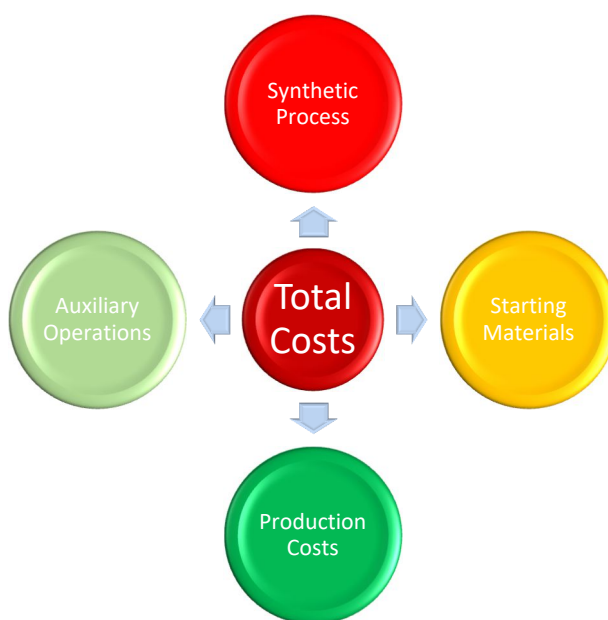
Scheme 1.2: Total cost relationships

As showed in scheme 1.2, four issues can be addressed in order to decrease the total cost:

- ❖ Synthetic process
- ❖ Starting material
- ❖ Auxiliary operations
- ❖ Production cost

The correct synthetic process is essential for the manufacturing of APIs. Several efforts are devoted to the identification of the best synthesis. One possible strategy is based on the reduction and optimisation of the synthetic steps. After the screening of the new and possible synthetic processes, one or two synthetic pathways are identified as the best.

Then, availability and price of the corresponding starting materials are to be defined as they play a crucial role in the synthetic processes. Much work is dedicated to identify the best supplier with the optimal features in terms of purity and cost. After this step, the reaction conditions are screened, in particular:

- Reagents
- Solvents (type and amount)
- Catalyst, if needed
- Operative conditions (concentrations, temperature, pressure, inert atmosphere)

In addition, calorimetric analysis is performed with the aim to detect the safety profile of the reaction analysing the energy produced during the reaction. After this study, the obtained parameters are used to define the correct reaction protocol: which reagent is added first, optimal concentration *etc.*

After this screening, work-up procedures are studied focusing the attention on the best and simple procedure to apply to obtain the desired product. Then, the complete analytical profile of the whole process is followed through HPLC/GC, NMR, and any other analytical technique that could be suitable to give full snapshot on the purity profile of the API.

The R&D working on the above cited steps, gives as a result a process that is nearly always completely different from the original synthesis of the

API applied by medicinal chemistry laboratories. The process is almost mature and ready to be scaled up to the industrial production.

The API can then be transferred in the industrial plant, classified on the base of the capacity of the manufacturing plant itself:

- Pilot plant
- Manufacturing plant

In the pilot plant, the synthesis starts to be applied on a wider scale, meaning hundred grams to kilogram-scale. This allows to identify scale-related problems and to solve them promptly. Once the process works on this scale reproducibly, it can be transferred on the final, large scale manufacturing plant. The latter can span from slightly more than a pilot plant, for high-potency specialty APIs, to very large 15-20000 L reactors with proportionally larger dedicated plants.

After these considerations on to the synthetic process and its costs, another important issue must be considered: the solid-state properties of the final APIs. The correct crystalline form is fundamental for the final formulation of the APIs because different crystalline forms possess different physico-chemical properties without altering the chemical properties of the APIs.

The presence of different crystal forms of the same compound is called polymorphism. The compound may show different crystal forms as a result of different crystal packing ("*packing polymorphism*") or arising from different molecular conformations ("*conformational isomerism*"). Moreover, the crystal may contain additional components, giving salts, solvates and cocrystals, collectively indicated as *pseudopolymorphs*.

Different pseudopolymorphs are present and were classified by *Grothe et al* as follows:[4]

- Salt

- Solvate

- Cocrystal

These three classes are further divided in to seven sub-classes, obtained by combination of different cases:

- True solvate (no ions)
- True salt (only ions)
- True cocrystal (only conformer)
- Salt solvate (no conformer)
- Cocrystal solvate (no ions)
- Cocrystal salt (no solvate)
- Cocrystal salt solvate

This important classification is a useful tool for the correct identification of the final crystalline form of the APIs. The presence of different crystal form can alter properties such as the solubility[5] or dissolution rate.[6] The "*actual*" crystalline form can be ascertained through different analytical methods such as X-ray diffractometry (single crystal or powder), DSC and TGA or combinations thereof.

1.2. References

1. Research & Market ltd, Active Pharmaceutical Ingredients (API) Global Market - Forecast to 2025 https://www.researchandmarkets.com/reports/4769388/active-pharmaceutical-ingredients-api-global (accessed Sep 30, 2019).

2. Global Active Pharmaceutical Ingredient/ API Market by Type, Synthesis, Drug, Therapeutic Application, Manufacturer, Region, Industry Analysis, Size, Share, Growth, Trends, and Forecast 2018 to 2025 https://www.fiormarkets.com/report/global-active-pharmaceutical-ingredient-api-market-by-type-376047.html (accessed Sep 30, 2019).

3. ICH Official web site: ICH https://www.ich.org/page/ich-guidelines (accessed Oct 29, 2019).

4. Grothe, E.; Meekes, H.; Vlieg, E.; ter Horst, J. H.; de Gelder, R. Solvates, Salts, and Cocrystals: A Proposal for a Feasible Classification System. *Cryst. Growth Des.* **2016**, *16* (6), 3237–3243. https://doi.org/10.1021/acs.cgd.6b00200.

5. Fini, A.; Fazio, G.; Feroci, G. Solubility and Solubilization Properties of Non-Steroidal Anti-Inflammatory Drugs. *Int. J. Pharm.* **1995**, *126* (1), 95–102. https://doi.org/10.1016/0378-5173(95)04102-8.

6. Ilarduya, M. C. T. de; Martín, C.; Goñi, M. M.; Martínez-uhárriz, M. C. Dissolution Rate of Polymorphs and Two New Pseudopolymorphs of Sulindac. *Drug Dev. Ind. Pharm.* **1997**, *23* (11), 1095–1098. https://doi.org/10.3109/03639049709150498.

Chapter 2: Outline of the Thesis

2.1. Outline of the Thesis

APIs (Active Pharmaceutical Ingredients) are compounds able to induce a biological effect interacting with specific targets. They are employed as tools for the treatment of infections, cardiovascular disease, cancer disease and many other pathologies, improving the global health.

APIs employed in the clinical practice are still the subject of a continue and vibrant research, finalised to the development of the synthetic process and to the comprehensive knowledge of their solid-state properties and the potential interaction with other excipients.

APIs require robust chemical processes in order to meet the requirements for a convenient industrial production and to satisfy the market requests. For these reasons, several efforts are devoted to the identification of the best synthetic process with the minimum number of synthetic steps and the maximum yield.

This PhD program is focused on different aspects of the work mentioned above. In particular, we concentrated our attention on the screening of alternative synthetic processes and on studying the solid-state chemistry for selected APIs.
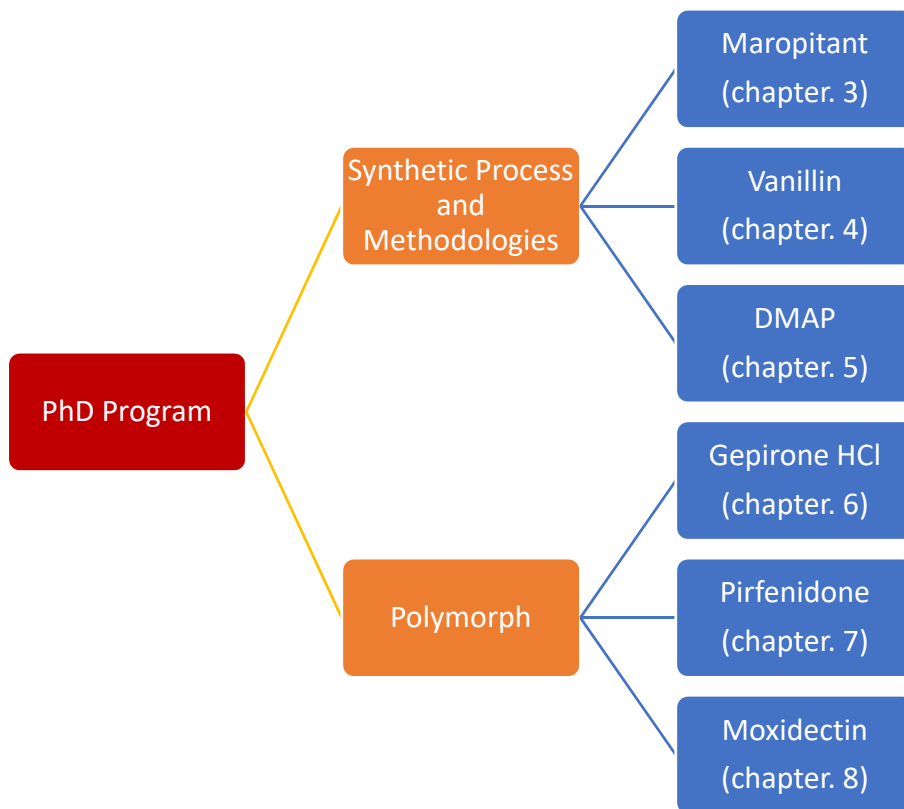
Scheme 2.1: PhD program scheme

In Chapter 3, a screening of alternative synthetic processes and reactions devoted to the preparation of the API maropitant citrate monohydrate, is described.

Chapter 4 reports on the unexpected reactivity of secondary amines and vanillin.

Chapter 5 describes the approach to the preparation of a supported catalyst (DMAP), with the first-time derivatisation of this important nucleophilic pyridine derivative.

In Chapter 6, 7 and 8, the polymorphism of selected APIs (gepirone hydrochloride, pirfenidone and moxidectin) are studied and discussed, respectively.

# Chapter 3: Synthesis and characterization of Maropitant Citrate Monohydrate

3.1. Introduction

Emesis and vomiting, induced by motion sickness, are two important syndromes in animals that can change their normal life. Emesis can be induced by several pathologies such as gastro-enteritis, pancreatitis, dietary problems and many others, but it is, also, correlated with the use of anti-cancer drugs[1]. It is regulated by a series of nuclei located in different parts of the body as well as in a specific zone called chemoreceptor trigger zone (CTZ).[2]

Otherwise, motion sickness induces vomiting by travelling by the car, boat, planes or other motion-related stimuli.[3] Generally, this condition is reported in puppies and young animals but decreasing during the aging.

In order to treats and solve these problems, Pfizer developed a new drug called maropitant (trade mark name Cerenia®). Maropitant is used for the treatment of emesis, vomiting induced by motion sickness, and it is a veterinary use-only, especially in dogs and cats.

1
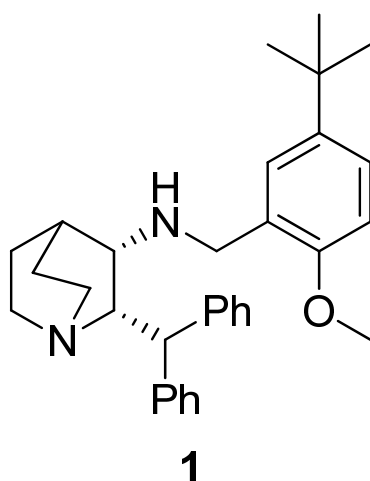
Figure 3.1: Maropitant free base

Maropitant is a neurokinin-1 (NK-1) receptor antagonist and its mechanism of action consists of binding and blocking the substance P, an endogenous peptide able to interact with NK-1 receptor inducing vomiting[4].

It was approved by FDA in 2007 for dogs then in 2012 for cats and it is commercialized as citrate monohydrate (Figure 3.2):

2
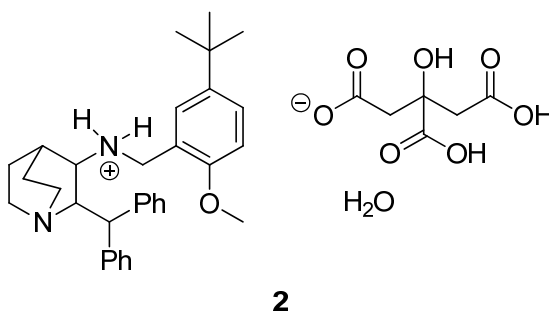
Figure 3.2: Maropitant citrate monohydrate

Maropitant shows an additional potential anti-inflammatory activity, and it was demonstrated by researcher group of Atsushi Tsukamoto that reported this anti-inflammatory activity in the treatment of acute pancreatitis[5] without losing the main antiemetic activity.

Maropitant is commercially available in different pharmaceutical forms such as tablets, with different dosages (16, 24, 60 or 160 mg of API), or injectable solution (10 mg/mL).

The IUPAC name of the free base of maropitant is (*2S,3S*)-2-benzhydryl-*N*-(5-tert-butyl-2-methoxybenzyl)-quinuclidine-3-amine, highlighting the different structural portions:

- a bicyclic disubstituted quinuclidine moiety,
- a benzhydryl group on C-2
- a 2-methoxy-5-*t*-butylbenzylamine residue on C-3.

The carbon atoms C-2 and C-3 are stereocenters, their substituents having relative stereochemistry *cis* and absolute configuration (2*S*,3*S*).

24

The API is the citrate salt of Maropitant free base, isolated as the citrate monohydrate. It is a white solid and it is characterised by the presence of two polymorphic forms named "A" and "B". The form A is more stable than B but both forms are suitable for treating emesis in animals.[6]

3.2. Original Synthesis

Maropitant is synthesised following a long and tedious synthetic process reported in Scheme 3.1.[7-10]
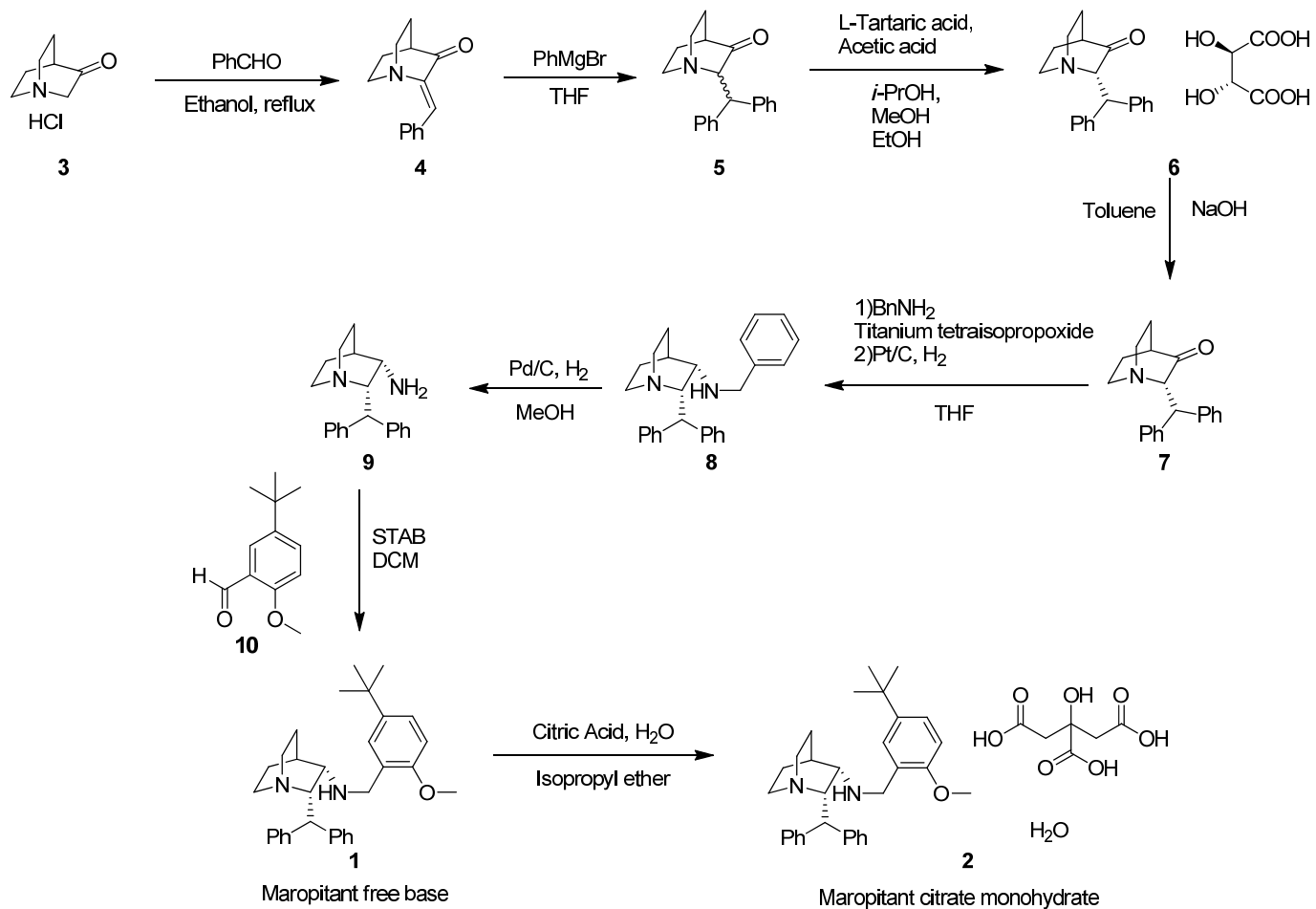
Scheme 3.1: Original synthesis of maropitant

Maropitant is synthesised in 8 synthetic steps starting from the commercially available starting material, 3-quinuclidinone hydrochloride.

The length of the synthesis prompted us to investigate possible improvements or alternatives, starting from a simple retrosynthetic analysis. This approach led us to the identification of two different strategies:

- Different approaches for the building of (2*S*)-2-benzhydryl-3-quinuclidinone (blue circle, Scheme 3.2) and
- Reductive amination for the set-up of the benzylamine residue (red circle, Scheme 3.2)
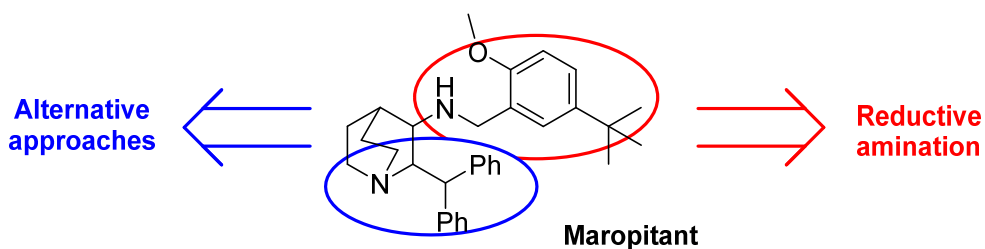
Scheme 3.2: Retrosynthetic analysis of maropitant

3.3. Direct Alkylation

(*2S*)-2-Benzhydryl-3-quinuclidinone (**7**) is a key intermediate in this process. Moreover it is involved in the synthesis of several correla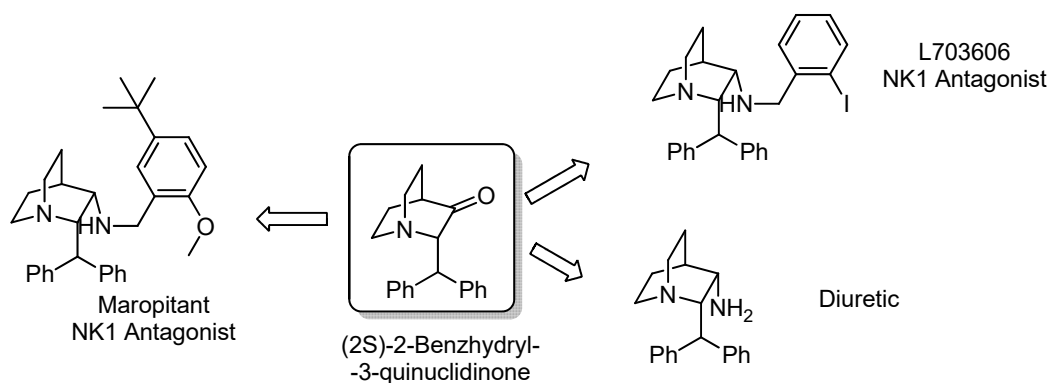ted bioactive molecules, such as L703606 (NK-1 antagonist)[6,11] and 3-amino-2-benzhydrylquinuclidine (diuretic)[12] (Scheme 3.3).

Scheme 3.3: Central role of (*2S*)-2-benzhydryl-3-quinuclidinone (**7**)

Usually, this intermediate, is prepared following established literature methods[8,9,13]. The first step involves a crossed-aldol condensation between 3-quinuclidinone hydrochloride and benzaldehyde in the presence of sodium hydroxide as base. The enone is isolated in nearly quantitative yield and this step does not need further optimisation.

A conjugate addition of phenylmagnesium bromide on the $\Delta^{\alpha,\beta}$ unsaturated system leads to the desired product. A dynamic resolution process with L-tartaric acid lead to the intermediate **6**. After treatment with an opportune base, the desired product (2S)-2-benzhydryl-3-quinuclidinone is obtained (Scheme 3.4).
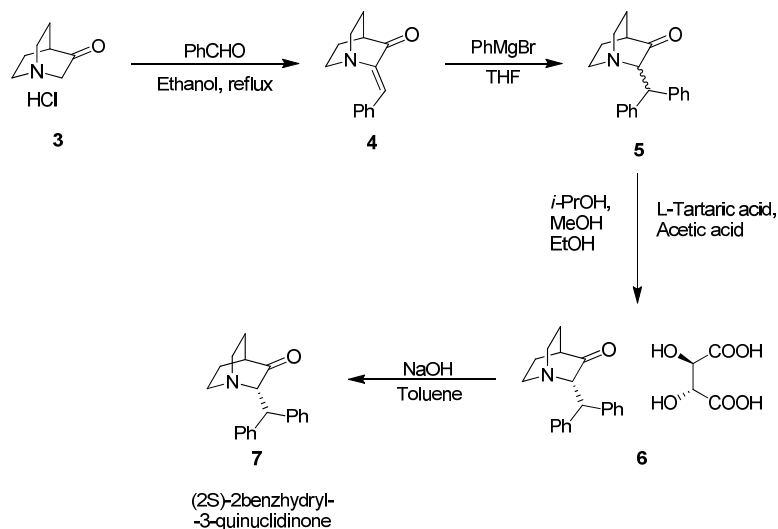
Scheme 3.4: Literature synthesis for the preparation of 2-benzhydryl-3-quinuclidinone

This second step is affected by the presence of by-products and low conversion of the starting material, limiting the yield less than 50%.

One of the main byproducts arising from the use of the Grignard reagent during the conjugate addition, arise from the double attack on the enone moiety (**11**, Figure 3.3):
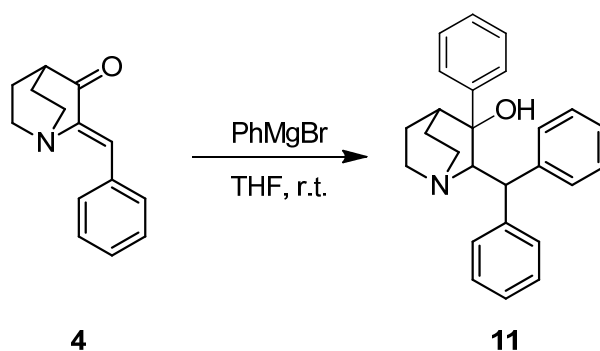
Figure 3.3: Double attack of Grignard reagent on the enone

For these reasons, during my PhD program, we focused our attention on an alternative synthetic process for the preparation of the important key intermediate (2S)-2-benzhydryl-3-quinuclidinone, avoiding as much as possible the formation of byproducts and improving the yield of the preparation.

3.3.1. Heck – arylation approach

Different synthetic approaches to (2S)-2-benzhydryl-3-quinuclidinone were investigated, maintaining 3-quinuclidinone hydrochloride as the starting material due to its convenient price and wide availability.

The first attempt was the introduction of the second aryl group through an alternative synthetic procedure, identified in the Mizoroki – Heck arylation[14]. In this reaction, the arylation mechanism is shifted from a conjugated addition to a transition metal-catalysed addition, with the enone compound as the acceptor and iodobenzene as the arylating agent. The reaction is run in the presence of tetrabutylammonium bromide, palladium(II)acetate as catalyst and DMF as solvent, respectively (Scheme 3.5).
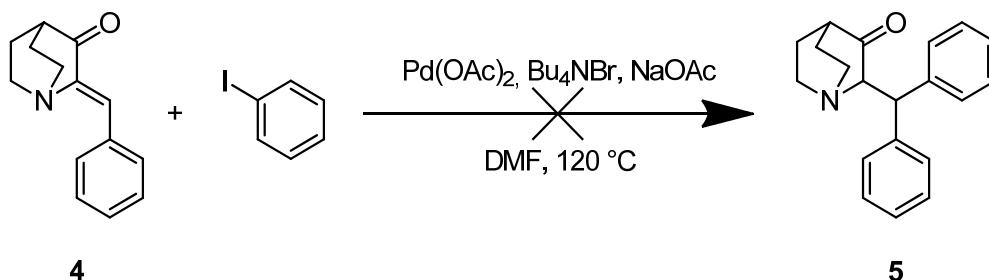
Scheme 3.5: Heck – arylation approach

Unfortunately, no evidence of the formation of the desired arylated product was observed, so we moved our attention on a completely different approach.

3.3.2. Stevens Rearrangement approach

The second strategy was based on the Stevens rearrangement. This rearrangement converts a quaternary ammonium salt into corresponding tertiary amine, through different sigmatropic rearrangements.
In general, the corresponding ylides, can evolve in two distinct pathways:

1) [1,2] shift of an ammonium ylide to the corresponding tertiary amine, and this pathway is called Stevens [1,2] rearrangement[15]

2) [2,3] shift of an ammonium ylide (**13**) to the corresponding tertiary amine (**14**) mediated by the presence of allylic substituent, and in this case, this pathway is called Stevens [2,3] rearrangement[16], also well known as Sommelet – Hauser rearrangement[17] (Scheme 3.6).
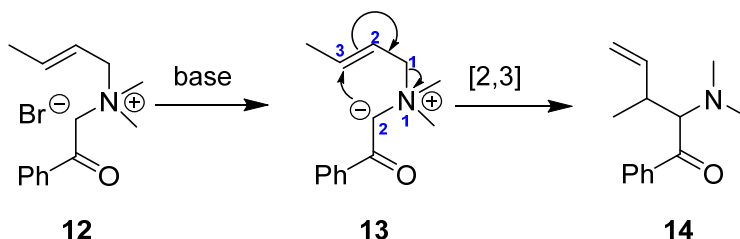
Scheme 3.6: Stevens [2,3] rearrangement

Both rearrangements take place in basic condition.
The product obtained by [1,2] rearrangement can be formed following two different mechanisms, as reported by Ollis et al[18] in 1983:

a- Concerted [1,2] sigmatropic rearrangement, with retention of configuration of the migrating group[16],

b- Homolysis of the C-N bond (**17**) between the migrating group and the quaternary nitrogen atom, to generate a radical pair that rapidly evolves to the corresponding product.

The first example of [1,2] rearrangement was reported by Stevens[15] in 1928. The first step was the reaction between 2-(*N,N*-dimethylamino)-1-phenylethanone (**20**) and benzylbromide (**21**), leading to a quaternary ammonium salt (**22**, Scheme 3.7):

20   **21**   **22**
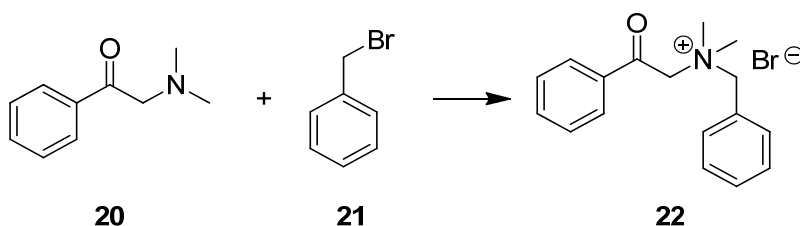
Scheme 3.7: Synthesis of the quaternary ammonium salt

The second step runs in the presence of a base or, if necessary, a strong base. The latter generates the intermediate ylide evolving spontaneously to the corresponding amine, 2-(*N,N*-dimethylamino)-1,3-diphenylpropan-1-one (**24**) (Scheme 3.8):

22   **23**   **24**

Stevens
Rearrangement
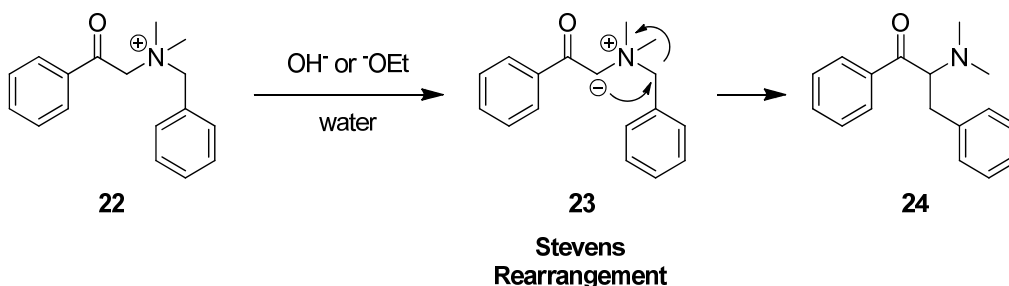
Scheme 3.8: Stevens rearrangement of the quaternary ammonium salt

This specific 1,2 electrophilic rearrangement requires the formation of the corresponding carbanion (ylide) as the intermediate. If no others electron withdrawing groups are present, except the quaternary ammonium group, strong bases are required, for example (Na, PhLi, fused KOH).

The presence of a disubstituted carbon atom in α to the tertiary amine in 2-benzhydryl-3-quinuclidinone prompted us to investigate the applicability of the Stevens rearrangement for the formation of the key intermediate (Scheme 3.9).

5

rac-2-benzhydryl-
-3-quinuclidinone

26

3

25
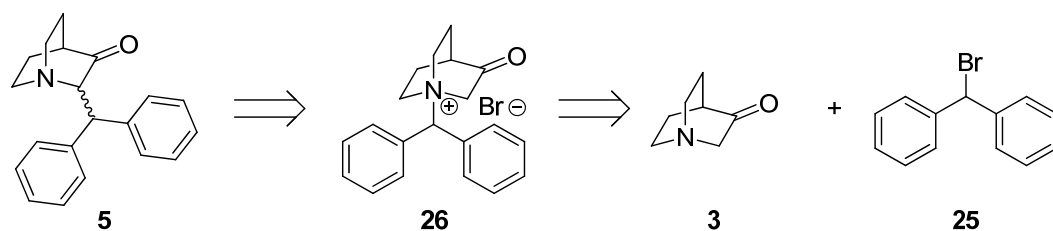
Scheme 3.9: Retrosynthetic analysis of 2-benzhydryl-3-quinuclidinone involving a Stevens rearrangement

At first, we synthesized the corresponding quaternary ammonium salt starting from 3-quinuclidinone and benzhydryl bromide, following the procedure reported in patent EP 0785198 A1[19] (Scheme 3.10). The quaternary salt is obtained in 93% yield.

3

25

MeCN

26
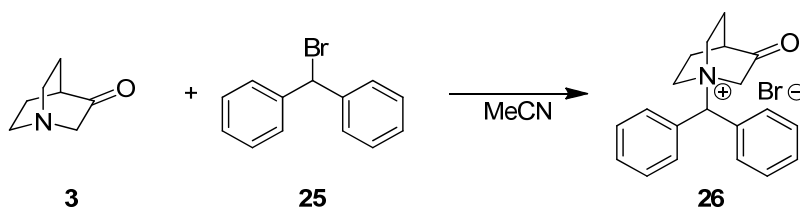
Scheme 3.10: Preparation of the quaternary quinuclidinium salt

Then, the Stevens [1,2] rearrangement was tested in the presence of different combinations base/solvent (Scheme 3.11).
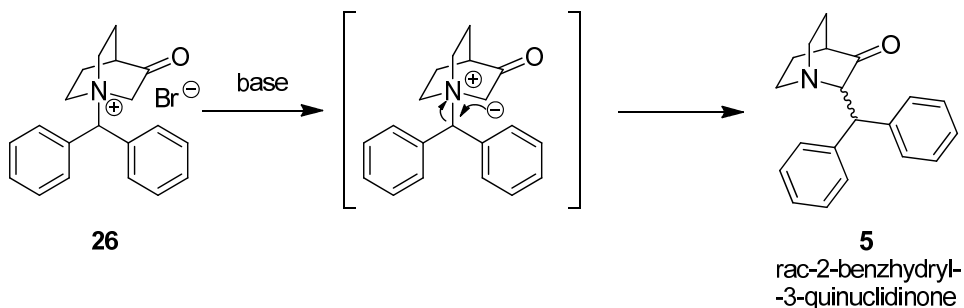
Scheme 3.11: Stevens [1,2] rearrangement

The combinations base/solvent investigated for this specific rearrangement are summarized in Table 3.1.

	Base	**Solvent**
#1	DBU	Acetonitrile
#2	t-BuO⁻K⁺	t-butanol
#3	NaOH	water

Table 3.1: different trials of Stevens rearrangement

All the reactions were run at room temperature. After 16 hours at room temperature, no evidence of the formation of the desired product was observed and for this reason all three reactions were warmed at 60°C. Reaction #2 and #3 did not proceed even after additional 16 hours at 60 °C. Nevertheless, the formation of a new product was observed in reaction #1.

The NMR analyses of the product of reaction #1 were not compatible with the expected structure. Careful analysis of the NMR spectra allowed to identify the product as the compound resulting from a competing Sommelet – Hauser [2,3] rearrangement (**27**, Scheme 3.12).
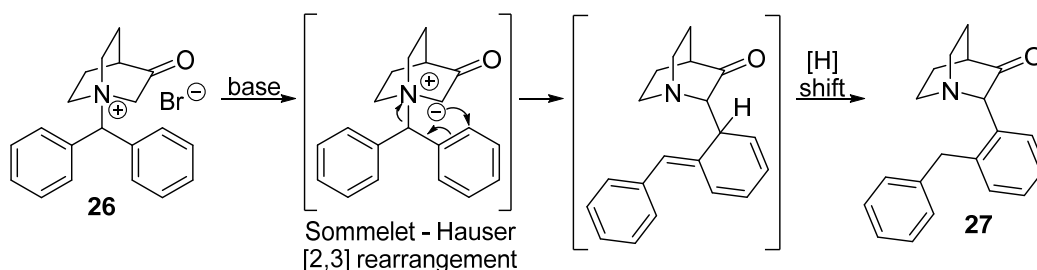
Scheme 3.12: Sommelet-Hauser rearrangement

The absence of products from the expected Stevens rearrangement suggests that the intermediate ylide reacts through the Sommelet-Hauser mechanism with complete selectivity. This approach was then abandoned.

3.3.3. Direct Benzhydrylation

We investigated the direct alkylation of 3-quinuclidinone using "benzhydrylating agents", and taking advantage of the easy enolisation of the starting aminoketone.

For this alternative synthetic approach, three different benzhydrylating agents were identified, in detail: benzophenone (**28**), dimethoxydiphenylmethane (**29**), diphenylmethanol (**30**), and corresponding reactions to be tested are showed in Scheme 3.13
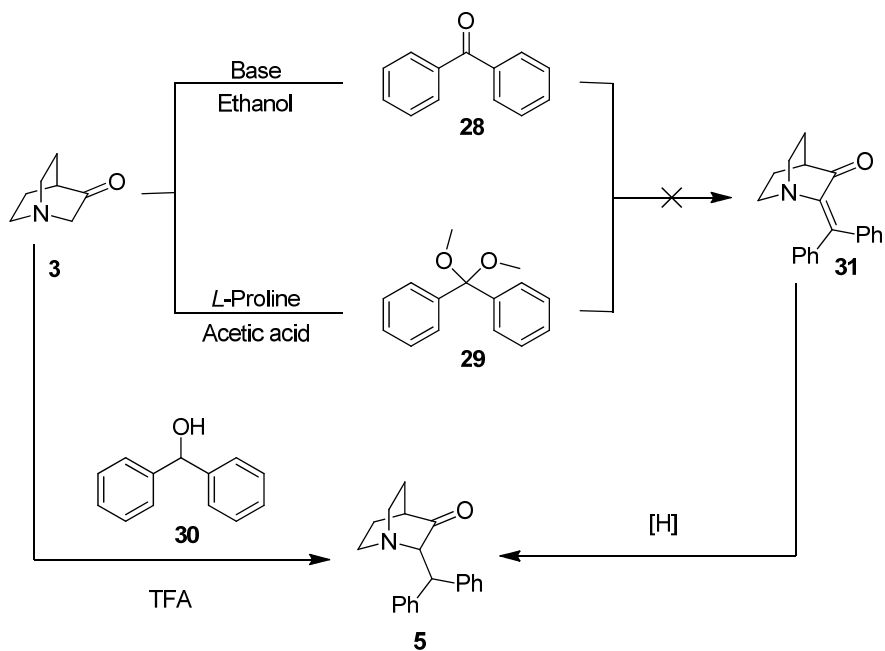
Scheme 3.13: Approaches to the introduction
of the benzhydryl(idene) moiety

Different combinations bases/solvents were investigated in order to perform these reactions. All the attempts are reported in Table 3.2.

Alkylating agent	Base	Solvent	T (°C)	Result
Benzophenone	DBU	CH_3CH_2OH	60 °C	NR
	DABCO			NR
	L-proline/ NaOH			NR
	TEA/ MgCl$_2$			NR
Dimethoxy--diphenylmethane	L-Proline	CH_3COOH	25 °C to 60 °C	NR
Diphenylmethanol	-	CF_3COOH	60 °C	NR

Table 3.2: Summary of reactions conditions

Unfortunately, applying the previous reported procedures, no evidence of the formation of the desired products was observed, probably related to the low reactivity of the benzhydrylating agents. The poor results obtained with this approach led us to the investigation of an alternative benzhydrylation method, enhancing the reactivity of the starting material through the formation of the corresponding silyl-enol ether.

3.3.4. Silyl-enol ether approach

The starting material (3-quinuclidinone), is known to form the corresponding enolate quite easily (**32**, Figure 3.4), as demonstrated by the efficient aldol condensation with benzaldehyde, catalysed by sodium hydroxide.
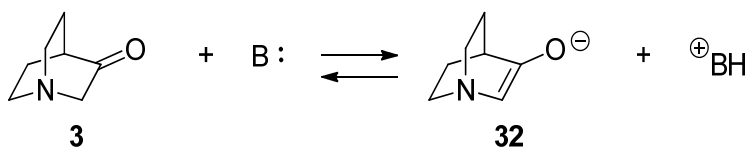
Figure 3.4: Base promoted formation of the 3-quinuclidinone enolate

Silylating agents (SAs) can trap the enol with the formation of the corresponding silyl enol ether derivatives (**33**), as reported in (scheme 3.14). This intermediate, can be reacted with alkylating agent, in general R-Br, in the presence of Lewis acid (Scheme 3.15).
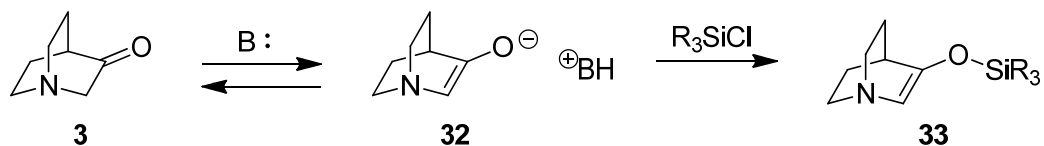
Scheme 3.14: Trapping of the enolate with silylating agents
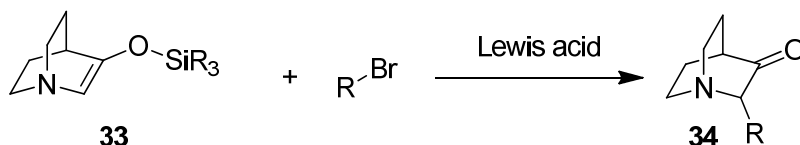
Scheme 3.15: Lewis acid-catalysed alkylation of silyl enol ether

For the investigation of this approach, the starting material 3-quinuclidinone was treated with a suitable base leading to the corresponding enol form, trapped by a suitable silylating agent giving the silyl enol ether intermediate. The latter was treated with an alkylating agent in presence of Lewis acid. In this investigation, two diphenylmethylating agents were used, in order to have a direct access to the desired product. In detail, we used for this screening bromodiphenylmethane and chlorodiphenylmethane.

In order to perform this synthetic approach, we screened different bases, silylating agents, Lewis acids and solvents and the results are reported in Table 3.3.

Starting material	Base	Silylating agent	Solvent/ Temperature	Lewis acid	Alkylating agent	Results
3-Quinuclidinone free base	DBU	TMSCl	DCM dry/ Reflux	ZnCl$_2$	Bromodiphenylmethane	32%
				BF$_3$ Et$_2$O		NR
				TiCl$_4$		NR
	DBU		THF dry/ 40°C	ZnCl$_2$		NR
			CHCl$_3$/ R.T			NR
	TEA		MeCN/ R.T	ZnCl$_2$		NR
			DCM dry/ 40°C			NR
	t-BuO⁻K⁺		THF dry/ R.T	ZnCl$_2$		NR
	…	…	THF dry/ R.T	ZnCl$_2$		NR
	t-BuO⁻K⁺					NR
	…	HMDS/TMSCl	MeCN/ R.T.	ZnCl$_2$		NR
	…	TMSOTf	DCM dry/ Reflux	ZnCl$_2$		NR
	DBU					70%
	t-BuO⁻K⁺	…	THF dry/ R.T	ZnCl$_2$	Chlorodiphenylmethane	NR

Table 3.3: Reaction conditions

After this screening, the desired product 2-benzhydryl-3-quinuclidinone was obtained only using the following two combinations:

- TMSCl/ DBU/ DCM dry/ ZnCl$_2$
- TMSOTf/ DBU/ DCM dry/ ZnCl$_2$

In particular, the silyl-enol-ether (**35**) intermediate described in the first combination system, was synthesized following the reported literature by Taniguchi et al[20], using trimethylsilylchloride and DBU as silylating agent and base, respectively. The resulting solution was added to a mixture containing freshly fused zinc chloride and bromodiphenylmethane (Scheme 3.16):
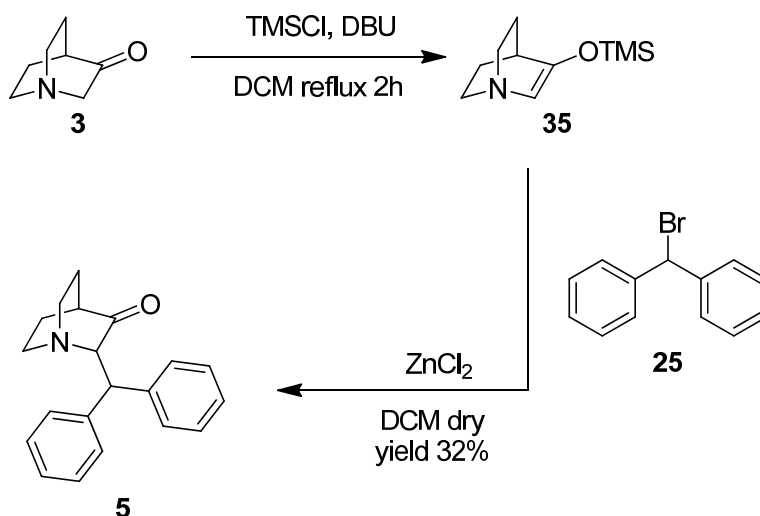
Scheme 3.16: Alkylation through S$_N$1 mechanism

The desired product (**5**) was obtained in 32% yield (determined on the crude by NMR with phenanthrene as internal reference standard).

Using, the silylating agent trimethylsilyltrifluoromethanesulfonate, as reported by Downey et al[21] and using DBU as base, the desired product

was obtained in 70% yield, determined by NMR with phenanthrene as internal reference standard.

Other combinations of bases, silylating agents and solvents were not successful, as summarised in table 3.3.

In conclusion, this approach allows direct access to α-alkylated derivatives exploiting the formation of silyl-enol ether intermediate followed by alkylation through S_N1 mechanism. Unfortunately, TMSOTf must be employed to obtain high yields, increasing considerably the production costs. As the latter is one of the most important issues in the development of an industrial process, this alternative approach at the present stage is not convenient.

3.4. Reductive Amination

The second approach identified during the retrosynthetic analysis of maropitant, was based on the reductive amination between (*2S*)-2-benzhydryl-3-quinuclidinone and a benzylamine derivative bearing all the final substituents, namely 5-*t*-butyl-2-methoxybenzylamine. Unfortunately, this amine is commercially available only in milligram-to-gram amounts, with a prohibitive cost for industrial applications. We decided to undertake the preparation of this amine, planning a synthesis suitable for the manufacturing of large-scale amounts.

We envisaged the preparation of 5-*t*-butyl-2-methoxybenzylamine through a Tscherniac-Einhorn reaction. This reaction was first reported by Tscherniac in 1901 and its potential further exploited by Einhorn in the following years[22]. The Tscherniac-Einhorn reaction is an alternative to the

classic Mannich reaction, in which the intermediate iminium ion is replaced by a more reactive acyliminium ion[23].

The driving force of this synthetic process is related to the formation of the superelectrophilic acyliminium ion (**38**, Scheme 3.17) from the starting material represented by a *N*-hydroxymethylamide (**36**, EWG = Electron withdrawing group). Acid conditions are mandatory for the success of this process.
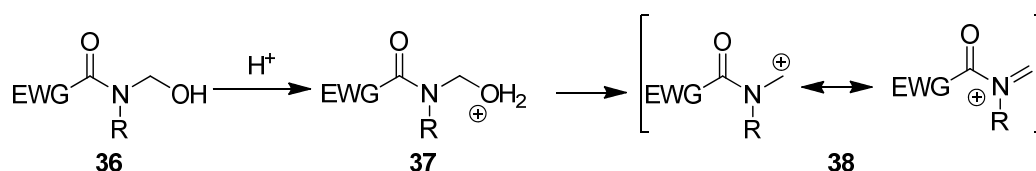
Scheme 3.17: Formation of a superelectrophilic acyliminium ion

The superelectrophilic acyliminium ion is able to react with aromatic substrate (39), ranging from activated ones to non-activated or even mildly deactivated arenes (Scheme 3.18)
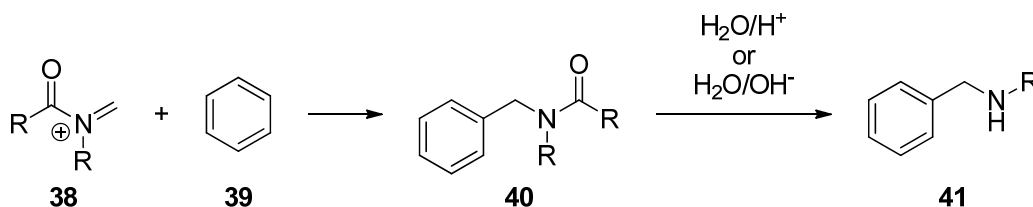
Scheme 3.18: Tscherniac-Einhorn reaction

The α-amidoalkylated arene can be hydrolysed, by both acid or basic conditions, to give a final aralkylamine, or more precisely a substituted benzylamine (**41**).

Synthetic applications of the Tscherniac-Einhorn reaction are extensively described in several articles and reviews[24,25] where different substrate, reaction conditions and α-amidoalkylating agents are discussed.

For our purpose, 5-*t*-butyl-2-methoxybenzylamine (**47**) was built using:

- 4-*t*-butylanisole as the substrate;
- *N*-hydroxymethyl-2-chloroacetamide (**44**) as the amidoalkylating agent.

The amidoalkylating agent was synthesized in quantitative yield using 2-chloroacetamide (**42**) and paraformaldehyde (**43**) following a reported procedure[26] (Scheme 3.19).
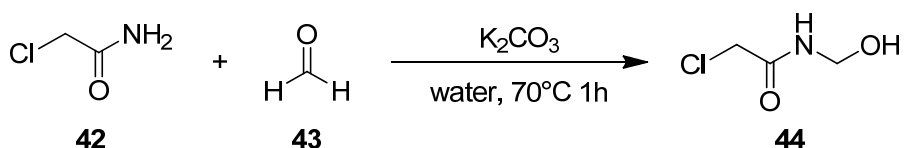
Scheme 3.19: *N*-hydroxymethyl-2-chloroacetamide preparation

After the preparation of the amidoalkylating precursor, the Tscherniac-Einhorn reaction was performed using a 9:1 mixture of acetic acid and sulphuric acid[27] and 4-*t*-butyl anisole (**45**) leading to the clean formation of a mono-substituted product (**46**, Scheme 3.20), isolated in very good yield and purity after a simple work-up.
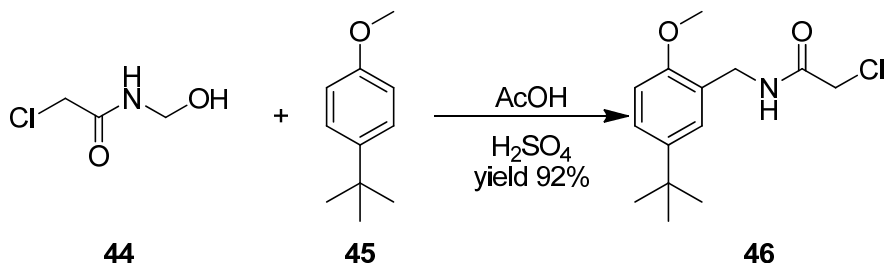
Scheme 3.20: Tscherniac-Einhorn reaction

The amide group was hydrolysed using 37% aq. HCl in 2-propanol in order to obtain (after basification) the free amine (**47**, Scheme 3.21):
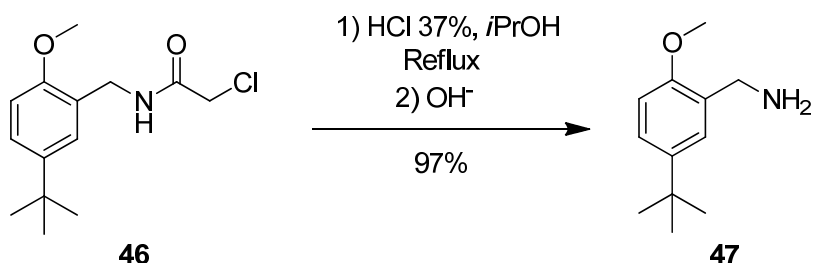
Scheme 3.21: Amide hydrolysis in acid condition

The desired 5-*t*-butyl-2-methoxybenzylamine (**47**) was obtained in a 2-step chromatography-free protocol, with an overall 89% yield from commercially available starting materials.

5-*t*-Butyl-2-methoxybenzylamine can be employed for the reductive amination *en route* to maropitant. This specific step was performed by reacting (2S)-2-benzhydryl-3-quinuclidinone (**7**) and 5-*t*-butyl-2-methoxybenzylamine (**47**), in dry DCM in presence of titanium(IV) tetraisopropoxide as drying agent and Pt/C as catalyst[8], under dihydrogen atmosphere (scheme 3.22).
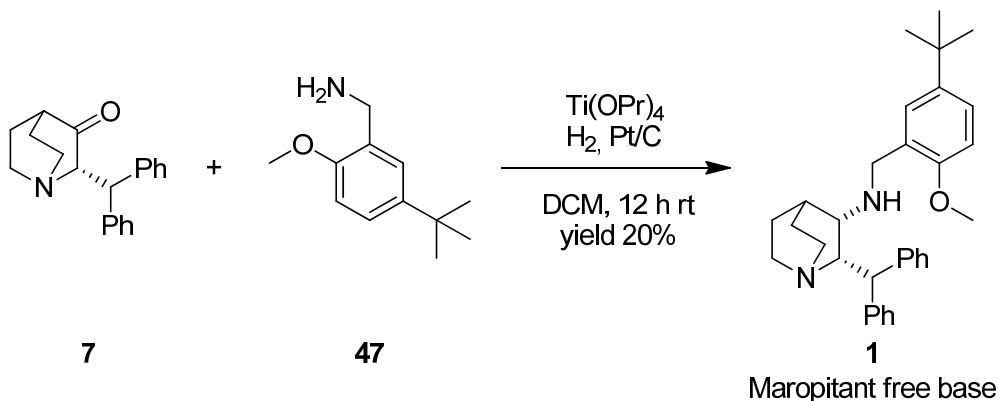
Scheme 3.22: Alternative maropitant synthesis

This approach to maropitant (**1**) avoids one combination of reductive amination/debenzylation and reduces the overall number of steps from 7 to 5. Unfortunately, at this stage, the last step suffers from a low yield and moreover, chiral HPLC analysis showed the formation of diastereomers (Figure 3.5). This step clearly requires an extensive optimisation to improve either the yield and the stereoselectivity, for this alternative synthesis to be comparable in efficiency with the previously reported one.

	Peak Name	RT	Area	% Area
1	(S,R)-MRP	5.241	87001	2.43
2	(R,R)-MRP	5.474	1057046	29.50
3	(S,S)-MRP	6.546	2402987	67.06
4	(R,S)-MRP	7.418	36190	1.01
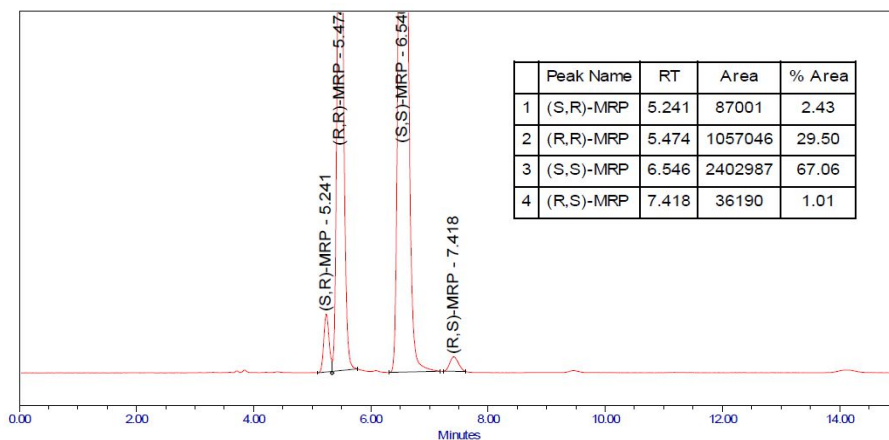
Figure 3.5: Chiral HPLC chromatogram of the reaction reported in Scheme 3.22

3.5. Current Maropitant synthesis

An alternative and complementary strategy to the design of a radically alternative synthetic process is to analyse and revise the originally reported synthesis, with the aim to trace the main drawbacks and to develop innovative solutions to these problems.

In the classical synthesis of maropitant[7,10], the first step involves a cross aldol condensation of the commercial starting material 3-quinuclidinone hydrochloride and benzaldehyde, in presence of sodium hydroxide as base, leading to the (2Z)-2-benzylidene compound (**4**). The use of the cheapest base and the almost quantitative yield exclude any possible improvement in this step.

The following conjugate addition of phenylmagnesium bromide on the $\Delta^{\alpha,\beta}$ unsaturated system of compound **4** generates the racemic 2-benzhydryl-3-quinuclidinone (**5**), but the yield of this step never exceeds a meagre 50%, due to the concomitant formation of byproducts. The byproducts arise from the high reactivity of the Grignard reagent that can react with the carbonyl group, too. The addition of phenylmagnesium bromide to the ketone may occur on the unsaturated starting material **4** or even on the desired product **5**, leading to the formation of misphenylated derivatives and eroding the yield.

The literature reports several attempts to increase the efficiency of this step, varying the organometallic reagent and the experimental conditions. Patent US 3560510[13] reports the conjugate addition procedure using phenylmagnesium bromide, previously generated, and 2-Z-benzylidenenone **4**, leading to compound **5** in 52% yield. A different procedure is reported by Boudhar et al,[28] using phenylmagnesium chloride

and copper iodide to give compound **5** in a poor 3% yield after chromatographic column and HPLC purification.

During the PhD, we undertook a methodical investigation on the experimental conditions of this step. Fixing the reactants, (**4** and PhMgBr), solvent, catalyst, concentrations, temperature and order and timing of addition were systematically varied. We were able to find a combination giving a strong improvement in the yield of this difficult step.

In detail, we discovered that the combined use of copper(I) iodide as a catalyst and 2-methyltetrahydrofuran as the solvent (scheme 3.23) and with specific temperature and addition time, the yield of the second step was raised from 52% to 90% with an almost complete suppression of the well-known misphenylated byproducts.
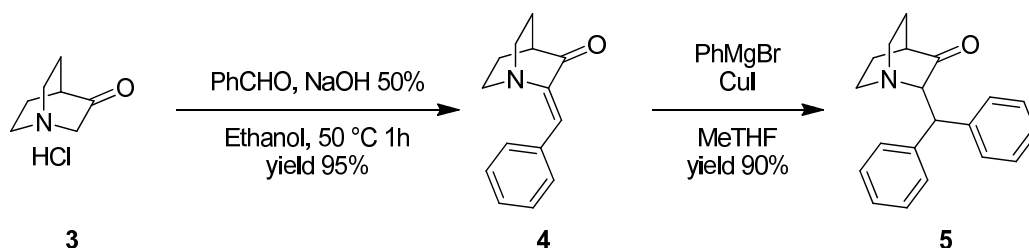
Scheme 3.23: Synthesis of the intermediate **5**

A patent covering IP issue related to the improved conditions for the selective conjugate addition was filed on the base of these results[29].

The synthesis of maropitant proceeds with the third step, involving a dynamic resolution of the racemic **5** with L-tartaric acid as the resolving agent, in ethanol with the addition of acetic acid. This procedure leads to the ketone with the correct configuration of benzhydryl moiety, i.e.: (*2S*)-2-benzhydryl-3-quinuclidinone as the tartaric acid salt (**6**).

Treatment of the salt with sodium hydrogen carbonate and extraction generated the free base *2S*-2-benzhydryl-3-quinuclidinone. Compound **7**

was obtained[8] with virtually complete retention of the stereochemistry (*S:R* 96:4) (**7**, Scheme 3.24).
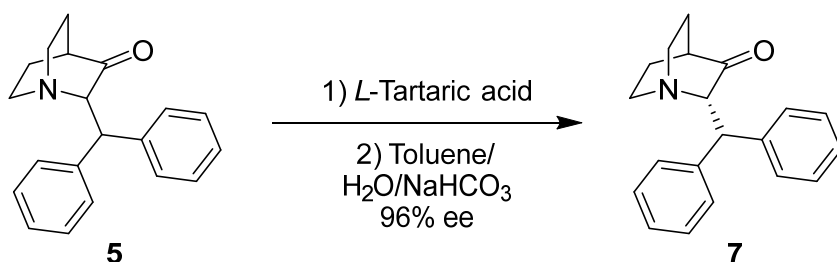
Scheme 3.24: Preparation of *2S*-2-benzhydryl-3-quinuclidinone (**7**)

Reductive amination of **7** with benzylamine was performed in a Parr reactor under hydrogen atmosphere (7 Atm) in the presence of titanium(IV)tetraisopropoxide as a drying agent, and Pt/C as catalyst[8]. The crude material was purified by crystallization leading to the desired product with an overall 61% yield for the two reactions (**8**, Scheme 3.25). Reductive amination by means of sodium triacetoxyborohydride (STAB) led to a complete erosion of the enantiomeric excess and to the formation of a large percentage of the unwanted stereoisomers.
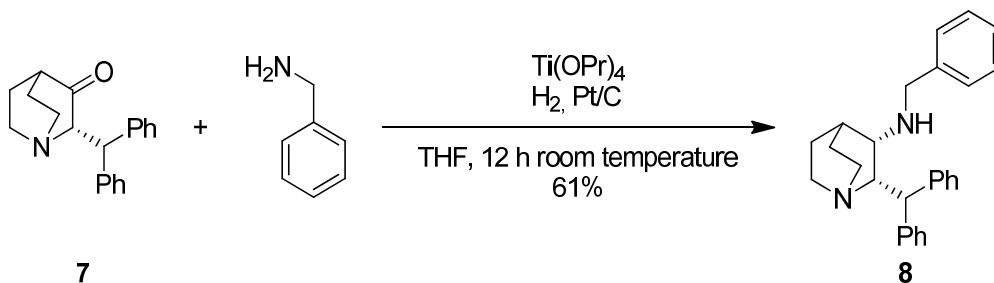
Scheme 3.25: Synthesis of the intermediate **8**

The benzylamine moiety was removed by a debenzylation procedure under hydrogen atmosphere in presence of Pd/C as catalyst leading to the free amine compound **9**[30]. The latter was isolated in quantitative yield and

treated with the commercial aldehyde (**10**) in a further reductive amination protocol relying on STAB as the reducing agent[10] that generates maropitant free base (**1**, Scheme 3.26).
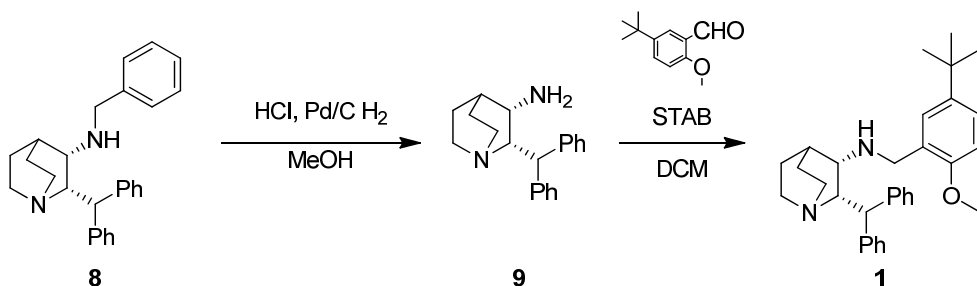
Scheme 3.26: Synthesis of maropitant free base

The preparation of the API is completed by treating the free base with citric acid, water and isopropyl ether[31] leading to the final commercial form: maropitant citrate monohydrate (Scheme 3.27).
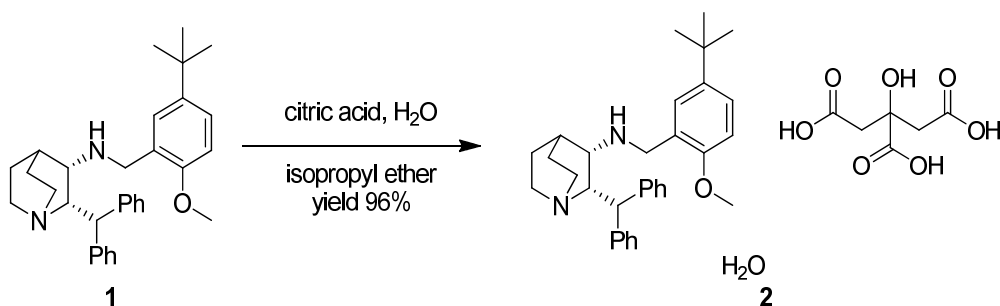
Scheme 3.27: Preparation of maropitant citrate monohydrate

The increase in the yield of the second step, almost doubled after the careful optimisation of the experimental conditions, led this process to be the most mature and convenient for the preparation of maropitant citrate monohydrate, not only in laboratory scale but even on larger scales.

Complete analytical characterisation of maropitant and all intermediates was achieved by different analytical methods (chiral HPLC, HPLC, UPLC-MS and NMR). Additional parameters were checked (ICH solvent guide and presence of catalysts or other metals) in order to confirm the purity of the API according to the AIFA, EMA and FDA standards.

3.6. Conclusion

Maropitant was the subject of the research activity of the first period of the PhD. The search of alternative and efficient syntheses was a complex task due to the variety of functional groups and stereocenters contained in this molecule.

The introduction of the benzhydryl group on the quinuclidinone bicyclic skeleton was investigated using different reactions and led to the identification of two successful approaches, different failures and the formation of byproducts arising by competing reactions. Further efforts were devoted to reducing the number of steps of the total synthesis, achieved by overturning the reductive amination step and preparing the corresponding alternative starting material through a Tscherniac-Einhorn reaction.

Among the two approaches leading to maropitant, one was selected in term of overall efficiency, stereochemical outcome and cost. This approach was positively scaled up to a larger scale and patented.

3.7. Experimental section

Solvents and reagents. Commercially available solvents and reagents were used without further purification. When needed, the reactions were performed under positive pressure of nitrogen or hydrogen.

Spectra. NMR spectra were recorded using either 300 MHz on a Jeol Eclipse ECP300 or Bruker Avance Neo 400 MHz spectrometer. All NMR spectra were registered at 298 K. Chemical shifts (δ) are quoted to parts per million referenced to the residual solvent peak. The multiplicity of each signals is designated using the following abbreviations: s, singlet; d, doublet; t, triplet, q, quartet; quint, quintet; sext, sextet; hept, heptet; m, multiplet, br s, broad singolet; br m, broad multiplet. Coupling constants (*J*) are reported in Hertz (Hz).

The reactions and mass analysis were monitored by UPLC-MS analysis, typically using a column ACQUITY UPLC® BEH C18 1.7 μm, 2.1x50 mm, with a mixture of water/acetonitrile/0.1 % formic acid as eluant.

N-Hydroxy-2-chloroacetamide (44)
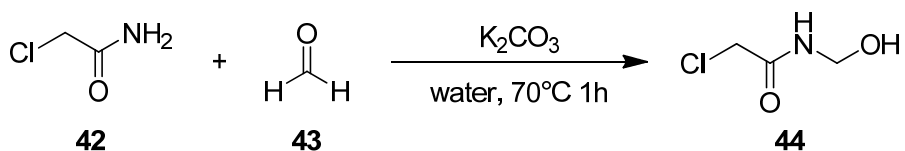
In a round 50 mL bottomed flask, equipped with magnetic stirrer, 2-chloroacetamide (10 g, 106.94 mmol, 1.00 eq), paraformaldehyde (3.44 g, 114.42 mmol, 1.07 eq) and potassium carbonate (4.88 g, 37.43 mmol, 0.35 eq) were dissolved in 10 mL of water. The resulting mixture was heated to 70 °C for 1 h then cooled to room temperature. The obtained white solid was filtered off, washed with cooled water and dried in vacuum at 40°C[26].

^{1}H (300 MHz, D$_2$O): δ 5.44 (s, 2H), 4.24 (s, 2H) ppm

^{13}C-APT (75 MHz, D$_2$O): δ 165.2, 67.7, 43.1 ppm.

N-(5-(*t-Butyl*)-2-methoxybenzyl)-2-chloroacetamide (46)
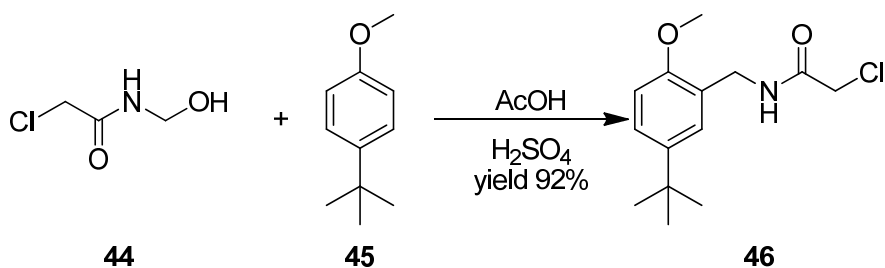
In a 25 mL round bottomed flask, equipped with magnetic stirrer, *N*-hydroxymethyl-2-chloroacetamide (**44,** 0.300 g, 2.43 mmol, 1.00 eq) was dissolved in acetic acid (2.7 mL). 4-*t*-Butylanisole (0.425 mL, 2.43 mmol, 1.00 eq) was added followed by conc. sulphuric acid (0.3 mL). The obtained solution was stirred until completion assessed by TLC (DCM/MeOH 9:1). Then, water (10 mL) was added followed by a saturated solution of sodium bicarbonate until pH 8. The mixture was extracted with DCM three times (3 x 10 mL) and the organic extracts were pooled and washed with brine (20 mL), dried with sodium sulphate, filtered and concentrated under vacuum to give a white solid (92%)[27].

^{1}H (300 MHz, CDCl$_3$): δ 7.32 (d, J = 2.7 Hz, 2H), 6.87 – 6.81 (m, 1H), 4.49 (d, J = 5.8 Hz, 2H), 4.02 (s, 2H), 3.86 (s, 3H), 1.30 (s, 9H).

^{13}C-APT (75 MHz, CDCl$_3$): δ 165.5, 155.7, 143.6, 127.2, 125.9, 124.7, 110.1, 55.5, 42.9, 40.6, 31.6 ppm

5-*t*-Butyl-2-methoxybenzylamine (47)
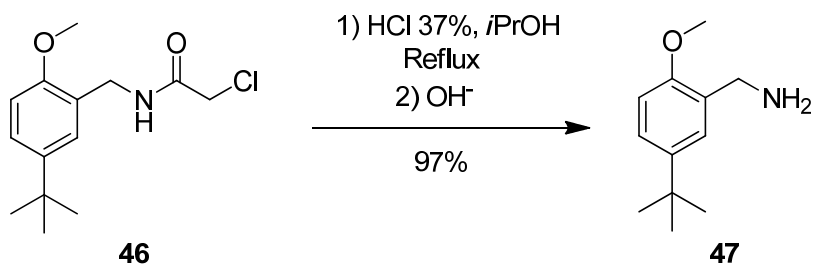
In a 25 mL round bottomed flask, equipped with magnetic stirrer, compound **46** (0.458 g, 1.70 mmol, 1.00 eq) was added followed by 2-propanol (5 mL). HCl 37% (2.8 mL) was added and the resulting mixture was heated to reflux until complete conversion of the starting material. The mixture was diluted with water and extracted with DCM (3 x 10 mL). The organic extracts were concentrated and the obtained residue was purified by column chromatography using DCM/MeOH 9:1 as mixture of solvents.

^{1}H (300 MHz, CDCl$_3$): δ 7.29-7.26 (m, 2H), 6.78 (d, J = 8.3 Hz, 1H), 3.95 (bs, 2H), 3.80 (s, 3H), 3.37-3.35 (m, 1 H), 1.27 (s, 9H) ppm.

^{13}C-APT (75 MHz, CDCl$_3$): δ 155.5, 143.5, 127.4, 126.3, 124.4, 110.0, 55.4, 41.4, 31.6 ppm.

(*2S,3S*)-*N*-(5-*t*-Butyl-2-methoxyphenyl)methyl-2-benzhydrylquinuclidin-3-amine (Maropitant free base, 1)
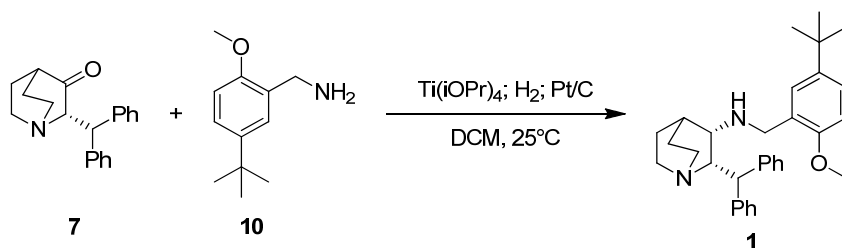
(*2S*)-2-Benzhydryl-3-quinuclidinone **7** (1.51 g, 5.17 mmol, 1.00 eq) was dissolved in anhydrous DCM (30 mL) and transferred to a Parr reactor under nitrogen atmosphere. 5-*t*-Butyl-2-methoxybenzylamine (**10,** 1.04 mL, 5.17 mmol, 1.00 eq) was added followed by titanium (IV) tetraisopropoxide (4.0 mL, 12.93 mmol, 2.50 eq). 5% Pt/C (0.192 g, 0.985 mmol, 0.19 eq) was added and the mixture was stirred at room temperature for 3 hours, then pressurized to 7 atm with hydrogen. The mixture was held in stirring for 12 hours at room temperature and monitored until conclusion. The mixture was filtered through a Celite™ pad under vacuum and the filtrate was washed with a saturated sodium carbonate solution (30 mL) and filtered through a Celite™ pad under vacuum to remove the titanium salts. The organic phase was washed with brine (20 mL), dried on sodium sulphate, filtered and concentrated under *vacuum.* The residue was purified by silica gel column chromatography using DCM/MeOH 95:5 as eluant leading to desired product (20% yield).

(2Z)-2-Benzylidene-3-quinuclidinone (4)
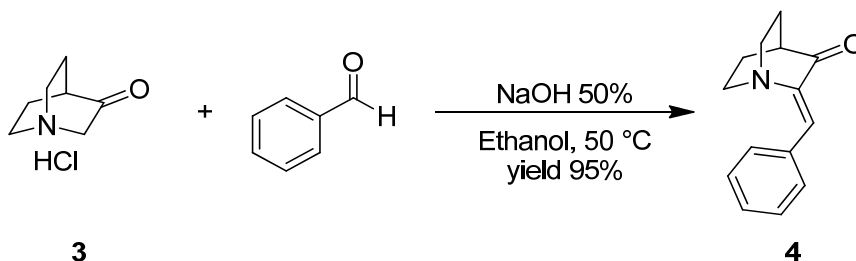
In a four necked round bottomed flask, equipped with a mechanical stirrer, 3-quinuclidinone hydrochloride (600.0 g, 3.71 mol, 1.0 eq) and ethanol (850 mL) were added under nitrogen atmosphere. Then, NaOH 50% (260 mL, 4.94 mol, 1.33 eq) was added dropwise over 15 minutes and the reaction mixture was warmed to 30 °C. A solution of benzaldehyde (379 mL, 3.71 mol, 1.0 eq) in ethanol (394 mL) was added and the resulting mixture was heated to 50 °C until completion (UPLC analysis). Water (780 mL) was added to the reaction at 50 °C and stirring was continued for 1 hour, then cooled to room temperature over 2 hours. After 1 additional hour, the yellow solid was collected by filtration under vacuum and washed with ethanol (910 mL) and water (600 mL). The solid was dried in vacuum at 50 °C for 1 day (yield 95%)[9].

^{1}H (400 MHz, CDCl$_3$): δ 8.03 (dd, J$_1$= 10.6, J$_2$= 2.84 Hz, 2H), 7.38-7.32 (m, 3H), 7.02 (s, 1H), 3.19-3.09 (m, 2H), 3.02-2.96 (m, 2H), 2.61 (q, J=2.9, 1H), 2.00 (td, J$_1$= 7.6, J$_2$= 2.8 Hz, 4H) ppm.

^{13}C-APT (101MHz, CDCl$_3$): δ 206.4, 144.7, 134.0, 132.2, 129.6, 128.4, 125.2, 47.5, 40.3, 25.9 ppm.

UPLC-MS. Calculated for C$_{14}$H$_{15}$NO: 213.28; found 214.30.

2-Benzhydryl-3-quinuclidinone (5)
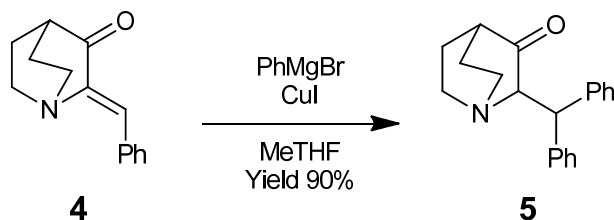
In a four necked 10 L round bottomed flask, equipped with a mechanical stirrer, a dropping funnel and a thermometer, MeTHF (3630 mL) and PhMgBr 45% in MeTHF 2.9M (645.0 mL, 1.86 mol, 1.20 eq) were added. The resulting solution was cooled to 0 °C and copper iodide (17.68 g, 0.093 mol, 0.06 eq) was added. The mixture was stirred at 0 – 2 °C for 10 minutes, under nitrogen atmosphere, then (2Z)-2-benzylidenequinuclidin-3-one (**4**, 330.0 g, 1.55 mol, 1.0 eq) was added in portions. The mixture was stirred until conclusion (30 minutes). The resulting solution was allowed to room temperature then slowly added over a solution of NH$_4$Cl (20% acq. solution, 238.38 g, 4.46 mol) in water (1188 mL) and the biphasic mixture was separated. The organic phase was washed with NH$_4$OH twice (2 x 1320 mL) followed by water (4 x 1320 mL) and brine (1320 mL). The solvent was removed in vacuum and a white solid was obtained. Ethanol (1320 mL) was added and heated until complete dissolution then cooled at room temperature over 16h. The resulting solid was filtered under vacuum, washed with ethanol (660 mL) and dried in vacuum stove for 16 h (yield 90%, purity > 99%)[29]. UPLC-MS calculated for C$_{14}$H$_{17}$NO: 291.38, found: 292.42.

NMR: ^{1}H (400 MHz, CDCl$_3$): δ 7.43-7.15 (m, 10H), 4.58 (d, J= 7.95 Hz, 1H), 4.02(d J= 7.95, 1H), 3.12 (t, J= 7.65 Hz, 2H), 2.68-2.42 (m, 3H), 2.08-1.88 (m, 4H) ppm.

^{13}C-APT (101 MHz, CDCl$_3$): δ 199.3, 128.5, 128.4, 126.6, 126.5, 72.6, 50.4, 49.7, 41.9, 40.8 ppm.

(2S)-2-Benzhydryl-3-quinuclidinone L-tartaric salt (6)
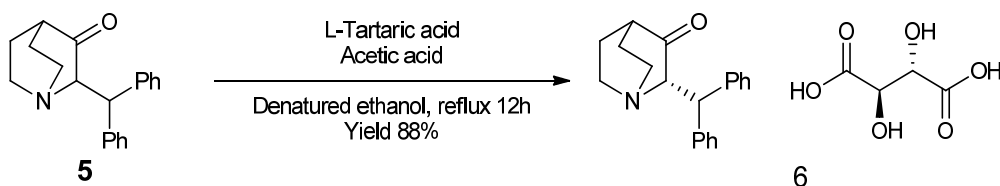
In a four necked 10 L round bottomed flask, equipped with mechanical stirrer and thermometer, *rac*-2-benzhydryl-3-quinuclidinone **5** (740.0 g, 2.54 mol, 1.00 eq) was dissolved in denatured ethanol (5% methanol, 5% 2-propanol) (7400 mL) with acetic acid (145 mL, 2.54 mol, 1.00 eq). L-tartaric acid (381.15 g, 2.54 mol, 1.00 eq) was added and the resulting mixture was heated to reflux for 12 h then cooled to room temperature. The white solid was collected by filtration under vacuum and dried under vacuum stove at 40 °C (yield 88%, *ee* 96%)[8].

^{1}H (400 MHz, DMSO-d$_6$): δ 7.42 – 7.35 (m, 4H), 7.21-7.18 (m, 4H), 7.11 – 7.06 (m, 2H), 4.35 – 4.28 (m, 4H), 3.04 – 2.80 (m, 3H), 2.52 – 2.45 (m, 2H), 2.23 – 2.20 (m, 2H), 2.03 – 1.85 (m, 2H) ppm.

^{13}C (101 MHz, DMSO-d$_6$): δ 219.2, 173.6, 144.2, 128.7, 128.5, 126.2, 72.6, 70.6, 50.9, 48.6, 41.0, 25.9, 25.8 ppm

UPLC-MS calculated for $C_{24}H_{27}NO_7$: 441.47, found: 442.50.

(2S)-2-Benzhydryl-3-quinuclidinone (7)
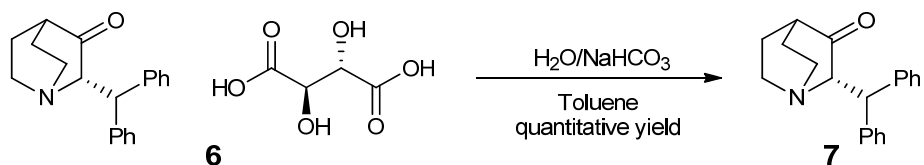
In a flask equipped with magnetic stirring bar and pH-meter, (2S)-2-benzhydryl-3-quinuclidinone L-tartaric salt **6** (500.0 g, 1.13 mol, 1.00 eq) was suspended in toluene (5000 mL) and cooled with an ice-water bath. NaHCO₃ saturated solution (3600 mL) was added dropwise maintaining the temperature under 25 °C. The clear biphasic solution was stirred for 30 minutes at 25 °C then separated. The organic phase was washed with water (750 mL) and concentrated under vacuum and dried in vacuum stove for 16h to provide the desired product in quantitative yield[8]. Chiral HPLC analysis: 96 % *ee*.

(*2S,3S*)-2-Benzhydryl-3-benzylaminoquinuclidine (8)
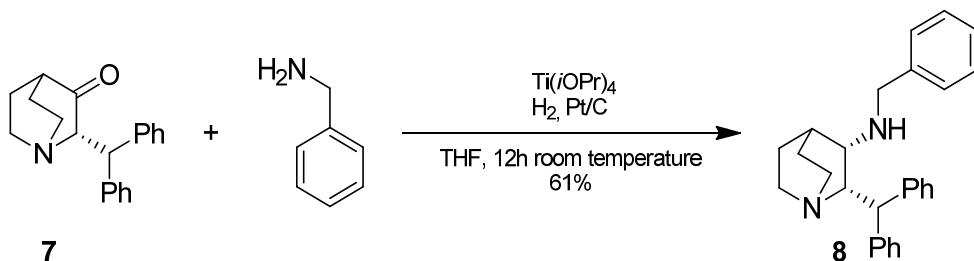
(*2S*)-2-Benzhydryl-3-quinuclidinone **7** (61.0 g, 0.209 mol, 1.0 eq) was dissolved in anhydrous THF (700 mL) and transferred to a Parr reactor under nitrogen atmosphere. Then, benzylamine (25.2 mL, 0.230 mol, 1.1 eq) and titanium (IV) tetraisopropoxide (93 mL, 0.314 mol, 1.50 eq) were added and the mixture was stirred at room temperature for 3 hours. 5% Pt/C (7.66 g, 0.039 mol, 0.19 eq) was added and the Parr reactor was pressurized to 7 atmospheres with hydrogen. The mixture was held in stirring for 12 hours at room temperature. The Parr reactor is vented and hydrochloric acid 12.4 % (190 mL H_2O + 95 mL HCl 37%, 285 mL) was added and the mixture was kept in stirring for 1 hour then filtered through a Celite™ pad under vacuum. The filter cake was washed with toluene (340 mL). The biphasic system was separated and the aqueous phase was transferred into flask. Toluene (340 mL) was added to the acid aqueous phase and NaOH was added until pH was 13. The mixture was filtered through a Celite™ pad under vacuum to remove the titanium salts. The cake was washed with toluene (2x100 mL) and the layers were separated. The organics were concentrated under vacuum leading to a solid. The latter was dissolved in freshly toluene (150 mL) and n-hexane (300 mL) was added and the mixture was cooled to 10°C over 2-3 hours. The white

precipitate was filtered and washed with toluene/n-hexane 1/6 (300 mL) and dried under vacuum stove at 40 °C (yield 61% over two steps).[8]

^{1}H (400 MHz, DMSO-d_6): δ 7.61 – 7.38 (m, 2H), 7.37 – 7.18 (m, 4H), 7.17 – 7.06 (m, 4H), 7.01 (t, J = 7.3 Hz, 1H), 6.74 – 6.39 (m, 2H), 4.40 (d, J = 12.2 Hz, 1H), 3.95 – 3.68 (m, 1H), 3.49 (d, J = 13.4 Hz, 1H), 3.09 (dd, J = 24.1, 12.4 Hz, 2H), 2.80 – 2.52 (m, 3H), 2.45 – 2.19 (m, 1H), 2.01 – 1.86 (m, 1H), 1.81 (d, J = 10.6 Hz, 1H), 1.66 – 1.34 (m, 3H), 1.15 (q, J = 10.2 Hz, 1H) ppm.

^{13}C NMR (101 MHz, DMSO-d_6) δ 140.6, 129.4, 128.4, 128.3, 128.1, 128.0, 126.8, 126.5, 60.8, 54.3, 51.7, 49.3, 41.9, 25.3, 24.7 ppm.

UPLC-MS calculated for $C_{27}H_{30}N_2$: 382.54, found: 383.60

(*2S,3S*)-2-Benzhydrylquinuclidin-3-amine (9)
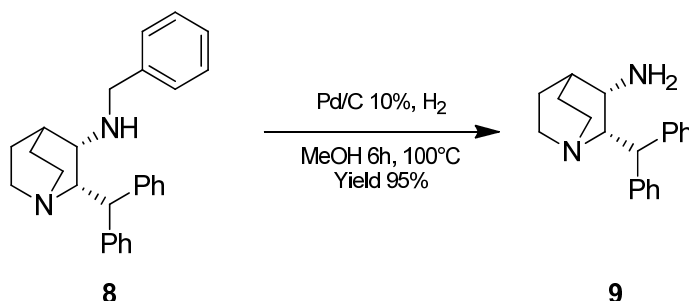
(*2S,3S*)-2-Benzhydryl-3-benzhydrylquinuclidine **8** (76.0 g, 0.199 mol, 1.0 eq) was dissolved in methanol (760 mL). The solution was transferred into a Parr reactor. Pd/C 10% (50% H_2O) (7.80 g, 0.073 mol, 0.37 eq) was added and hydrogen was charged (7 atm) and heated for 6h at 100 °C. The catalyst was removed by filtration under vacuum on a Celite™ pad, and the filtrate was treated with NaOH 2M (760 mL) then separated. The organic phase was concentrated under vacuum giving a white solid (yield 95%)[12].

^{1}H (400 MHz, CDCl$_3$): δ 7.48 - 7.09 (m, 10H), 4.59 (d, J= 12.24 Hz, 1H), 3.69 (dt, J$_1$= 12.2 Hz, J$_2$ = 7.6 Hz, 1H), 3.31 - 3.20 (m, 2H), 2.85 (t, J = 7.95 Hz, 2H), 2.68 (t, J = 11.9 Hz, 1H), 1.98 – 1.87 (m, 1H), 1.81 – 1.80 (m, 1H), 1.69 – 1.60 (m, 2H), 1.36 – 1.25 (m, 1H), 1.08 (s, 2H) ppm.

^{13}C-APT (101 MHz, CDCl$_3$): δ 145.2, 144.1, 129.2, 128.5, 127.9, 127.7, 126.6, 126.1, 62.4, 49.8, 49.7, 49.4, 41.5, 29.5, 26.6, 19.9 ppm

UPLC-MS calculated for $C_{20}H_{24}N_2$: 292.42, found 243.47

(*2S,3S*)-*N*-(5-*t*-Butyl-2-methoxyphenyl)methyl-2-benzhydrylquinuclidin-3-amine (Maropitant free base, 1)
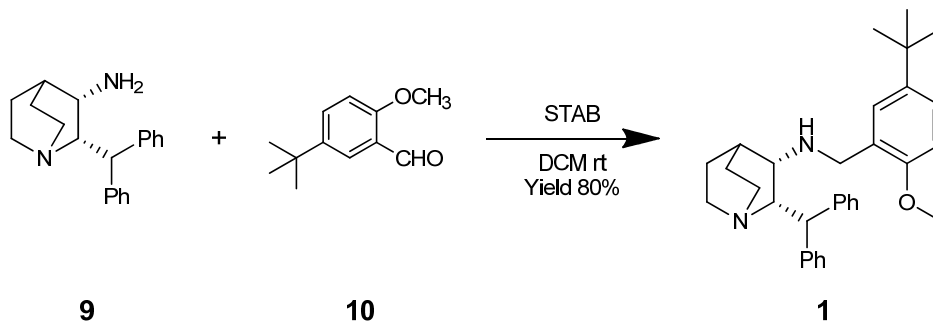
To a solution of 5-*t*-butyl-2-methoxybenzaldehyde **10** (59.17 g, 0.308 mol, 1.00 eq) and (*2S,3S*)-2-benzhydryl-3-aminoquinuclidine **9** (108.0 g, 0.369 mol, 1.20 eq) in methylene chloride (1100 mL), sodium triacetoxyborohydride (97.84 g, 0.462 mol, 1.50 eq) was added in small portions. The mixture was stirred at room temperature for 2 h then transferred into flask and neutralized using NaHCO$_3$ until pH was 8. The biphasic system was separated and the organic phase was dried over sodium sulphate, filtered and concentrated under vacuum to give a white solid (yield 80%)[10].

^{1}H (400 MHz, CDCl$_3$): δ 7,40 - 7,37 (m, 2H), 7,31 - 7,27 (m, 2H), 7.25 – 7.17 (m, 6H), 7.13 – 7.08 (m, 1H), 6.97 (d, J = 2.6 Hz, 1H), 6.70 (d, J = 8.5 Hz, 1H), 4.57 (d, J = 12.1 Hz, 1H), 3.79 – 3.62 (m, 2H), 3.58 (s, 3H), 3.31 – 3.13 (m, 2H), 2.98 (dd, J$_1$ = 7.9 Hz, J$_2$ = 4.2 Hz, 1H), 2.85 – 2.80 (m, 2H), 2.68 – 2.61 (m, 1H), 2.17 – 2.13 (m, 1H), 2.03 – 1.96 (m, 1H), 1.75 – 1.67 (m, 1H), 1.65 – 1.58 (m, 2H), 1.34 (s, 9H) ppm

^{13}C-APT (101 MHz, CDCl$_3$): δ 155.3, 145.6, 143.4, 142.6, 128.9, 128.3, 127.6, 127.6, 127.0, 126.3, 125.8, 124.3, 109.5, 61.9, 55.3, 55.1, 49.3, 31.6, 25.1 ppm

UPLC-MS calculated for C$_{34}$H$_{40}$N$_2$O: 468.67, found: 469.69

Maropitant citrate monohydrate (2)
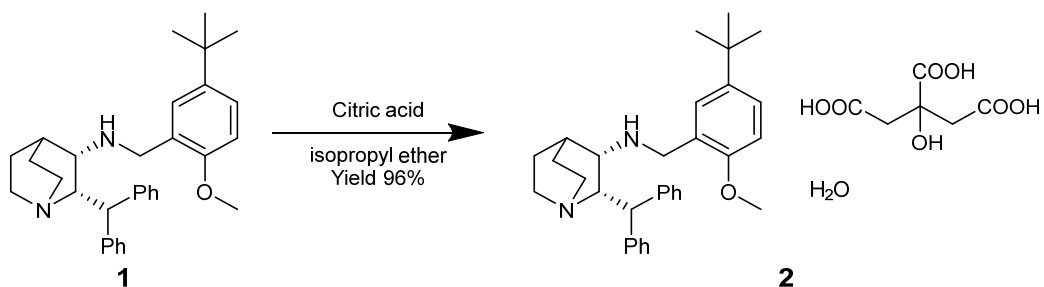
To a white slurry of maropitant free base **1** (90.0 g, 0.192 mol, 1.0 eq) in isopropyl ether (900 mL), anhydrous citric acid (36.89 g, 0.192 mol, 1.0 eq) was added at room temperature. Water (270 mL) was added and the resulting mixture was held in stirring for 18 hours. The desired product was collected by filtration under vacuum[31] (yield 96%).

^{1}H (400 MHz, CD$_3$OD): δ 7,45 - 7,42 (m, 4H), 7,35 - 7,31 (m, 4H), 7.26 (t, J = 7.12 Hz, 2H), 7.22 (dd, J1 = 8.6 Hz, J2 = 2.5 Hz, 1H), 6.93 (d, J = 2.5 Hz, 1H), 6.72 (d, J = 8.6 Hz, 1H), 4.73 (dd, J1 = 12.5 Hz, J2 = 7.3 Hz, 1H), 4.68 (d, J = 12.4 Hz, 1H), 3.72 (m, 1H), 3.54 (d, J = 12.2 Hz, 1H), 3.5 (s, 3H), 3.38 – 3.24 (m, 3H), 3.22 (d, J = 12.2 Hz, 1H), 3.10 (bt, J = 11.6 Hz, 1H), 2.80 (d, J = 15.4 Hz, 2H), 2.73 (d, J = 15.4 Hz, 2H), 2.47 (m, 1H), 2.30 (m, 1H), 2.11 – 1.88 (m, 2H), 1.81 (m, 1H), 1.26 (s, 9H) ppm
^{13}C (101 MHz, CD$_3$OD): δ 177.90, 173.6, 155.40, 142.6, 140.1, 140.0, 129.7, 129.3, 128.0, 127.6, 127.4, 127.0, 126.8, 125.7, 125.1, 109.6, 72.6, 63.2, 54.7, 52.8, 49.0, 47.1, 46.9, 43.5, 42.3, 33.4, 30.6, 23.8, 20.8, 16.7 ppm
UPLC-MS calculated for C$_{38}$H$_{50}$N$_2$O$_9$: 678.81, found 679.85

3.8. References

1. Lesman, S. P.; Boucher, J. F.; Grover, G. S.; Cox, S. R.; Bidgood, T. L. The Pharmacokinetics of Maropitant Citrate Dosed Orally to Dogs at 2 mg/Kg and 8 mg/Kg Once Daily for 14 Days Consecutive Days. *J. Vet. Pharmacol. Ther.* **2013**, *36* (5), 462–470. https://doi.org/10.1111/jvp.12027.

2. de la Puente-Redondo, V. A.; Tilt, N.; Rowan, T. G.; Clemence, R. G. Efficacy of Maropitant for Treatment and Prevention of Emesis Caused by Intravenous Infusion of Cisplatin in Dogs. *Am. J. Vet. Res.* **2007**, *68* (1), 48–56. https://doi.org/10.2460/ajvr.68.1.48.

3. Benchaoui, H. A.; Siedek, E. M.; De La Puente-Redondo, V. A.; Tilt, N.; Rowan, T. G.; Clemence, R. G. Efficacy of Maropitant for Preventing Vomiting Associated with Motion Sickness in Dogs. *Vet. Rec.* **2007**, *161* (13), 444–447. https://doi.org/10.1136/vr.161.13.444.

4. Hickman, M. A.; Cox, S. R.; Mahabir, S.; Miskell, C.; Lin, J.; Bunger, A.; McCALL, R. B. Safety, Pharmacokinetics and Use of the Novel NK-1 Receptor Antagonist Maropitant (Cerenia ™) for the Prevention of Emesis and Motion Sickness in Cats. *J. Vet. Pharmacol. Ther.* **2008**, *31* (3), 220–229. https://doi.org/10.1111/j.1365-2885.2008.00952.x.

5. Tsukamoto, A.; Ohgoda, M.; Haruki, N.; Hori, M.; Inomata, T. The Anti-Inflammatory Action of Maropitant in a Mouse Model of Acute Pancreatitis. *J. Vet. Med. Sci.* **2018**, *80* (3), 492–498. https://doi.org/10.1292/jvms.17-0483.

6. Massett, S. S.; Quallich, G. J.; Rose, P. R.; Wint, L. T. Polymorphs of Crystalline (2-Benzhydryl-1-Azabicyclo[2.2.2]Oct-3-Yl)-(5-Isopropyl-2-

Methoxybenzyl)-Amine Citrate as Nk-1 Receptor Antagonists. WO0073303 (A1), December 7, 2000.

7. Basford, P. A.; Post, R. J.; Smith, J. D.; Taber, G. P. Process for Preparation of 1-(2S,3S)-2-Benzhydryl-N-(5-*t*-Butyl-2-Methoxybenzyl) Quinuclidin-3-Amine. WO2005075473 (A1), August 18, 2005.

8. Nugent, T. C.; Seemayer, R. An Efficient Enantiopure Synthesis of a Pivotal Precursor to Substance P Antagonists. *Org. Process Res. Dev.* **2006**, *10* (1), 142–148. https://doi.org/10.1021/op050213e.

9. Chandramouli, S. V.; Ayers, T. A.; Wu, X.-D.; Tran, L. T.; Peers, J. H.; Disanto, R.; Roberts, F.; Kumar, N.; Jiang, Y.; Choy, N.; et al. Scale-Up of an Enantioselective Overman Rearrangement for an Asymmetric Synthesis of a Glycine Transporter 1 Inhibitor. *Org. Process Res. Dev.* **2012**, *16* (3), 484–494. https://doi.org/10.1021/op200378r.

10. Ito, F.; Kondo, H.; Nakane, M.; Lowe, I. J. A.; Rosen, T. J.; Shimada, K. Quinuclidine Derivatives. US6222038 (B1), April 24, 2001.

11. McCarson, K. E. L703606. In *xPharm: The Comprehensive Pharmacology Reference*; Elsevier, 2007; pp 1–4. https://doi.org/10.1016/B978-008055232-3.62000-8.

12. Warawa, E. J.; Mueller, N. J.; Fleming, J. S. Quinuclidine Chemistry. 4. Diuretic Properties of Cis-3-Amino-2-Benzhydrylquinuclidine. *J. Med. Chem.* **1975**, *18* (6), 587–593. https://doi.org/10.1021/jm00240a013.

13. Warawa, E. J. 2-Benzhydrylquinuclidines. US3560510 (A), February 2, 1971.

14. Aggarwal, V. K.; Staubitz, A. C.; Owen, M. Optimization of the Mizoroki−Heck Reaction Using Design of Experiment (DoE). *Org.*

Process Res. Dev. **2006**, *10* (1), 64–69. https://doi.org/10.1021/op058013q.

15. *Progress in Organic Chemistry*; Cook, J., Carruthers, W., Eds.; Springer US: Boston, MA, 1968. https://doi.org/10.1007/978-1-4899-7315-3.

16. Millard, B. J.; Stevens, T. S. 630. Electrophilic Rearrangements: Stereochemistry and Allylic Transformations. *J. Chem. Soc. Resumed* **1963**, No. 0, 3397–3403. https://doi.org/10.1039/JR9630003397.

17. Hoffmann, R. W. Stereochemistry of [2,3]Sigmatropic Rearrangements. *Angew. Chem. Int. Ed. Engl.* **1979**, *18* (8), 563–572. https://doi.org/10.1002/anie.197905633.

18. Ollis, W. D.; Rey, M.; Sutherland, I. O. Base Catalysed Rearrangements Involving Ylide Intermediates. Part 15. The Mechanism of the Stevens [1,2] Rearrangement. *J. Chem. Soc. Perkin 1* **1983**, No. 0, 1009–1027. https://doi.org/10.1039/P19830001009.

19. Brieden, W. D. Method for the Preparation of Optically Active 3-Hydroxyquinuclidine. EP0785198 (A1), July 23, 1997.

20. Taniguchi, Y.; Inanaga, J.; Yamaguchi, M. Use of 1,8-Diazabicyclo[5.4.0]Undec-7-Ene in Preparation of Trimethylsilyl Enol Ethers and Trimethylsilylacetylenes. *Bull. Chem. Soc. Jpn.* **1981**, *54* (10), 3229–3230. https://doi.org/10.1246/bcsj.54.3229.

21. Downey, C. W.; Johnson, M. W.; Tracy, K. J. One-Pot Enol Silane Formation-Mukaiyama Aldol-Type Addition to Dimethyl Acetals Mediated by TMSOTf. *J. Org. Chem.* **2008**, *73* (8), 3299–3302. https://doi.org/10.1021/jo8001084.

22. Tscherniac-Einhorn Reaction: (Tscherniac-Einhorn Amidomethylation, Tscherniac-Einhorn Amidoalkylation). In *Comprehensive Organic*

Name Reactions and Reagents; John Wiley & Sons, Inc.: Hoboken, NJ, USA, 2010. https://doi.org/10.1002/9780470638859.conrr629.

23. Olah, G. A.; Wang, Q.; Sandford, G.; Oxyzoglou, A. B.; Surya Prakash, G. K. Superelectrophilic Tscherniac Amidomethylation of Aromatics with *N* -Hydroxymethylphthalimide in Trifluoromethanesulfonic Acid. *Synthesis* **1993**, *1993* (11), 1077–1079. https://doi.org/10.1055/s-1993-26001.

24. Zaugg, H. E. α-Amidoalkylation at Carbon: Recent Advances - Part I. *Synthesis* **1984**, *1984* (02), 85–110. https://doi.org/10.1055/s-1984-30740.

25. Zaugg, H. E. α-Amidoalkylation at Carbon: Recent Advances - Part II. *Synthesis* **1984**, *1984* (03), 181–212. https://doi.org/10.1055/s-1984-30772.

26. Murata, H. Method for Synthesizing N-Methylol Compound. JP2003171357 (A), June 20, 2003.

27. Tamura, K.; Kato, Y.; Ishikawa, A.; Kato, Y.; Himori, M.; Yoshida, M.; Takashima, Y.; Suzuki, T.; Kawabe, Y.; Cynshi, O.; et al. Design and Synthesis of 4,6-Di- *Tert* -Butyl-2,3-Dihydro-5-Benzofuranols as a Novel Series of Antiatherogenic Antioxidants. *J. Med. Chem.* **2003**, *46* (14), 3083–3093. https://doi.org/10.1021/jm030062a.

28. Boudhar, A.; Ng, X. W.; Loh, C. Y.; Chia, W. N.; Tan, Z. M.; Nosten, F.; Dymock, B. W.; Tan, K. S. W. Overcoming Chloroquine Resistance in Malaria: Design, Synthesis and Structure–Activity Relationships of Novel Chemoreversal Agents. *Eur. J. Med. Chem.* **2016**, *119*, 231–249. https://doi.org/10.1016/j.ejmech.2016.04.058.

29. Donnola, M.; Mossotti, M.; Barbero, M.; Roletto, J.; Paissoni, P. Process for the Synthesis of 2-Benzhydryl-3 Quinuclidinone. WO2019086434 (A1), May 9, 2019.

30. Swain, C. J.; Seward, E. M.; MacIntyre, D. E.; Merchant, K. J.; Owen, S. N.; Owens, A. P.; Sabin, V.; Teall, M.; VanNiel, M. B.; Williams, B. J.; et al. Identification of a Series of 3-(Benzyloxy)-l-Azabicyclo[2.2.2]Octane, Human NK-1 Antagonists.

31. Castaldi, M. J.; Quallich, G. J.; Wint, L. T. Polymorphs of a Crystalline Azabicyclo (2,2,2) Octan-3-Amine Citrate and Their Pharmaceutical Compositions. WO0073304 (A1), December 7, 2000.

Chapter 4: Oxidative Degradation-Amination of Vanillin

4.1. Introduction

Vanillin (**1**, 4-hydroxy-3-methoxybenzaldehyde) is one of the most common flavouring agent, widely used in foods, beverages, food-supplements, perfumes and pharmaceuticals[1]. This aromatic aldehyde is extracted from the berries of orchids of the genus Vanilla. Due to the high extraction costs and the low yield of extraction, synthetic vanillin is available to satisfy the worldwide request. More recently, a new synthetic derivative of vanillin was produced, *i.e.*: ethyl-vanillin **2** (bourbonal, 3-ethoxy-4-hydroxybenzaldeyde), is gaining space in the flavouring industry, due to its stronger and persistent aroma (Figure 4.1).

1	**2**
Vanillin	Ethylvanillin (Bourbonal)
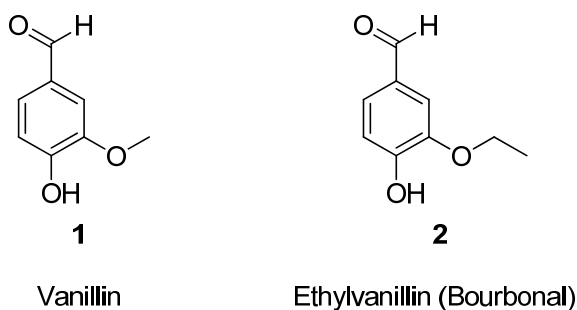
Figure 4.1: Structures of Vanillin and Ethylvanillin

As mentioned above, different synthetic strategies have been developed for the production of synthetic vanillin. Recent examples include the work of the research group of Liu et al[2] involving a method based on the iron-catalized oxidative C-C bond cleavage of allylarenes to the corresponding arylaldehyde. Following this procedure, vanillin is produced in 84% yield. An alternative method was reported by Taber at al[3] in which vanillin was synthesised in two steps: bromination of 4-hydroxybenzaldehyde **3**,

followed by substitution of the bromine atom with a methoxide group in the presence of copper(I)bromide as catalyst, in 74% yield (Scheme 4.1).
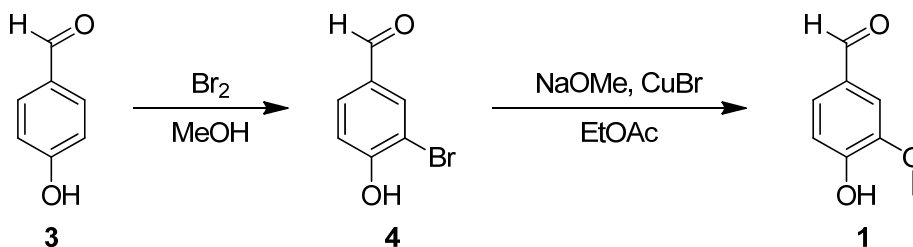
Scheme 4.1: Reported synthesis of vanillin

Both the two cases reported the use of a chromatographic separation in order to obtain the pure vanillin. The latter technology cannot be applied in industries due to the high associated costs. For these reasons, alternative production processes were developed based on the biotechnological transformations, employing different microorganisms and starting materials. Kaur – Chakraborty[4], Chattopadhyay[5], Banerjee – Chattopadhyay[1] and Gallage – Møller[6], reported different and alternative methods for the biotechnological production of vanillin using different starting material like ferulic acid, eugenol, isoeugenol and lignin. These transformations can be made using several microorganisms as bacteria (*S. sannanensis MTCC 6637*), fungi and genetic modified organisms. The aims of these researches were focused on the identification of large scale inexpensive starting materials (agro-residues) suitable for the production of vanillin. FDA approved the use of vanillin in 1977 in foods and beverages. This compound shows a robust safety profile and several studies even claimed the potential anti-bacteria[7], anti-oxidant[8] and anti-mutagens[9,10] activities. Nevertheless, Chen and co. workers[11], showed that vanillin (or ethylvanillin) are an inductor of the CYP2E1 as well as

inhibitor of the CYP1A2. These data revealed that the drug interaction between vanillin and CYP2E1/1A2 can be possible. This result suggests that use of this additive in foods should be accompanied with more attention. Moreover, these results can suggest that vanillin could interact with endogenous molecules even if no data are available to support this theory.

Vanillin is widely used in foods, especially in cooked products (biscuits, cakes), increasing the possibility of the vanillin to take a role during reactions involving functional groups presents in other ingredients, as for example eggs and flour. To our knowledge, the literature does not report any evidence of the formation of vanillin-related by-products during the use of this flavouring compound.

This work complements and completes an investigation started in a previous PhD work[12]. During the investigation of the reactions of vanillin with amines, initially addressed to the isolation of quinomethides, we registered a surprising and efficient formation of coloured products with secondary amines. Treatment of vanillin (**1**) with excess morpholine (**2a**) in alcoholic solution at room temperature gave an initially complex mixture of coloured compounds as evidenced by TLC analysis, evolving overnight towards the precipitation of a brick red crystalline compound. Isolation of the precipitate and analysis by NMR and HRMS led to the identification of this product as 2,5-dimorpholino-1,4-benzoquinone (**3a**) (Scheme 4.2). Comparison of the product with a sample prepared by an independent procedure[13] confirmed its identity.
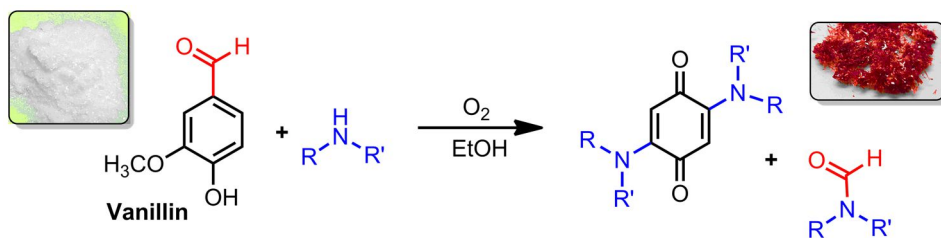
Scheme 4.2: Reaction of vanillin with secondary amines in aerobic conditions

Startled by this initial result, we undertook a systematic investigation of this strange reaction by exploring its versatility towards different amines. Different secondary aliphatic amines (**2a-e**, Figure 4.2) were found to react in the same way, providing good to excellent yields of the corresponding substituted 2,5-diamino-1,4-benzoquinones (**3a-e**). Proline (**2f**) reacts leading the corresponding quinone **3f**, in the presence of Na_2CO_3. This is especially noteworthy as this proteinogenic amino acid may be present in the free form in some foods. Secondary aromatic amines failed to react significantly while aliphatic and aromatic primary amines yielded variable amounts of "simple" imines (drying agents were not present).
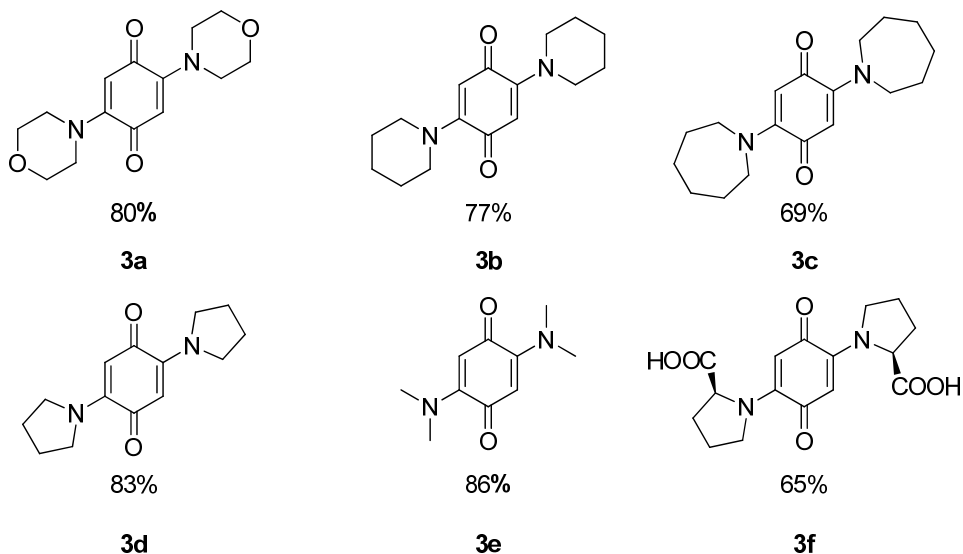
Figure 4.2: Disubstituted 1,4-benzoquinone with relative yields.

We examined the experimental conditions in order to gain additional information on the possible mechanism. The reactions run at room temperature for 24h yielded 2,5-diamino-1,4-benzoquinones as summarised in Scheme 1. Heating or refluxing speeded up the formation of the 2,5-diamino-1,4-benzoquinones. Alcoholic solvents like methanol and ethanol were the best solvents, while either apolar or more polar solvents led to incomplete reactions and/or complex mixtures, mainly ascribed to the limited solubility of the reagents. The reaction atmosphere was the subject of particular attention. The reactions proceeded sluggishly under nitrogen atmosphere but restoring the aerobic condition the reactions reached complete conversion, suggesting a direct role of oxygen in the reaction mechanism. Atom mapping allowed to trace back the quinone skeleton to the aromatic ring of vanillin, with the evident excision of the carbon atom of the aldehyde group. Analysis of the residual mother liquor of the reaction originally leading to **3a** allowed to isolate a byproduct,

identified by NMR as *N*-formylmorpholine (**4a**), later confirmed by comparison with the commercially available compound by GC. An analogous reaction between vanillin and dimethylamine (**2e**) clearly showed by GC analysis the formation of *N,N*-dimethylformamide (DMF), identifying the fate of the missing carbon atom.

The experimental evidences arising by this preliminary investigation led us to sketch a possible mechanism for this reaction (Scheme 4.3). The transformation of vanillin to 2,5-diamino-1,4-benzoquinones starts with a dehydrative condensation of the arylaldehyde with the secondary amine (morpholine **2a** in Scheme 3.3) to give an intermediate iminium ion **5a**. Deprotonation gives the morpholinoquinomethide **6a**. Structural analogues of **6a** were described as intermediates in cycloadditions[14] ad sometimes isolated[15]. Aerobic oxidation of the enamine portion[16] of the dialkylaminoquinomethide is known to take place on similar compounds through a SET mechanism[17] generating the unstable dioxetane **7a**. The four-membered ring promptly fragments[18] to 2-methoxy-1,4-benzoquinone **8a** and to the identified byproduct N-formylmorpholine **4a**. Conversion of the quinone **8a** to the final 2,5-dimorpholino-1,4-benzoquinone **3a** may occur through two alternative and converging pathways, involving standard quinone chemistry[19]: i) the secondary amine undergoes to a conjugate addition to giving 2-amino-5-methoxyhydroquinone **9a**, then oxidised (by oxygen or by the quinones present in the reaction mixture) to the corresponding 1,4-benzoquinone **10a**; finally giving **3a** by an *ipso*-substitution of the -OCH$_3$ group operating through a combined addition-elimination[19]; ii) preliminary nucleophilic *ipso*-substitution of the -OCH$_3$ group by the secondary amine leading to an intermediate 2-amino-1,4-benzoquinone **11a** and afterward addition of a second molecule of amine

to give the intermediate 2,5-diaminohydroquinone **12a**, finally oxidised (by oxygen or by the quinones present in the reaction mixture) to the stable end-product **3a**.
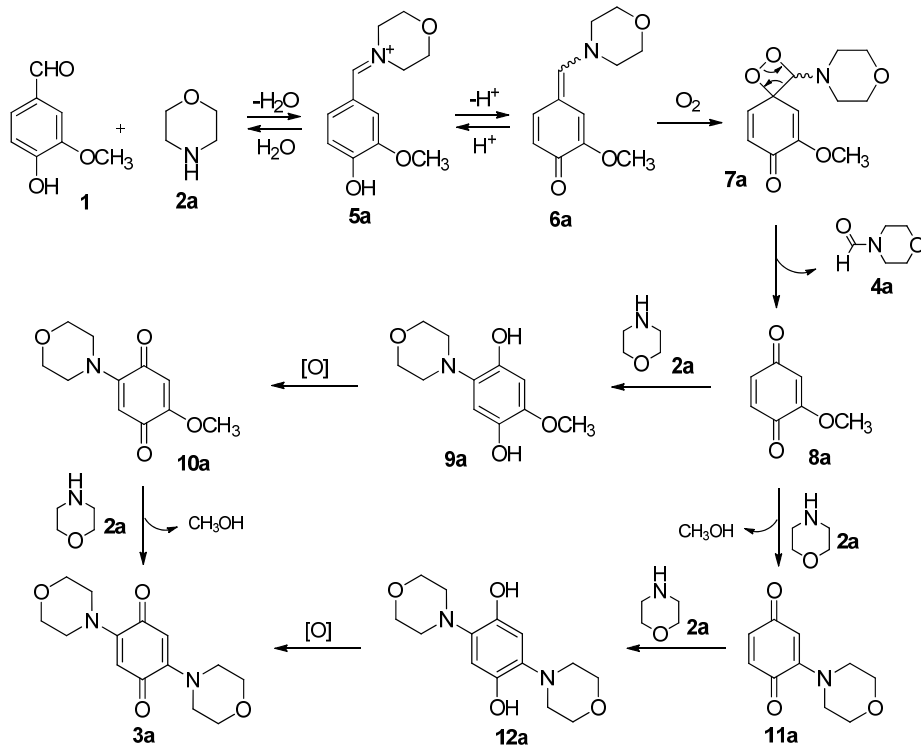
Scheme 4.3: Proposed mechanism for the formation of disubstituted 1,4-benzoquinones

Two additional experiments endorse the proposed mechanism. Reaction of the commercially available quinone **8a** with excess morpholine in ethanol at room temperature in aerobic conditions overnight gave good yields of **3a**, confirming its involvement as intermediate in the reaction pathway. Moreover, "bourbonal" gave as expected the same 2,5-diamino-1,4-benzoquinones on reaction with amines **2a-f**. Slightly longer reaction times were needed to reach complete conversion. Due to the efficiency of the reaction of vanillin with secondary amines, proceeding in mild

conditions and with good to excellent yields, the possibility of this reaction to take place during cooking processes in the hot aerobic environment of baking ovens may raise some safety concerns.

Vanillin is commonly added to foods before baking or sprayed as an ethanolic solution after cooking on their surface, with the aim to aromatise the baked product. In addition, free proline can be present in different ingredients (milk powders, flours), as well as other secondary amines released during the Maillard's reaction. The formation of 2,5-diamino-1,4-benzoquinones (namely **3f**) is then conceivable in products enriched by free amino acids (*e.g.*: baked enriched foods or food for medical uses).

For this reason, we undertaken preliminary toxicity tests (in collaboration with Prof. F. Condorelli, Dipartimento di Scienze del Farmaco) to evaluate the potential biological effect of 2,5-diamino-1,4-benzoquinone. No literature data are available for this family of compounds except for the 2,5-diaziridino analogues, where cytotoxicity and mutagenicity is well documented[20] but obviously related to the presence of the strained three-membered heterocyclic rings rather than to the benzoquinone. These tests show that 2,5-diamino-1,4-benzoquinones are not toxic even at 100 µM concentrations. In detail, MTT-based assays were exploited *in vitro* to test the effect of our compounds on viability of renal (HEK293T) and hepatocytic (HepG2) human cell lines, pointing out to a negligible toxicity at concentrations compatible with alimentary exposure. Thus, although more detailed investigation is needed, our observations exclude at this stage undesired biological activities for these compounds.

Colour is a fundamental attractive sensorial feature of baked products, and the Maillard reactions are well known to contribute to the development of the brown colour during food processing. The wide range of brilliant orange

to brilliant dark red tones shown by the 2,5-diamino-1,4-benzoquinones could be a contributor to the overall colour perceived in bakery products. Furthermore, the colouring properties of these compounds can be estimated to select novel potential candidates as "new" colorant additives in foods, following a mandatory deeper safety assessment.

4.2. Conclusion

In conclusion, in this work we report the observation of an unprecedented reaction of vanillin with secondary alkylamines in aerobic conditions, generating 2,5-diamino-1,4-benzoquinones. This complex reaction appears to involve several steps and intermediates, as typified by the proposed reaction mechanism, sketched following the results of suitably designed experiments and on the base of literature records in quinone chemistry. The relevance of this novel transformation resides in the possibility of this reaction to happen more frequently than considered until now, due to the widespread use of vanillin (and its derivatives as ethylvanillin) and the occurrence of secondary amines, either biogenic or thermally/chemically generated during food processing. These outcomes give new insights on the potential red-orange colour tone development in baked foods, complementary to the browning correlated to the well know Maillard reactions and paves the way to consider the use of 2,5-diamino-1,4-benzoquinones as potentially safe dyes (*e.g.*: as pigments for foods or other colourants for pharmaceuticals products).

4.3. Experimental section

Solvents and starting materials were purchased from Sigma-Aldrich, Carlo Erba Reagents or TCI Europe and used without further purification. All aqueous solutions were prepared from ultrapure laboratory grade water (18 MΩ・cm) obtained from Millipore/MilliQ purification system. ^{1}H and ^{13}C NMR spectra were recorded at 300 MHz on a Jeol Eclipse ECP300 spectrometer. Chemical shifts are reported in ppm with the protic impurities of the deuterated solvent as the internal reference. All NMR spectra were conducted at 333 K. Mass spectra were obtained with a TSQ Quantum Access Max Triple Quadrupole Mass Spectrometer (Thermo Scientific) equipped with an electrospray ionization (ESI) source; analysis by direct infusion. High resolution mass spectra were registered on a Thermo Fisher Scientific Orbitrap Q-Exactive Plus mass spectrometer (San Josè, CA, USA), with 70.000 as resolution (FWHM) and methanol as solvent for infusion. All spectra were registered in positive ion mode. Chromatographic analyses were performed using a Thermo Fisher Scientific TRACE 1300 gas chromatography system with Flame Ionization Detector, the apparatus used was equipped with a split/splitless injector and column TG-WAXMS (30 m x 0.25 mm i.d. x 0.25 μm film thickness). Separation was performed starting at 50 °C, held for 2 min, temperature increased at a rate of 10 °C/min to 180 °C, temperature increased at a rate of 15 °C/min to 240 °C and finally held for 10 min. Analysis was performed at 1.5 mL min $^{-1}$ constant flow; hydrogen is the carrier gas. Injection temperature: 250 °C. Detector temperature: 350 °C Analysis was performed with 50:1 split ratio. TLC were performed with silica gel (MN Kieselgel 60F254) and visualized by UV or sprayed with Dragendorff reagent or alkaline $KMnO_4$.

General procedure

Vanillin (1.00 g, 6.57 mmol, 1.0 eq) was dissolved in ethanol (10 mL), then the corresponding amine (3.2 eq) was added, and the resulting solution was stirred in an open flask at room temperature for 16 hours. The obtained crystals were collected by filtration under vacuum and dried in air.

The reaction with L-proline was carried out using the same procedure, adding sodium carbonate (2.2 eq) to the reaction mixture. The reaction progress was monitored by TLC then HCl 2M was added until pH 1. The resulting precipitate was filtered and dried in air.

MTT assay were conducted following the procedure below:
Human cell lines (HepG2, HEK293T) were cultured according to the ATCC guidelines. For cytotoxicity assays, cells were re-suspended in Dulbecco Modified Eagle Medium (DMEM) without phenol red, supplemented with 10% heat-inactivated fetal calf serum. Cells were plated in 96-well polystyrene cell culture plates (30,000 to 50,000 cells/well depending on the cell type) and incubated at 37 °C in 5% CO_2 for 24 hours to promote cell adhesion to the well's surface. Compounds, with exception of **3f** which was re-suspended in cell culture media (DMEM), were solubilized in DMSO at 1M concentration. Cells were incubated at 37 °C in 5% CO_2 for 12 hours at concentrations ranging between 100 nM up to 100 μM. Experiments were performed in Locke solution (134 mM NaCl, 5 mM KCl, 4 mM $NaHCO_3$, 10 mM HEPES [pH 7.6], 2.3 mM $CaCl_2$, 1 mM $MgCl_2$, 5 mM sucrose) with a final concentration of 250 μg/ml of the tetrazolium dye 3-(4,5-dimethylthiazol-2-yl)-2,5-diphenyltetrazolium bromide (MTT). In brief,

cells were washed twice in Locke to be incubated for 1 h with MTT at 37°C. Reactions were then stopped and the formazan crystals produced by cellular oxidoreductase enzymes were solubilized in isopropyl alcohol/HCl before being read at 600 nm in a spectrophotometer.
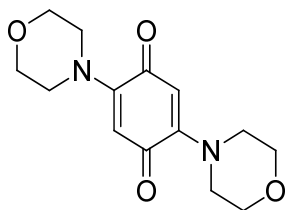
2,5-Dimorpholinocyclohexa-2,5-diene-1,4-dione (**3a**), brick-red solid, m.p.: 239 - 240 °C (238 - 243 °C)[21], yield: 83%): ^{1}H NMR (300 MHz, CDCl$_3$): δ 5.52 (s, 2H), 3.79 (t, J = 4.3 Hz, 8H), 3.55 (t, J = 4.3 Hz, 8H) ppm. ^{13}C NMR (75.6 MHz, CDCl$_3$): δ 182.8 (C), 152.2 (C), 106.9 (CH), 66.5 (CH$_2$), 49.1 (CH$_2$) ppm. MS: Calc. [C$_{14}$H$_{18}$N$_2$O$_4$+H]$^+$: 279.13393, found 279.13362, calc. [C$_{14}$H$_{18}$N$_2$O$_4$+Na]$^+$: 301.11588, found 301.11542.
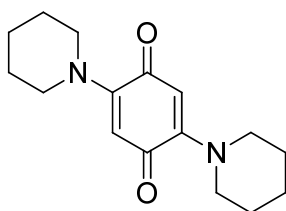
2,5-Di(piperidin-1-yl)cyclohexa-2,5-diene-1,4-dione (**3b**), dark-red solid, m.p: 173 - 175 °C (176 °C)[13], yield: 77%: ^{1}H NMR (300 MHz, CDCl$_3$): δ 5.44 (s, 2H), 3.47 (br s, 8H), 1.60 (br s, 12H) ppm. ^{13}C NMR (75.6 MHz, CDCl$_3$): δ 182.6 (C), 153.0 (C), 105.5 (CH), 50.2 (CH$_2$), 25.9 (CH$_2$), 24.3 (CH$_2$) ppm. MS: Calc. [C$_{16}$H$_{22}$N$_2$O$_2$+H]$^+$: 275.17540, found 275.17438. calc. [C$_{16}$H$_{22}$N$_2$O$_2$+Na]$^+$: 297.15735, found 297.15619.
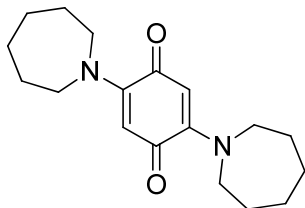
2,5-Di(azepan-1-yl)cyclohexa-2,5-diene-1,4-dione (**3c),** brick-red solid, m.p.: 157 °C (157 °C), yield: 69**%.** ^{1}H NMR (300 MHz, CDCl$_3$): δ 5.32 (s, 2H), 3.62 (t, J = 5.9 Hz, 8H), 1.74 (br s, 8H), 1.50 (d, J = 9.5 Hz, 8H) ppm. ^{13}C NMR (75.6 MHz, CDCl$_3$): δ 181.8 (C), 151.5 (C), 101.3 (CH), 52.4 (CH$_2$), 27.7 (CH$_2$), 26.8 (CH$_2$) ppm. MS: Calc. [C$_{18}$H$_{26}$N$_2$O$_2$+H]$^+$: 303.20670, found 303.20618. Calc. [C$_{18}$H$_{26}$N$_2$O$_2$+Na] $^+$: 325.18865, found 325.18802.
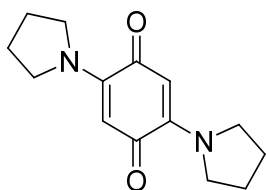
2,5-Di(pyrrolidin-1-yl)cyclohexa-2,5-diene-1,4-dione (**3d),** glittery red crystals, m.p.: 244 – 246 °C (238 - 240 °C)[13], yield: 80**%.** ^{1}H NMR (300 MHz, CDCl$_3$): δ 5.28 (s, 2H), 3.64 (br s, 8H), 1.91 (m, 8H) ppm. ^{13}C NMR (75.6 MHz, CDCl$_3$): δ 180.6 (C), 149.8 (C), 100.0 (CH), 50.9 (CH$_2$), 25.3 (CH$_2$) ppm. MS: Calc. [C$_{14}$H$_{18}$N$_2$O$_2$+H]$^+$: 247.14410, found 247.14371. Calc [C$_{14}$H$_{18}$N$_2$O$_2$+Na]$^+$: 269.12605, found 269.12552.
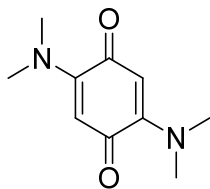
2,5-Bis(dimethylamino)cyclohexa-2,5-diene-1,4-dione (**3e),** dark-red solid, m.p.: 156.6 °C (171-172 °C)[21], yield**:** 86%: ^{1}H NMR (300 MHz, CDCl$_3$): δ 5.30 (s, 2H), 3.14 (s, 12 H) ppm. ^{13}C NMR (75.6 f   MHz, CDCl$_3$): δ 181.7 (C), 152.3 (C), 102.2 (CH), 42.5 (CH$_3$) ppm.   MS: Calc. [C$_{10}$H$_{14}$N$_2$O$_2$+H]$^+$:195.11280, found 195.11279. Calc . [C$_{10}$H$_{14}$N$_2$O$_2$+Na]$^+$: 217.09475, found 217.09454.
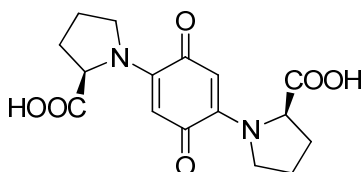
L-**2,5-Diprolincyclohexa-2,5-diene-1,4-dione (3f),** brick-red solid, m.p.: 385 °C dec, yield 65%. ^{1}H NMR (300 MHz, D$_2$O): δ 5.20 (s, 2H), 4.74 (br s, 2H), 3.47 (br s, 4H), 218 – 1.78 (m, 8H) ppm. ^{13}C NMR (75.6 MHz, D$_2$O): δ 180.2 (C), 180.0 (C), 151.2 (C), 99.7 (CH), 66.5 (CH), 52.3 (CH$_2$), 32.0 (CH$_2$), 22.0 (CH$_2$) ppm. MS: Calc. [C$_{16}$H$_{18}$N$_2$O$_6$+H]$^+$: 335.12376, found 335.12326. Calc. [C$_{16}$H$_{18}$N$_2$O$_6$+Na]$^+$: 357.10571, found 357.10504.
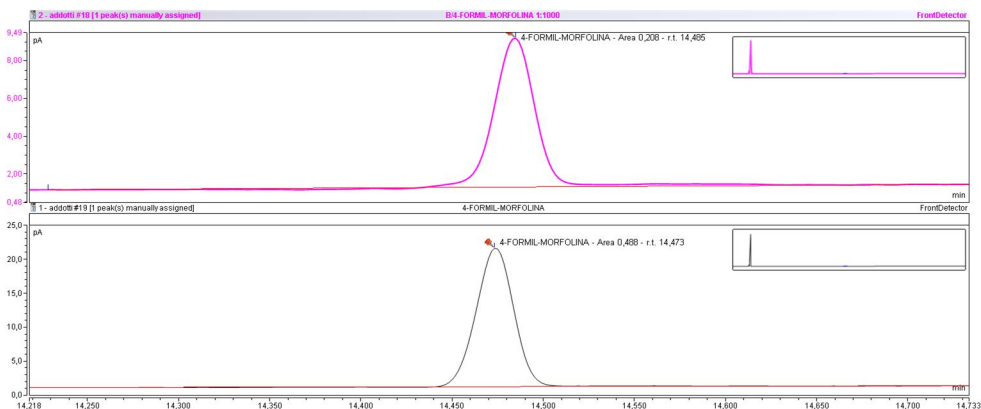
Figure 4.3: Top: GC trace of the reaction mixture vanillin – morpholine. Bottom, GC trace of standard *N*-formylmorpholine (TCI Europe F0157)
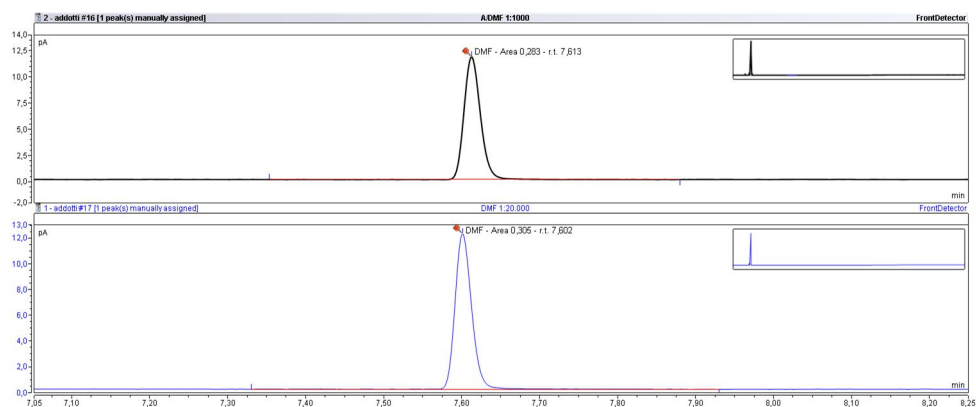
Figure 4.4: Top: GC trace of the reaction mixture vanillin – dimethylamine. Bottom, GC trace of standard *N,N*-dimethylformamide (Carlo Erba reagents 444923).

MTT assays
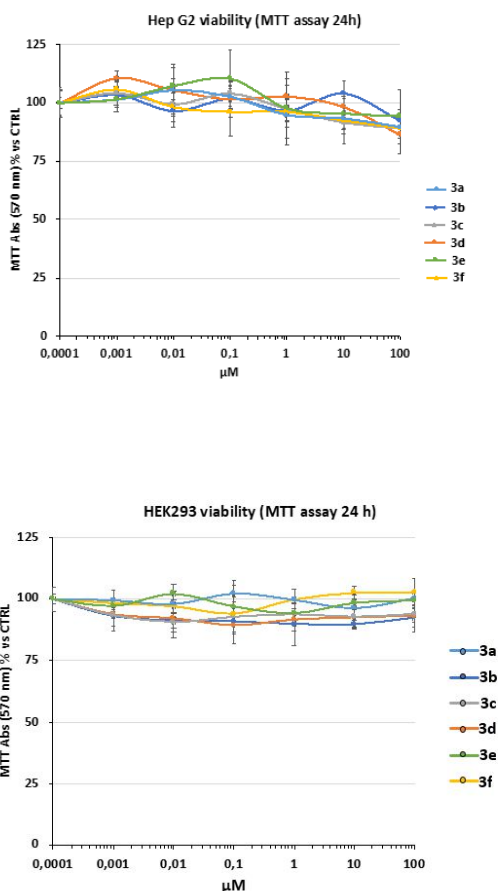
Figure 4.5: MTT cytotoxicity tests. Dose-response curves of Hep G2 (top) and HEK293 (bottom) human cell lines treated with increasing concentrations of each compound (1 nM – 100 µM). Results are expressed as percent reduction *vs* vehicle- (DMEM or 0.1% DMSO) treated cells. Values are means from three independent experiments ± S.D.M.

4.4. References

1. Banerjee, G.; Chattopadhyay, P. Vanillin Biotechnology: The Perspectives and Future. *J. Sci. Food Agric.* **2019**, *99* (2), 499–506. https://doi.org/10.1002/jsfa.9303.

2. Liu, B.; Cheng, L.; Hu, P.; Xu, F.; Li, D.; Gu, W.-J.; Han, W. Iron-Catalyzed Oxidative C–C(Vinyl) σ-Bond Cleavage of Allylarenes to Aryl Aldehydes at Room Temperature with Ambient Air. *Chem. Commun.* **2019**, *55* (33), 4817–4820. https://doi.org/10.1039/C9CC01995B.

3. Taber, D. F.; Patel, S.; Hambleton, T. M.; Winkel, E. E. Vanillin Synthesis from 4-Hydroxybenzaldehyde. *J. Chem. Educ.* **2007**, *84* (7), 1158. https://doi.org/10.1021/ed084p1158.

4. Kaur, B.; Chakraborty, D. Biotechnological and Molecular Approaches for Vanillin Production: A Review. *Appl. Biochem. Biotechnol.* **2013**, *169* (4), 1353–1372. https://doi.org/10.1007/s12010-012-0066-1.

5. Chattopadhyay, P.; Banerjee, G.; Sen, S. K. Cleaner Production of Vanillin through Biotransformation of Ferulic Acid Esters from Agroresidue by Streptomyces Sannanensis. *J. Clean. Prod.* **2018**, *182*, 272–279. https://doi.org/10.1016/j.jclepro.2018.02.043.

6. Gallage, N. J.; Møller, B. L. Vanillin–Bioconversion and Bioengineering of the Most Popular Plant Flavor and Its De Novo Biosynthesis in the Vanilla Orchid. *Mol. Plant* **2015**, *8* (1), 40–57. https://doi.org/10.1016/j.molp.2014.11.008.

7. Rupasinghe, H. P. V.; Boulter-Bitzer, J.; Ahn, T.; Odumeru, J. A. Vanillin Inhibits Pathogenic and Spoilage Microorganisms in Vitro and Aerobic Microbial Growth in Fresh-Cut Apples. *Food Res. Int.* **2006**, *39* (5), 575–580. https://doi.org/10.1016/j.foodres.2005.11.005.

8. Tai, A.; Sawano, T.; Yazama, F.; Ito, H. Evaluation of Antioxidant Activity of Vanillin by Using Multiple Antioxidant Assays. *Biochim. Biophys. Acta BBA - Gen. Subj.* **2011**, *1810* (2), 170–177. https://doi.org/10.1016/j.bbagen.2010.11.004.

9. Ho, K.; Yazan, L. S.; Ismail, N.; Ismail, M. Apoptosis and Cell Cycle Arrest of Human Colourectal Cancer Cell Line HT-29 Induced by Vanillin. *Cancer Epidemiol.* **2009**, *33* (2), 155–160. https://doi.org/10.1016/j.canep.2009.06.003.

10. Sasaki, YūF.; Ohta, T.; Imanishi, H.; Watanabe, M.; Matsumoto, K.; Kato, T.; Shirasu, Y. Suppressing Effects of Vanillin, Cinnamaldehyde, and Anisaldehyde on Chromosome Aberrations Induced by X-Rays in Mice. *Mutat. Res. Lett.* **1990**, *243* (4), 299–302. https://doi.org/10.1016/0165-7992(90)90146-B.

11. Chen, X.; Wei, M.; Zhang, H.; Luo, C.; Chen, Y.; Chen, Y. Effect of Vanillin and Ethyl Vanillin on Cytochrome P450 Activity in Vitro and in Vivo. *Food Chem. Toxicol.* **2012**, *50* (6), 1897–1901. https://doi.org/10.1016/j.fct.2012.03.060.

12. Giani, A. M. A JOURNEY THROUGH THE CHEMISTRY OF DIAGNOSTIC IMAGING PROBES. 121.

13. Marxer, A. Über 2,5-Bisäthylenimino-Hydrochinon, Eine Carcinostatisch Wirksame Verbindung. *Helv. Chim. Acta* **1955**, *38* (6), 1473–1489. https://doi.org/10.1002/hlca.19550380620.

14. Ukhin, L. Yu.; Belousova, L. V.; Orlova, Zh. I.; Shishkina, S. V.; Shishkin, O. V. Reactions of Nitrogenous Derivatives of Substituted Salicylaldehydes with Cyclic Ketones and Enamines. *Russ. Chem. Bull.* **2002**, *51* (7), 1262–1269. https://doi.org/10.1023/A:1020956614588.

15. Gazizov, M. B.; Ismagilov, R. K.; Shamsutdinova, L. P.; Karimova, R. F.; Sinyashin, O. G. Reactions of 4-Hydroxy-3,5-Di-Tert-Butylbenzylidene Chloride with Aminals. *Russ. J. Gen. Chem.* **2006**, *76* (7), 1176–1177. https://doi.org/10.1134/S1070363206070322.

16. Tiwari, B.; Zhang, J.; Chi, Y. R. Facile Access to Chiral Ketones through Metal-Free Oxidative C-C Bond Cleavage of Aldehydes by O_2. *Angew. Chem. Int. Ed.* **2012**, *51* (8), 1911–1914. https://doi.org/10.1002/anie.201107473.

17. Malhotra, S. K.; Hostynek, J. J.; Lundin, A. F. Autoxidation of Enamines and Schiff Bases of alpha-beta Unsaturated Ketones. A New Synthesis of Unsaturated 1,4-Diones. *J. Am. Chem. Soc.* **1968**, *90* (23), 6565–6566. https://doi.org/10.1021/ja01025a086.

18. Vacher, M.; Fdez. Galván, I.; Ding, B.-W.; Schramm, S.; Berraud-Pache, R.; Naumov, P.; Ferré, N.; Liu, Y.-J.; Navizet, I.; Roca-Sanjuán, D.; et al. Chemi- and Bioluminescence of Cyclic Peroxides. *Chem. Rev.* **2018**, *118* (15), 6927–6974. https://doi.org/10.1021/acs.chemrev.7b00649.

19. Harger, R. N. THE OXIDATION OF HYDROQUINONE IN THE PRESENCE OF ALIPHATIC AMINES. FORMATION OF BIS(ALKYLAMINO) QUINONES. J. Am. Chem. Soc. 1924, 46 (11), 2540–2551. https://doi.org/10.1021/ja01676a027.

20. Córdoba-Pedregosa, M. C. D.; Villalba, J. M.; González-Aragón, D.; Bello, R. I.; Alcaín, F. J. Cellular Density and Cell Type Are the Key Factors in Growth Inhibition Induced by 2,5Bis [1-Aziridinyl]-1,4 Benzoquinone (DZQ). *Anticancer Res.* **2006**, *26* (5A), 3535–3540.

21. Golabi, S. M.; Nourmohammadi, F.; Saadnia, A. Electrosynthesis of Organic Compounds.: Part II: Electrooxidative Amination of 1,4-

Dihydroxybenzene Using Some Aliphatic Amines. *J. Electroanal. Chem.* **2003**, *548*, 41–47. https://doi.org/10.1016/S0022-0728(03)00218-3.

Chapter 5: Approaches to heterogenised DMAP

5.1. Introduction

Catalysts play a central role during reactions, decreasing the activation energy barrier of the reagents and leading to the desired products easier and faster than for un-catalysed reactions. These goals are very important aspects for industries continuously involved in the development of new processes related to decrease of production costs.

Catalysis in chemistry may be divided in:

- Homogeneous catalysis
- Heterogeneous catalysis

Homogeneous catalysis involves the presence of organic or inorganic catalysts in the same phase of the reagents, generally represented by the liquid phase. On the other hand, heterogeneous catalysis involves the use of a catalyst linked to an inorganic and inert support; the catalyst and the reagents are then in two distinct different phases.

Heterogeneous catalysis offers different advantages over homogeneous catalysis, among them an easy workup facilitated by the straightforward separation of the catalyst from the reaction mixture.

Different inorganic supports are used depending on their specific properties like surface area, chemical stability and pore size.

The principal materials used as supports in catalysis are:

- alumina (aluminium oxide, in its different versions)
- silica (hydrated silicon dioxide), characterized by weakly Brønsted acidity
- zeolites, aluminosilicates characterized by well-defined pore sizes[1] and tunable Brønsted acidity. Zeolites can be modified to

aluminophosphates, silicoaluminophosphates (SAPO) or MCM-type (mesoporous support)

- MOFs (Metal-Organic-Frameworks) three-dimensional networks of metals bound to bi/tridentate-organic molecules

- Organic polymers and copolymers as polystyrene/divinylbenzene, cellulose, etc.

Heterogenising a catalyst is a common strategy to transfer a well-established activity showed by a homogeneous catalyst in heterogeneous phase catalysis. Nevertheless, heterogenisation of a homogeneous catalyst is not straightforward, as it requires to bind the catalyst (generally an organic species or a metal complex) to the inorganic support through a suitable linker (Figure 5.1).

Figure 5.1: General scheme of heterogenisation of a catalyst

The catalyst has to be endowed with a functional group, whose role is to react with the linker, usually represented by a homo- or hetero-bifunctional molecule of a predefined length. The functional group should be implanted in a remote position with respect to the catalytically active site, so to reduce any possible interference with it, and should present and orthogonal reactivity with the functional group(s) of the active site, to avoid the mutual deactivation.

During the PhD project we focused our attention on a well-known catalyst, *i.e.*: 4-(*N,N*-dimethylamino)pyridine **1** (DMAP).

DMAP is an organic compound widely used as nucleophilic catalyst in different types of organic reactions. This pyridine derivative shows a greater nucleophilicity than the parent heterocycle due to the resonance of the azine ring with the dimethylamino substituent (Figure 5.2):
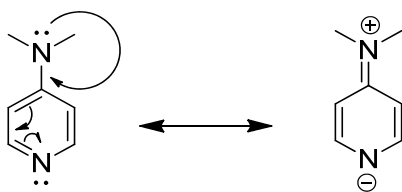
Figure 5.2: Resonance of DMAP, **1**

Examples of reactions accelerated by DMAP include the acylation of tertiary or generally hindered alcohols, DCC-mediated esterification and amidation of carboxylic acid[2] and silylation of alcohols and so on, all of them extremely important for the preparation of APIs and many other chemicals.

Nevertheless, the structure of DMAP does not offer any possibility for its direct binding to an inorganic support and we decided to explore the possibility to introduce a reactive functional group on this important catalyst as a viaticum to its heterogenisation.

A literature search pointed out the paucity of direct functionalisation of DMAP, limited to the direct bromination using NBS[3] or direct formylation promoted by litium salt[4].

The pyridine ring of DMAP is well known to be scarcely reactive towards electrophilic aromatic substitution, due to the electron withdrawing effect of the endocyclic nitrogen atom. The dimethylamino- substituent improves

somewhat the situation, pumping electron density in the ring through the mesomeric effect, overcoming the opposite inductive effect. In principle, it is possible to perform electrophilic aromatic substitutions, provided that the electrophile has a marked reactivity.

In Chapter 3 we demonstrated the superelectrophilic character of the diacylminium ion generated in the Tscherniac-Einhorn reaction. We envisaged the possibility to take advantage of this remarkable reactivity to introduce a functionality on DMAP that could be really suitable for our original purpose.

We applied the Tscherniac-Einhorn to DMAP using *N*-hydroxymethyl-phthalimide as the amidoalkylating agent. As *N*-hydroxymethylphthalimide can be generated *in situ* by the reaction of phthalimide (**2**) and paraformaldehyde, we developed a one-pot procedure involving DMAP, phthalimide and paraformaldehyde, reacting in concentrated sulfuric acid at 70°C (Scheme 5.1).
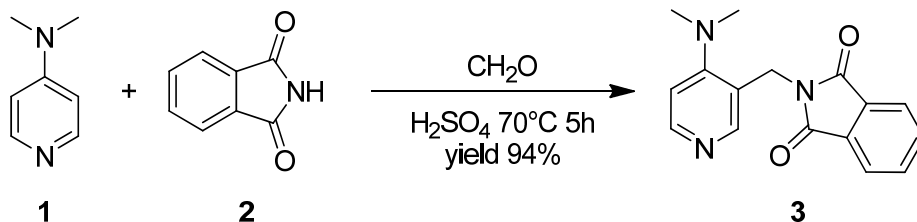
Scheme 5.1: Synthesis of DMAP derivative

To our delight, the conversion of DMAP to a single product was completed in 5 h. Standard workup of the homogeneous reaction mixture lead to the isolation of a the analytically pure 3-monophthalimidoalkylated product (**3**) in 94% yield.

The phthalimide group was removed using hydrazine hydrate in refluxing ethanol for 4 h, giving after workup 3-(aminomethyl)-*N,N*-dimethylpyridin-4-amine (**4**) in 74% yield (Figure 5.4).
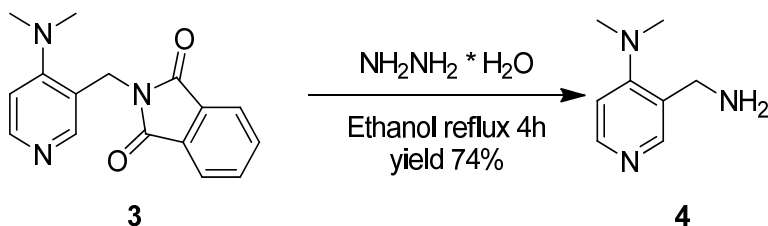
Scheme 5.4: Hydrolysis of the phthalimide group

The structure of compound **4** exemplifies our goal: a DMAP bearing a single reactive functional group (primary aliphatic amine), in a relatively remote position with respect to the active site (the catalytically active site is the anular nitrogen atom and in this derivative the ortho (2,6) positions are kept free).

We exploited these properties by reacting DMAP with triethoxysilylpropyl isocyanate **5** (Scheme 5.2), the latter playing the role of the linker and showing a reactive tail represented by the trialkoxysilyl group, routinely employed for the grafting to hydroxyl-rich material surfaces such as silica and derivatives thereof.

Scheme 5.2: Grafting reaction between modified DMAP compound **4** and isocyanate derivative **5**

5.2. Conclusion

In this chapter we reported the successful design and synthesis of a functionalised derivative of the important catalyst DMAP, *i.e.*: 3-aminomethyl-4-(*N,N*-dimethylamino)pyridine. The additional functional group has been exploited for the preparation of a silylated derivative, useful for grafting DMAP to an heterogenous inorganic support. The preparation of the functionalised DMAP was accomplished in two steps taking advantage of the strong electrophile involved in the Tscherniac-Einhorn reaction. The desired product is obtained in high yields and avoiding chromatographic separations, optimal prerequisites for a future large-scale preparation.

Future development of this work will deal with the grafting of the functionalised DMAP to silica-based inorganic supports for the preparation of organic-inorganic hybrid catalysts and with the evaluation of their propertied in heterogeneously catalysed acylation reactions.

5.3. Experimental Section

Solvents and reagents. Commercially available solvents and reagents were used without further purification. When needed, the reactions were performed under positive pressure of nitrogen.

NMR spectra were recorded using a JEOL ECP 300 MHz spectrometer. All NMR spectra were registered at 298 K. Chemical shifts (δ) are quoted to parts per million referenced to the residual solvent peak. The multiplicity of each signals is designated using the following abbreviations: s, singlet; d, doublet; t, triplet, q, quartet; quint, quintet; sext, sextet; sept, septet; m, multiplet, br s, broad singolet; br m, broad multiplet. Coupling constants (*J*) are reported in Hertz (Hz). Mass spectra were obtained with a TSQ Quantum Access Max Triple Quadrupole Mass Spectrometer (Thermo Scientific) equipped with an electrospray ionization (ESI) source; analysis by direct infusion.

4-Dimethylamino-3-phthalimidomethylpyridine (3)
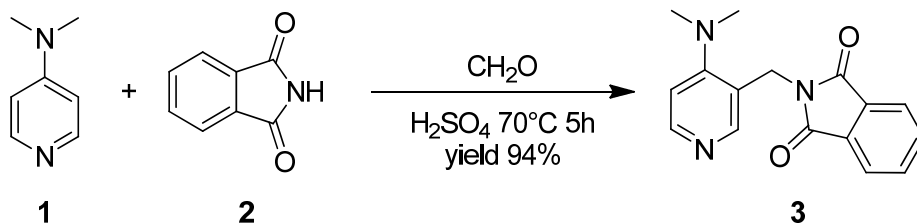
In a round bottomed flask, conc. sulphuric acid (80 mL) was added and cooled to 0 °C with an ice/water bath. DMAP, **1** (15.0 g, 0.123 mol, 1.00 eq) was added in small portions. Phthalimide, **2** (21.70 g, 0.147 mol, 1.20 eq) and paraformaldehyde (5.53 g, 0.184 mol, 1.50 eq) were added and the mixture was heated at 70 °C for 5 hours. After complete conversion (TLC: DCM/ MeOH: conc. NH_4OH 92/8/0.2), the mixture was cautiously poured in cold water and slowly basified to pH = 10 with Na_2CO_3. A white solid is formed and removed by filtration under *vacuum,* washed with distilled water and dried in air to constant weight (yield 94%).

[1]H (300 MHz, $CDCl_3$): δ 8.24 (d, J= 5.5 Hz, 1H), 8.11 (s, 1H), 7.80 (m, 2H), 7.68 (m, 2H), 6.77 (d, J= 5.7 Hz, 1H), 4.87 (s, 2H), 2.81 (s, 6H) ppm.

[13]C-APT (75 MHz, $CDCl_3$): δ 168.1, 158.3, 149.5, 149.0, 134.4, 132.0, 123.5, 123.2, 112.5, 43.5, 36.4 ppm.

Calculated mass: $C_{16}H_{15}N_3O_2$: 281.31, found: 282.54. Calculated mass: $C_{16}H_{15}N_3O_2Na^+$: 304.29, found: 304.34.

3-(Aminomethyl)-4-(*N,N*-dimethylamino)pyridine (4)
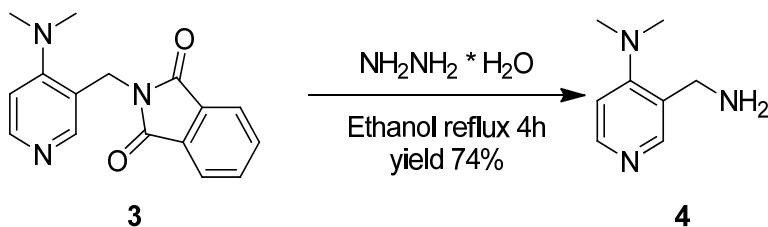
In a 2 necked 500 mL round bottomed flask, compound **3** (30.0 g, 0.107 mol, 1.00 eq) was suspended in ethanol (250 mL). Hydrazine hydrate (6.66 mL, 0.149 mol, 1.4 eq) was added and the mixture was heated to reflux for 4 hours. After complete hydrazinolysis (TLC: DCM/MeOH/conc. NH_4OH 92/8/0.2), the mixture was cooled to room temperature using an ice/water bath and the precipitate was filtered off and the mother liquors discarded. The solid was dissolved in 120 mL of warm NaOH 30% and extracted with toluene (6x50 mL). The organic extracts were dried on sodium carbonate, filtered and concentrated under vacuum to give the product ad a yellow oil (yield 74%).

^1H (300 MHz, $CDCl_3$): δ 8.04 (s, 1H), 7.95 (d, J= 5.2 Hz, 1H), 6.42 (d, J= 5.2 Hz, 1H), 3.58 (s, 2H), 2.53 (s, 6H) ppm.

^{13}C-APT (75 MHz, $CDCl_3$): δ 157.0, 150.0, 148.3, 128.0, 111.2, 42.2, 41.4 ppm.

Calculated mass: $C_8H_{13}N_3$: 151.21, found: 152.30. Calculated mass: $C_8H_{13}N_3Na^+$: 174.20, found: 174.26.

1-((4-(Dimethylamino)pyridin-3-yl)methyl)-3-(3-(triethoxysilyl)propyl)urea (6)
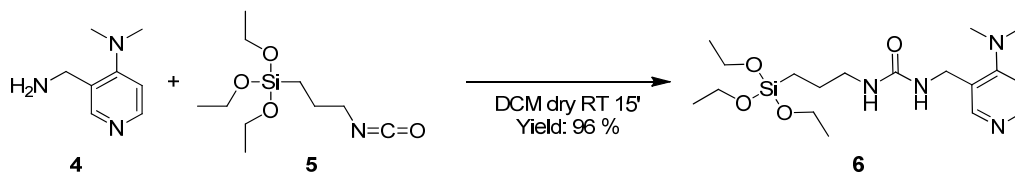
In a round bottomed flask, 3-(aminomethyl)-4-(*N,N*-dimethylamino)pyridine **4** (1.00 g, 0.0066 mol, 1.00 eq) was dissolved under nitrogen atmosphere in dry DCM (10 mL). Triethoxysilylpropyl isocyanate **5** (1.72 g, 0.0069 mol, 1.00 eq) was added in one portion. The resulting solution was kept at room temperature and, after 15 minutes, TLC analysis (DCM/ MeOH 8/2) showed complete conversion. The reaction mixture was concentrated under vacuum to give the product as a white solid (yield 96%).

[1]H (300 MHz, CDCl$_3$): δ 8.20 (s, 1H), 8.11 (d, J= 5.5 Hz, 1H), 6.61 (d, J= 5.5 Hz, 1H), 5.67 (bs, 1 NH), 5.60 (bs, 1H), 4.31 (d, J= 5.2 Hz, 2H), 3.71 (q, 6H), 3.09 (q, J= 7.0 Hz, 2H), 2.74 (s, 6H), 1.50 (q, J= 7.7 Hz, 2H), 1.12 (t, J= 7.0 Hz, 9H), 0.54 (t, J= 8.2 Hz, 2H) ppm

[13]C-APT (75 MHz, CDCl$_3$): δ 158.7, 157.8, 150.3, 148.8, 125.1, 111.7, 54.4, 42.9, 42.8, 39.6, 23.7, 18.3, 7.7 ppm

Calculated mass: C$_{18}$H$_{34}$N$_4$O$_4$Si: 398.57, found: 399.23.

5.4. References

1. Deutschmann, O.; Knözinger, H.; Kochloefl, K.; Turek, T. Heterogeneous Catalysis and Solid Catalysts, 2. Development and Types of Solid Catalysts. In *Ullmann's Encyclopedia of Industrial Chemistry*; Wiley-VCH Verlag GmbH & Co. KGaA, Ed.; Wiley-VCH Verlag GmbH & Co. KGaA: Weinheim, Germany, 2011. https://doi.org/10.1002/14356007.o05_o02.

2. Neises, B.; Steglich, W. Simple Method for the Esterification of Carboxylic Acids https://doi.org/10.1002/anie.197805221.

3. Shi, Y.; Ke, Z.; Yeung, Y.-Y. Environmentally Benign Indole-Catalyzed Position-Selective Halogenation of Thioarenes and Other Aromatics. *Green Chem.* **2018**, *20* (19), 4448–4452. https://doi.org/10.1039/C8GC02415D.

4. Gros, P. C. Trimethylsilylmethyllithium–Lithium Dimethylaminoethoxide. In *Encyclopedia of Reagents for Organic Synthesis*; American Cancer Society, 2009. https://doi.org/10.1002/047084289X.rn01093.

Chapter 6: Synthesis and Characterization of Gepirone Hydrochloride

6.1. Introduction

Major Depressive Disorder (MDD) is a complex mental disease characterized by loss of interest, esteem, low energy, anxiety and irritability and other symptoms. This pathology is the third global disease affecting more than 350 million people worldwide each year and negatively conditioning their normal life.[1]

The causes of MDD is yet unknown although some hypothesis are raised on the genesis of the pathology, such for example dietary programs, stress, drug abuse, genetic factors and childhood abuse.[2] This pathology is serious because it can lead to death by suicide. The onset of this disease arises at 25 years old to reach the maximum level at 40s and women are more susceptible to MDD than men, generally. There is never a complete regression of this pathology, and after many years, second or more episodes of depression may occur.

The mental equilibrium is finely regulated by different substances called neurotransmitters. In particular, monoaminergic neurotransmitters as serotonin, norepinephrine, dopamine and adrenaline play a central role in this regulation, leading to the hypothesis of the monoaminergic deficit for the onset of this disease. It has been demonstrated that increasing the monoaminergic level inside the central nervous system (CNS) decreases the symptoms associated to MDD. On the base of this theory, different drugs were developed with the aims to increase the basal level of these monoaminergic neurotransmitter.

The most important APIs developed are drugs which act as inhibitor of monoaminergic re-uptake pathway. In particular, three different inhibitors were developed[3]:

- SSRIs (selective serotonin re-uptake inhibitors) act on transporters devoted to the re-uptake of serotonin neurotransmitter (SERT). This class includes drugs such as fluoxetine, paroxetine, citalopram and many others.

- SNaRIs (serotonin-nonepinephrine re-uptake inhibitors) act on two transporters devoted to the re-uptake of serotonin and norepinephrine neurotransmitter (SERT and NET). At this class belong drugs such as duloxetine and venlafaxine.

- NRIs (selective nonepinephrine re-uptake inhibitors) act on transporters devoted the re-uptake of norepinephrine neurotransmitter (NET). At this class belong drugs such as viloxazine.

Tricyclic antidepressants (TCA) such as amitriptyline and imipramine can be used for the treatment of MDD, too. These APIs molecules are unselective antagonists of the serotonin receptor, the muscarinic receptor and the histamine receptors, leading to several and serious side effect. For this reason, TCAs have been displaced by SSRIs and SNaRIs due to their better safety profile[2].

Alternative therapies target monoamine oxidases (MAO-A and MAO-B), enzymes involved in oxidative deamination of monoaminergic neurotransmitters. These enzymes are probably involved in other neurodegenerative pathologies as the Parkinson disease and the Lewy

body dementia[4]. To this class belongs drugs like selegiline, moclobemide and iproniazid.

Another important family of APIs used for the treatment of depression is that of the azapirones. These molecules act as partial agonists of postsynaptic 5-HT$_{1A}$ receptors, increasing the concentration/level of serotonin[4]. Generally, these types of drugs are used as add-on[5] for the MDD patients with inadequate response to one of the previously described classes. The main representatives of this family are gepirone (**1**), buspirone (**2**), and tandospirone(**3**)[6,7] (Figure 6.1).

1
Gepirone

2
Buspirone

3
Tandospirone
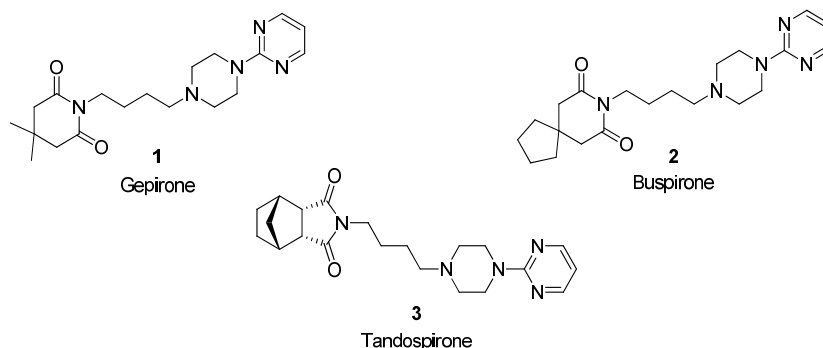
Figure 6.1: The family of azapirones

Azapirones share three common structural features:
- the 2-(1-piperazinyl)pyrimidine double ring system;
- a 4-carbon chain (*n*-butyl) acting as a linker
- a 5- or 6-membered cyclic or bicyclic imide

Although the scientific literature lists several papers and patent on the synthesis and bioactivity of these molecules, scarce information is available for the solid-state properties of the azapirone family, with only a single crystal diffractometric analysis reported for buspirone.

6.2. Discussion and Results

During the PhD, we focused our attention on gepirone with the aim to characterise the crystal forms of this API and to investigate the eventual presence of additional polymorphs. The solid state behaviour of gepirone hydrochloride is mentioned in a single article by Behme et al.[8] In detail, they reported the evidence of three distinct polymorphs named: form I, form II and form III. DSC analysis revealed that form I has melting point at 180 °C, form II 212 °C and form III 200 °C. As the study is based on thermal analysis only, no structural data is reported in this manuscript for the three claimed polymorphs.

In order to confirm or integrate the information on the polymorph of gepirone hydrochloride and to extract the structural parameters of all its solid-state forms, we undertook a comprehensive study on this API.

The investigation of additional polymorphs was focused on free base, too. The study of free base is important for the sake of comparison with the hydrochloride form, in order to gain information on the microscopic protonation site and the conformational changes determined by this process.

Several attempts were made, employing different solvents for the crystallization of gepirone free base and the hydrochloride form.

Gepirone free base was crystallised using solvents such as:

- MIBK (Methyl Isobutyl Ketone)
- 2-Propanol
- Toluene
- *n*-Heptane
- Acetonitrile

Gepirone free base crystallizes in the monoclinic P2$_1$/c space group, with one molecule in general position (Figure 6.2). The conformation of the molecule is quite planar, mainly due to the fully extended chain conformation of the butyl C$_4$ spacer. Only one weak inter-molecular interactions may be found and it is of the type C-H···N between a methylene group of the glutarimide portion and the nitrogen atom of the piperazine ring linked to the butyl chain (H-bond distance is 3.592 Å). The piperazine ring is found to be in the chair conformation. Conformation of the whole molecule, and crystallographic details (*i.e.*: space group, unit cell volume) are found to be quite similar to the ones reported in the literature for buspirone free base[9].
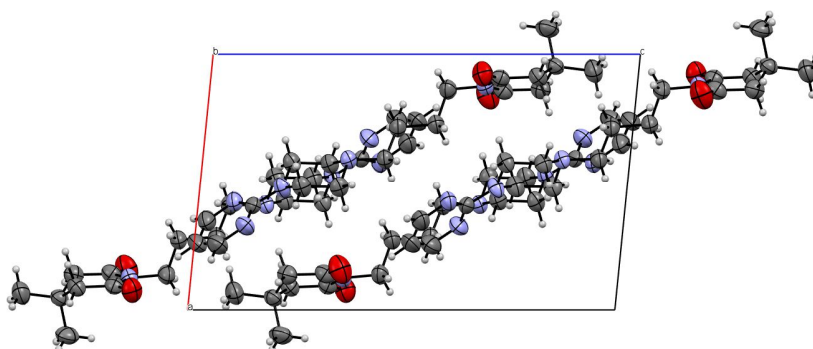
Figure 6.2: Crystal packing of gepirone free base viewed down to the [010] crystallographic direction. Colour code: N, blue; O, red; C, gray; H, white. Ellipsoids are depicted at the 50% probability level.
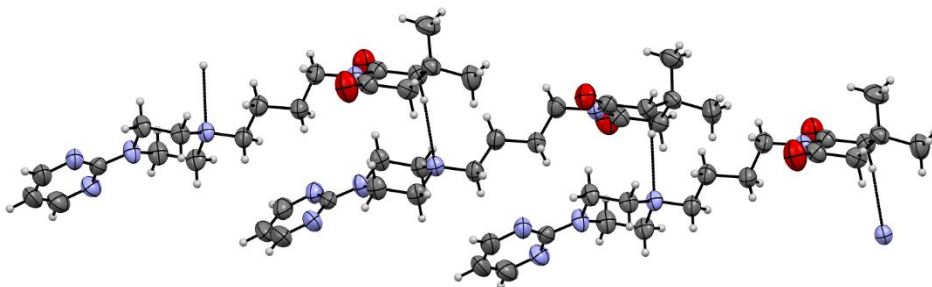
Figure 6.3. Depiction of the weak interactions of the type C-H…N between gepirone molecules in the crystal lattice. Colour code: N, blue; O, red; C, gray; H, white. Ellipsoids are depicted at the 50% probability level.

The thermal behavior of gepirone free base was elucidated by means of Differential Scanning Calorimetry (DSC) and *in situ* variable-temperature X-ray diffraction analysis. The DSC curve shows that there are no other thermal events other than the melting of the form at about 110 °C. Gepirone free base appears to be stable up to 350°C (figure 6.4).
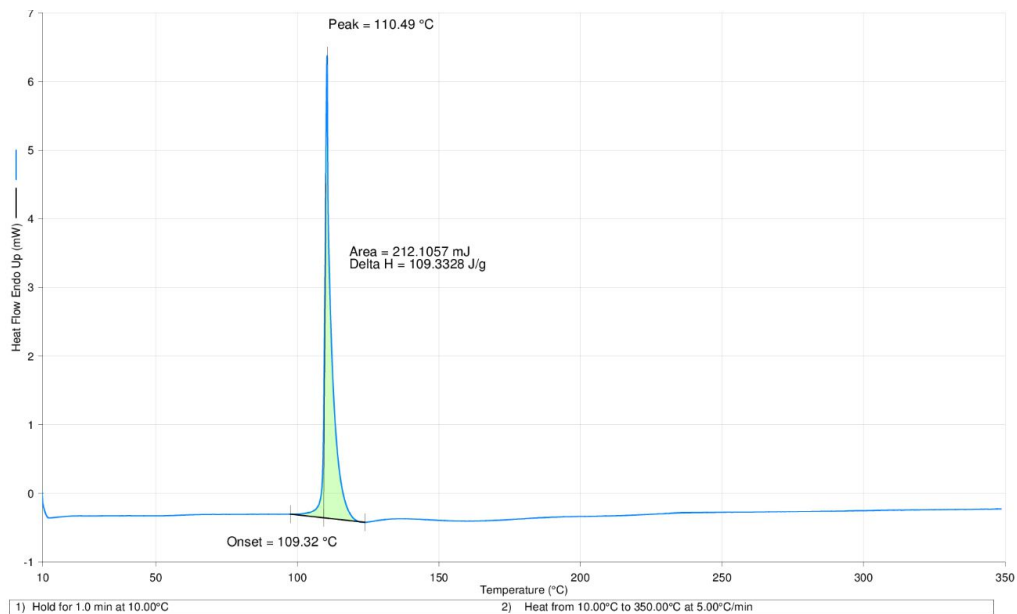
Figure 6.4: DSC analysis of gepirone free base

Gepirone free base was further analysed by variable temperature XRD analysis (Figure. 6.5). Data were collected up to amorphization of the sample. While rising the temperature an effect of induced preferential orientation is observed, with the reflection at about 2θ 18.5 ° that becomes sharper. This is probably due to fusion-recrystallization of small crystallites on the sample holder. No other phenomena are observed, in agreement with the DSC curve.
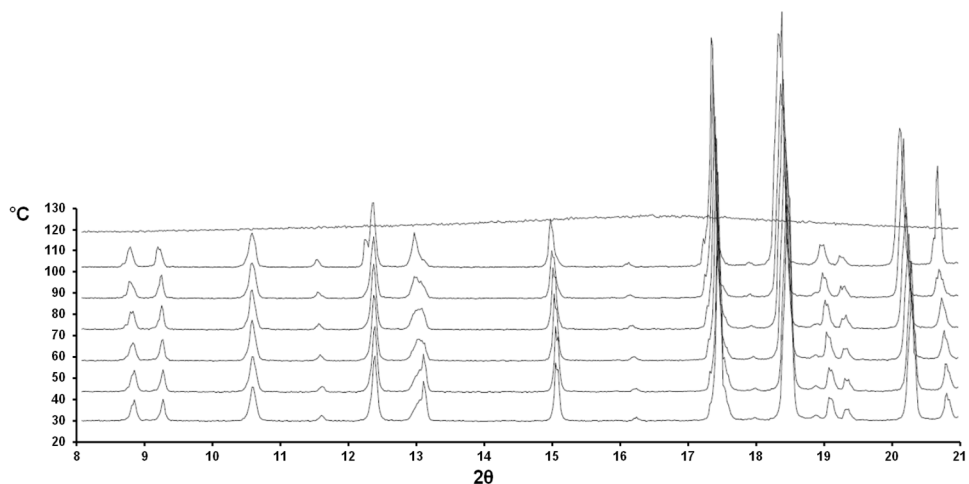
Figure 6.5: Variable-temperature XRPD analysis of gepirone free base.

The study of gepirone hydrochloride started with an acquisition of the DSC curve (Figure 6.6), in order to confirm the behaviour observed by Behme[8] for our samples of this API or possibly to highlight eventual differences.
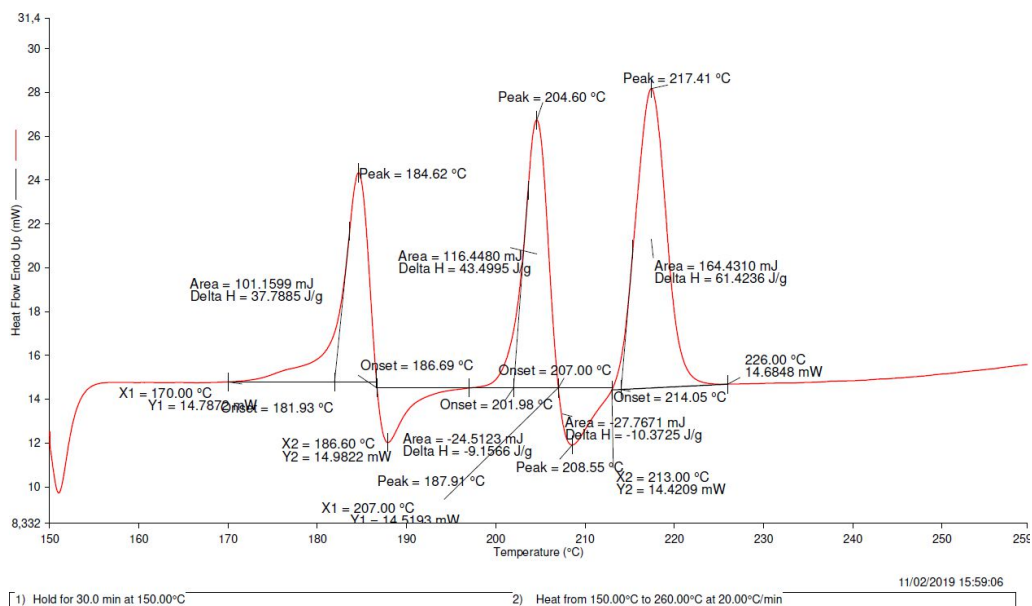
Figure 6.6: DSC analysis of gepirone hydrochloride.

The DSC analysis of our sample of gepirone hydrochloride paralleled the curve reported by Behme[8], with the clear evidence three thermal events attributable to three crystal forms: form I, form III and form II, respectively. Crystals of gepirone hydrochloride (Form I) suitable for single crystal X-ray diffraction were obtained heating gepirone hydrochloride in acetonitrile until dissolution. The clear solution was kept at 22-25 °C until the formation of the crystals. The analysis of these crystals revealed that gepirone hydrochloride form I belongs to the monoclinic $P2_1/c$ space group with one molecule in general position (Figure 6.7).
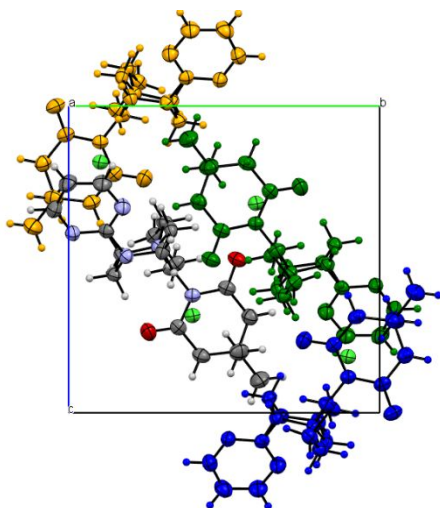

Figure 6.7: Crystal packing for gepirone hydrochloride form I viewed down to the [100] direction. Colour code: Cl, green; N, blue; O, red; C, gray; H, white. Ellipsoids are depicted at the 50% probability level. Three of the four molecules in the unit cell have been coloured for helping the reader in the visualization of the structure.

Gepirone hydrochloride presents the (HCl) acid proton bonded to a nitrogen atom of the piperazine ring. As expected, the protonation electron lone pair takes place on the piperazine nitrogen atom linked to the aliphatic

butyl chain. The opposite nitrogen atom, linked to the pyrimidine ring, has its lone pair involved in the resonance with the heteroaromatic ring, thus strongly reducing its basicity.

Moreover, the overall molecular conformation of gepirone hydrochloride is quite different from that observed for the free base. Figure 6.8 clearly shows the effect of the protonation in Form I, that may be summarized in the loss of the extended chain conformation of the butyl chain spacer, the latter "wrapping" around the chlorine atom in this form.
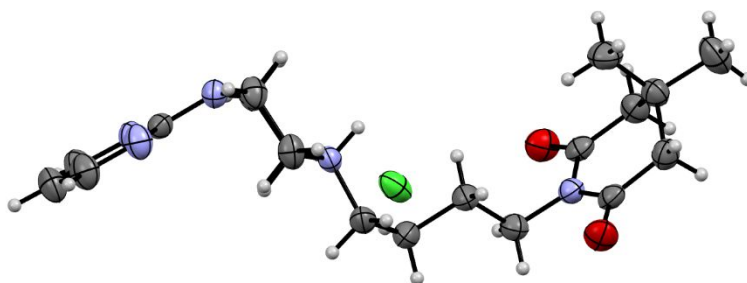
Figure 6.8: Depiction of the asymmetric unit for Gepirone HCl form I to highlight the conformation of the molecule. Colour code: Cl, green; N, blue; O, red; C, gray; H, white. Ellipsoids are depicted at the 50% probability level.

The chlorine atom is the centre of several interactions, among them the hydrogen bond N-H⋯Cl with the protonated nitrogen atom of the and additional short contacts with hydrogen atoms of methylene groups of the butyl chain and of the piperazine ring.

While performing the *in situ* variable temperature X-ray powder diffraction experiment, after the melting of form I, we were able to observe the recrystallization of the sample in small crystals, which were found to be of a quality suitable to perform a single crystal XRD analysis. This allowed us to retrieve the crystal structure information for the second polymorph of gepirone HCl, which as later recognized as form II previously claimed by Behme[8] with no associated structural data.

The form II of gepirone hydrochloride crystallizes in the $P2_12_12_1$ orthorhombic space group, still with one molecule in general position (Figure 6.9).
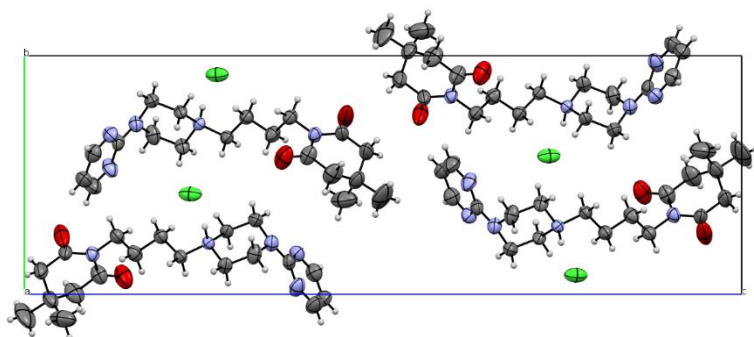
Figure 6.9: Crystal packing for gepirone hydrochloride form II, viewed down to the [100] crystallographic direction. Colour code: Cl, green; N, blue; O, red; C, gray; H, white. Ellipsoids are depicted at the 50% probability level.

In Figure 6.10 it is possible to note that this high melting point form II is endowed with more intermolecular interactions than those observed in gepirone hydrochloride form I.
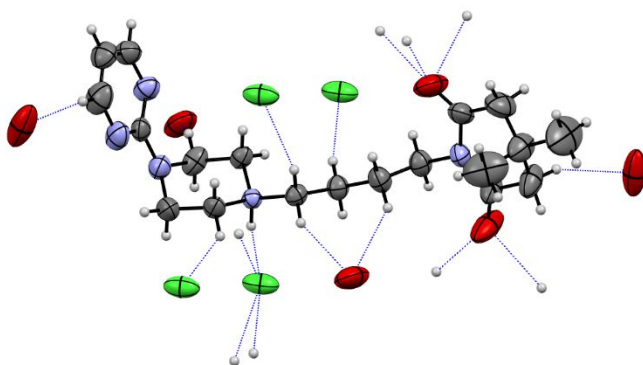
Figure 6.10: H-bond and close contacts pattern (in blue dotted lines) for gepirone hydrochloride, form II. Colour code: Cl, green; N, blue; O, red; C, gray; H, white. Ellipsoids are depicted at the 50% probability level.

The chlorine atom is still interested in an H-bond with the protonated nitrogen of the piperazine ring, while short contacts may be found involving three out of four methylene groups of the butyl chain, methylene groups of the piperazine ring, one C-H of the pyrimidine ring and the oxygen atoms of the carbonyl groups of the glutarimide portion.

Figure 6.11a-b, shows the comparison between the conformations of the two molecules of gepirone hydrochloride in form I and form II, respectively. While the pyrimidine-piperazine system appears to be substantially unchanged, the main variation may be ascribed to the aliphatic C_4 chain, wrapped in Form I and extended in Form II. The different conformation of this chain leads to a different positioning in the two forms of the glutarimide residue.

Figure 6.11: Comparison between the conformations of the two molecules in a) gepirone HCl form I and b) gepirone HCl form II. The molecules are oriented keeping fixed the chair conformation of the piperazine ring. Colour code: Cl, green; N, blue; O, red; C, gray; H, white. Ellipsoids are depicted at the 50% probability level.

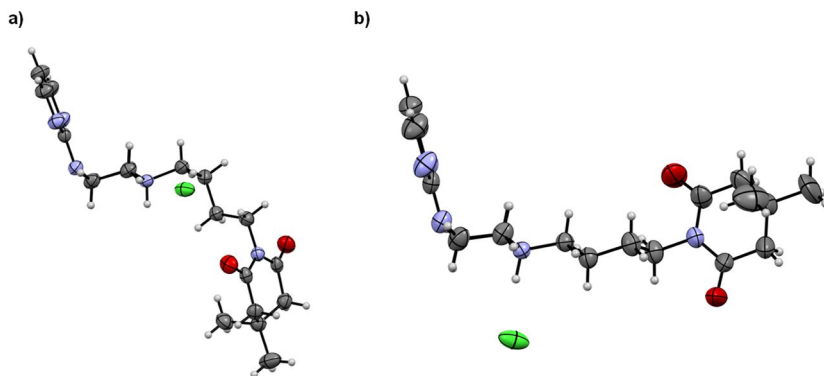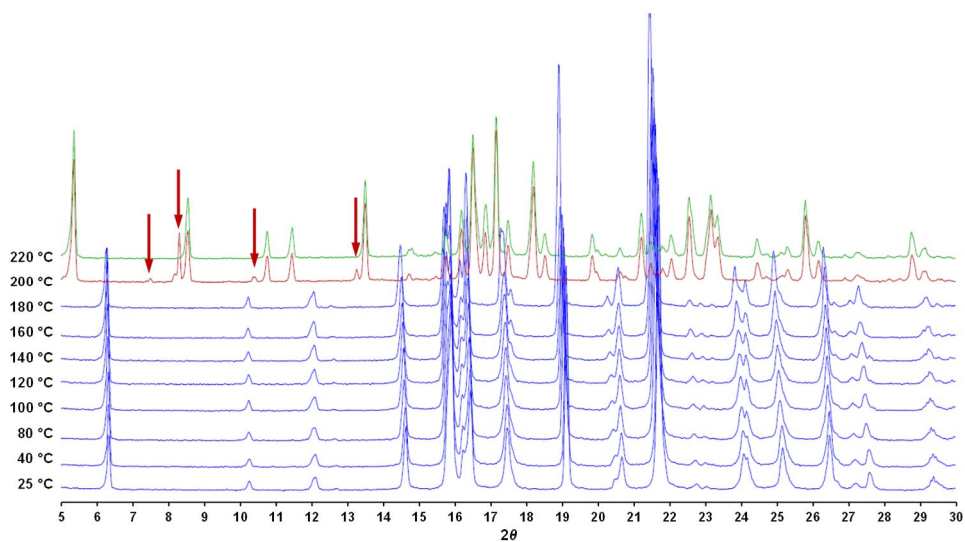**Figure 6.12:** Variable temperature X-ray powder diffraction analysis. Bottom to up, from room temperature up to complete transformation of the form I into the form II. Blu patterns correspond to form I; green pattern corresponds to form II. Peaks of the transient form III are highlighted with red arrows.

The variable temperature PXRD analysis reported in Figure 6.12 clearly shows the thermal evolution of the initial Form I, finally leading at high temperatures (220°C) to pure Form II. Signals of the transient Form III may be detected at 200°C, as indicated by the DSC analysis, but Form III is always accompanied by variable amounts of Form II, the latter being predominant and even exclusive at higher temperatures. The transience of Form III is probably the reason of our failure to isolate crystals of this form.

Crystallographic data obtained for gepirone free base and for gepirone hydrochloride, Form I and Form II, are summarised in Table 6.1.

	Form I	Form II	FB
Formula	$C_{19}H_{30}N_5O_2Cl$	$C_{19}H_{30}N_5O_2Cl$	$C_{19}H_{29}N_5O_2$
Fw	395.9	395.9	359.47
System	Monoclinic	Orthorhombic	Monoclinic
Space Group	$P2_1/c$	$P2_12_12_1$	$P2_1/c$
a, Å	13.9240(9)	6.146(3)	10.1000(16)
b, Å	12.2460(8)	10.897(6)	11.7068(19)
c, Å	12.1075(8)	32.823(17)	16.800(3)
α, °	90	90	90
β, °	90.6090(10)	90	95.718(3)
γ, °	90	90	90
V, Å^3	2064.4(2)	2198(2)	1976.5(5)
Z	4	4	4
Temperature (K)	293(2)	293(2)	293(2)
$\rho_{(calcd)}$, g cm^{-3}	1.274	1.196	1.208
μ, mm^{-1}	0.209	0.074	0.081
F(000)	848	848	776
cryst size, mm	0.20	0.10	0.25
	0.20	0.20	0.20
	0.10	0.10	0.10
θ range for data collection, deg	1.463-24.759	1.969-23.182	2.026-22.013
limiting indices	$-16 \leq h \leq 6$	$-6 \leq h \leq 6$	$-10 \leq h \leq 10$
	$-14 \leq k \leq 14$	$-12 \leq k \leq 12$	$-12 \leq k \leq 12$
	$-14 \leq l \leq 14$	$-36 \leq l \leq 36$	$-17 \leq l \leq 17$
reflns collected/unique	14978/3530 [R_{int} = 0.0201]	12884/3098 [R_{int} = 0.0496]	11590/2425 [R_{int} = 0.0417]
final R indices [$I > 2\sigma(I)$]	R1 = 0.0377 wR2 = 0.0316	R1 = 0.0438 wR2 = 0.806	R1 = 0.0396 wR2 = 0.0699
R indices (all data)	R1 = 0.0876 wR2 = 0.0832	R1 = 0.0793 wR2 = 0.0889	R1 = 0.0880 wR2 = 0.1000
GOF on F^2 ^{c}	1.079	0.976	1.010
largest diff peak and hole, e Å^{-3}	0.148 and -0.176	0.148 and -0.179	0.102 and -0.145

[a] $R_{int} = \Sigma|F_o^2 - F_o^2(mean)|/\Sigma F_o^2$, $R_\sigma = \Sigma\sigma(F_o^2)/\Sigma F_o^2$, $R1 = \Sigma||F_o| - |F_c||/\Sigma|F_o|$, $wR2 = \{\Sigma[w(F_o^2 - F_c^2)^2]/\Sigma[w(F_o^2)^2]\}^{1/2}$, $GOF = \{S/(n-p)\}^{1/2} = \{\Sigma[w(F_o^2 - F_c^2)^2]/(n-p)\}^{1/2}$.

Table 6.1: Crystallographic data for gepirone hydrochloride, Form I and Form II, and gepirone free base.

6.3. Conclusion

In this chapter, we focused our attention on the solid-state properties of gepirone hydrochloride, in order to obtain further information about its crystalline form and the presence of others polymorphic forms.

In 1985, Behme et al.[8] reported the alleged presence of three polymorphic forms (Form I, II and III) of gepirone hydrochloride. The form I is reported to melt at 180°C, form II at 212 °C and form III at 200 °C. Unfortunately, no structural data for these forms were reported as their existence was ascertained only by DSC analysis.

Thermal analysis on our samples of gepirone hydrochloride confirmed the presence of three forms of this API and we succeeded in isolating crystals of two of these forms, along with crystals of the free base. Single crystal X-ray diffraction analysis of these forms allowed to obtain detailed structural information. In addition, variable temperature PXRD studies defined the stability range of these forms.

6.4. Experimental Section

Gepirone compound was prepared following the literature reported methods[10-13].

Then, several crystallisations tests were made in order to obtain suitable crystals for the X-ray analysis. In particular, we focused our attention on:

- Gepirone free base
- Gepirone HCl (commercial form)

The free base form was added in 3 mL of the appropriate solvent (MIBK) and dissolved by heating. The obtained solution was kept at 22 – 25 °C until crystals, suitable for X-ray analyses, were obtained.

Gepirone hydrochloride was suspended in 3 mL of acetonitrile and dissolved by heating. The resulting solution was kept at 22 – 25 °C until crystals, suitable for X-ray analyses, were obtained.

6.5. References

1. Zhao, Q.; Swati, Z. N. K.; Metmer, H.; Sang, X.; Lu, J. Investigating Executive Control Network and Default Mode Network Dysfunction in Major Depressive Disorder. *Neurosci. Lett.* **2019**, *701*, 154–161. https://doi.org/10.1016/j.neulet.2019.02.045.

2. Otte, C.; Gold, S. M.; Penninx, B. W.; Pariante, C. M.; Etkin, A.; Fava, M.; Mohr, D. C.; Schatzberg, A. F. Major Depressive Disorder. *Nat. Rev. Dis. Primer* **2016**, *2*, 16065. https://doi.org/10.1038/nrdp.2016.65.

3. Celada, P.; Bortolozzi, A.; Artigas, F. Serotonin 5-HT1A Receptors as Targets for Agents to Treat Psychiatric Disorders: Rationale and Current Status of Research. *CNS Drugs* **2013**, *27* (9), 703–716. https://doi.org/10.1007/s40263-013-0071-0.

4. Cai, Z. Monoamine Oxidase Inhibitors: Promising Therapeutic Agents for Alzheimer's Disease (Review). *Mol. Med. Rep.* **2014**, *9* (5), 1533–1541. https://doi.org/10.3892/mmr.2014.2040.

5. Kishi, T.; Meltzer, H. Y.; Matsuda, Y.; Iwata, N. Azapirone 5-HT1A Receptor Partial Agonist Treatment for Major Depressive Disorder: Systematic Review and Meta-Analysis. *Psychol. Med.* **2014**, *44* (11), 2255–2269. https://doi.org/10.1017/S0033291713002857.

6. Eison, A. S. Azapirones: History of Development. *J. Clin. Psychopharmacol.* **1990**, *10* (3), 2S.

7. Chessick, C. A.; Allen, M. H.; Thase, M. E.; Cunha, A. A. B. M. da; Kapczinski, F.; Lima, M. S. de; Souza, J. J. dos S. Azapirones for Generalized Anxiety Disorder. *Cochrane Database Syst. Rev.* **2006**, No. 3. https://doi.org/10.1002/14651858.CD006115.

8. Behme, R. J.; Brooke, D.; Farney, R. F.; Kensler, T. T. Characterization of Polymorphism of Gepirone Hydrochloride. *J. Pharm. Sci.* **1985**, *74* (10), 1041–1046. https://doi.org/10.1002/jps.2600741004.

9. Koziol, A. E.; Chilmonczyk, Z.; Cybulski, J. Buspirone Free Base. *Acta Crystallogr. Sect. E* **2006**, *62* (12), o5616–o5618. https://doi.org/10.1107/S1600536806047726.

10. Kamal, A.; Satyanarayana, M.; Devaiah, V.; Rohini, V.; Yadav, J.; Mullick, B.; Nagaraja, V. Synthesis and Biological Evaluation of Coumarin Linked Fluoroquinolones, Phthalimides and Naphthalimides as Potential DNA Gyrase Inhibitors. *Lett. Drug Des. Discov.* **2006**, *3* (7), 494–502. https://doi.org/10.2174/157018006778194862.

11. Glennon, R. A.; Naiman, N. A.; Lyon, R. A.; Titeler, M. Arylpiperazine Derivatives as High-Affinity 5-HT1A Serotonin Ligands. *J. Med. Chem.* **1988**, *31* (10), 1968–1971. https://doi.org/10.1021/jm00118a018.

12. Paluchowska, M. H.; Bugno, R.; Bojarski, A. J.; Charakchieva-Minol, S.; Duszyńska, B.; Tatarczyńska, E.; Kłodzińska, A.; Stachowicz, K.; Chojnacka-Wójcik, E. Novel, Flexible, and Conformationally Defined Analogs of Gepirone: Synthesis and 5-HT$_{1A}$, 5-HT$_{2A}$, and D$_2$ Receptor Activity. *Bioorg. Med. Chem.* **2005**, *13* (4), 1195–1200. https://doi.org/10.1016/j.bmc.2004.11.019.

13. Temple, J. D. L. 2-[4-[(4,4-Dialkyl-2,6-Piperidinedion-1-yl)Butyl]-1-Piperazinyl]Pyrimidines. US4423049 (A), December 27, 1983.

Chapter 7:
Pirfenidone: Crystal Structure Characterization

7.1. Introduction

Idiopathic Pulmonary Fibrosis (IPF) is a debilitating lungs disease characterised by cough, scars and dyspnoea that lead to progressive degeneration of lungs reaching an irreversible loss of function. This pathology is common in patients over 60 years' old, and male patient are more affected[1]. After the diagnosis of this pathology, the life expectancy is drastically reduced to few years, generally 3-5 years[2] without lung transplantation.

In 2019 in USA and Europe, more than 100.000 peoples are affected by IPF, but detailed data, today, are scarcely available. This serious pathology, is associated to different risk factors like cigarettes smoke, sarcoidosis and various genetic factors[3].

Pirfenidone is to date the only API used for the treatment of IPF. It was approved Japan in 2008 (trade mark Pirespa®) and in Europe in 2011 (trade mark Esbriet®). Pirfenidone (IUPAC name: 5-methyl-1-phenyl-1*H*-pyridin-2-one) is a heterocyclic compound with a 2-pyridone ring with a *N*-phenyl substituent and a methyl group in position 5, being a small and very simple molecule.

Pirfenidone (Figure 7.1) shows a well-known activity as anti-fibrotic and anti-inflammatory compound[4]. Moreover, this API, reduces fibroblast proliferation[5] and it is able to interact with other proteins like TGF-β, and other cytokines[5], but the exact molecular target has not been highlighted. Several clinical studies were directed to understand the mechanism of action, safety profile, and other important parameters (bioavailability, dose, toxicity etc.)[4] as well as side effects[6]. Pirfenidone is generally very well

tolerated[7] leading this molecule as the only lead compound in the treatment of IPF.

Different synthetic procedure for the synthesis of pirfenidone are reported in the scientific literature[8-12], but much less is reported on the solid state properties, of this important API. As mentioned in the chapter 1, the presence of one or more crystalline forms may affect significantly the chemical stability of API and as a consequence, the final stability of pharmaceutical forms.
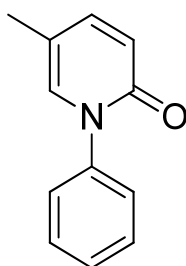
Figure 7.1: Molecular structure of pirfenidone

Our work was focused on the screening of the eventual crystalline forms of pirfenidone, gaining a comprehensive solid-state characterisation of this molecule. To this purpose a systematic series of experiments involving the crystallization of pirfenidone from different solvents (alcohols, acetone, acetonitrile, nitromethane, toluene) were performed.

The starting material pirfenidone was prepared according to a previously reported method[8], with a purity >99.5 %.

Although various solvents and mixtures thereof produced a crystalline precipitate of pirfenidone, large transparent crystals suitable for SCXRD analysis were obtained by solutions of the API.

Data of the pirfenidone crystal, collection and structure refinement details are summarized in Table 7.1. The crystals of pirfenidone belong to the monoclinic space group $P2_1$.

Crystal data

Chemical Formula	$C_{12}H_{11}NO$
M_r	185.22
Crystal system, space group	Monoclinic, $P2_1$
Temperature (K)	293
a (Å)	6.2525(8)
b (Å)	7.797(1)
c (Å)	10.2810(13)
α, β, γ (°)	90, 104.744(2), 90
V (Å^3)	484.70(11)
Z	2
Radiation type	Mo $K\alpha$
μ (mm^{-1})	0.08
Crystal size (mm)	0.5 x 0.45 x 0.05

Data Collection

Diffractometer	Bruker SMART APEX CCD
Absorption correction	Multi-scan (*SADABS*; Bruker, 2010)
T_{min}; T_{max}	0.692, 0.746
No of measured, independent and observed [$I > 2\sigma(I)$] reflections	4547, 2128, 1879
R_{int}	0.019
$(\sin \theta/\lambda)_{max}$ (Å^{-1})	0.643

Refinement

$R[F^2 > 2\sigma(F^2)], wR(F^2), S$	0.037, 0.095, 1.04
No. of refelctions	2128
No. of parameters	127
No. of restraints	1
H-atom treatment	H-atom parameters constrained
$\Delta\rho_{max}, \Delta\rho_{min},$ (e Å^{-3})	0.11, -.20
Absolute structure	Flack x determined using 762 quotients [(I$^+$)-(I$^-$)]/(I$^+$)+(I$^-$)
Absolute structure parameters	0.3 (4)

Table 7.1: Experimental details of the SCXRD analysis of pirfenidone

The phenyl substituent and the pyridinone ring are not coplanar (Figure 7.2), subtending a dihedral angle of 50.30(11) and implying a negligible resonance between the two π-systems.
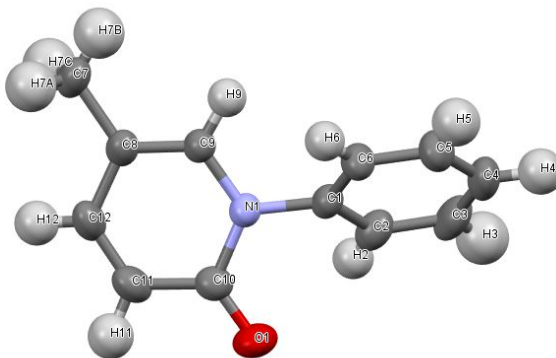
Figure 7.2: Molecular structure of pirfenidone

In the crystal, pirfenidone molecules are linked in the crystal by C—H···O pseudo-hydrogen bonds with the same acceptor atom, generating an undulating network, enclosing R^3_4 (20) ring motifs, parallel to the *ab* plane (Figs. 7.3 and 7.4). No additional significant intermolecular contacts may be found by analysis of the crystal structure with PLATON[13].
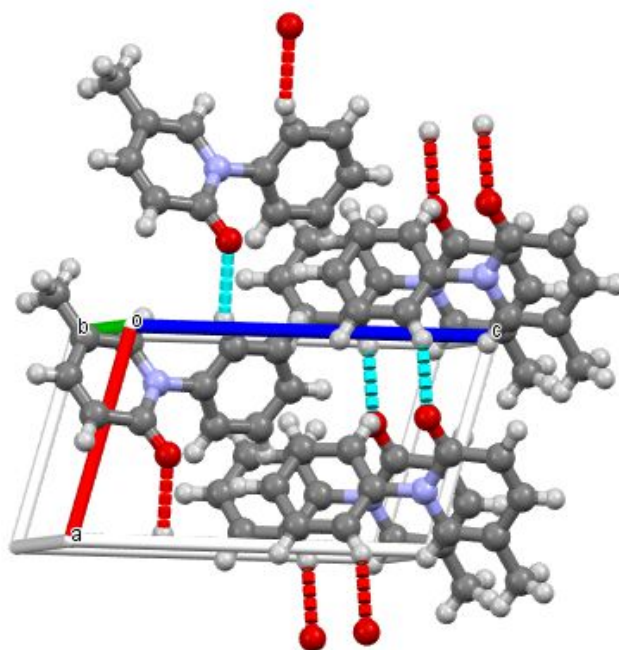
Figure 7.3: View of CH···O interactions in the crystal packing of pirfenidone
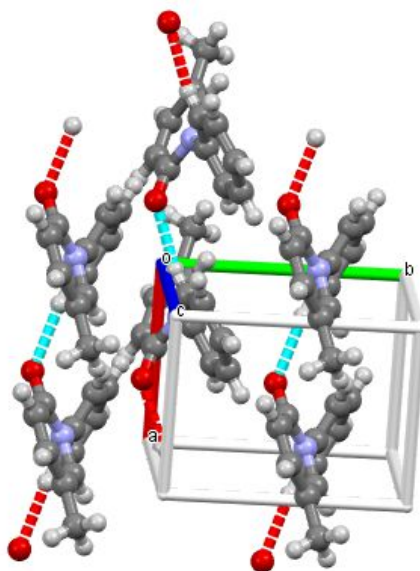
Figure 7.4: View of the undulating network of CH···O interaction in the crystal packing of pirfenidone

Finally, the PXRD pattern calculated on the base of the SCRXD data was compared with the PXRD pattern registered on a sample of commercial pirfenidone powder, prepared according to the reported procedure.[8] The very good agreement implies that the crystal phase of the commercial powder is the same of that of the isolated single crystal obtained by toluene (Figure 7.5).
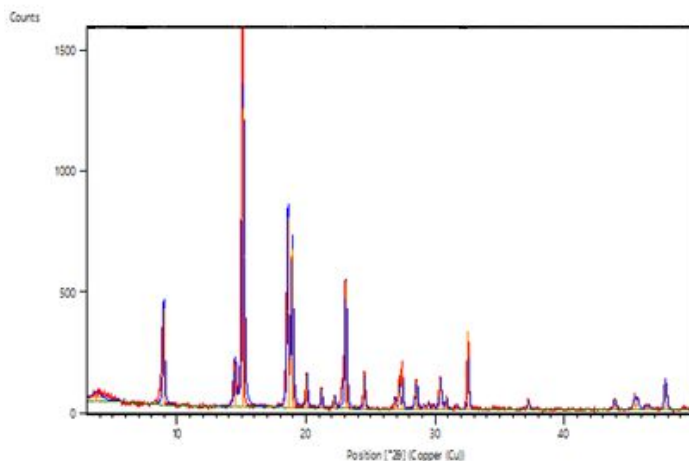
Figure 7.5: Comparison of PXRD patterns of pirfenidone. Red line = experimental pattern of a commercial sample. Blue line = calculated pattern based on the SCXRD data.

Comm.	UPO.
8.9599	8.89
14.4965	14.44
15.1304	15.08
18.5862	18.56
18.9272	18.91
20.0387	20.02
21.2012	21.18
22.1902	22.19
	22.80
23.0790	23.07
24.4826	24.51
26.8686	26.88
27.1859	27.18
27.4654	27.45
	28.37
28.5421	28.57
29.1277	29.09
	29.26
29.4621	29.52
29.8306	29.85
30.3791	30.43
	30.52
30.8702	30.84
31.6665	31.72
32.5596	32.58

7.2. Conclusion

In conclusion, in this work we investigated the solid-state features of pirfenidone. A thorough screening of solvents and mixtures thereof, allowed to identify a single crystal phase for this specific API. No additional forms were isolated, nor were adducts, solvates or inclusion compounds. The structural details of the molecule of pirfenidone and its packing in the monoclinic crystal were determined by single-crystal X-ray analysis.[14]

The limited number of polar residues and functional groups along with the few degrees of rotational freedom of this small molecule are likely at the base of the absence of alternative polymorphs.

7.3. Experimental Section

Solvents and reagents. Commercially available solvents and reagents were used without further purification.

Single crystal X-ray analysis. Bruker SMART APEX CCD diffractometer ω scans Absorption Correction: multi-scan (SADABS), T_{min} = 0.692, T_{max} = 0.746, 4547 measured reflections.

Computing details. Data collection: *APEX2;* cell refinement: *SAINT*; data reduction: *SAINT*;

program(s) used to solve structure: *SHELXT2017*[15]; program(s) used to refine structure: *SHELXL2017*[16]; molecular graphics: *ORTEP-3 for Windows*[17] and *Mercury*[18]; software used to prepare material for publication: *SHELXL2017*[16], *PLATON*[13] and *publCIF*[19].

Preparation of Pirfenidone single crystal

Pirfenidone (approx. 100 mg) was heated in toluene (2 mL) until complete dissolution. The clear solution was closed and kept at 0-5 °C for one week obtaining colourless crystals of pirfenidone.
The melting point determined through DSC is 383 K.

The same protocol was applied with different solvents. The same crystal form was obtained in all instances.

7.4. References

1. Strongman, H.; Kausar, I.; Maher, T. M. Incidence, Prevalence, and Survival of Patients with Idiopathic Pulmonary Fibrosis in the UK. *Adv. Ther.* **2018**, *35* (5), 724–736. https://doi.org/10.1007/s12325-018-0693-1.

2. Kropski, J. A.; Blackwell, T. S. Progress in Understanding and Treating Idiopathic Pulmonary Fibrosis. *Annu. Rev. Med.* **2019**, *70* (1), 211–224. https://doi.org/10.1146/annurev-med-041317-102715.

3. Thomson, C. C.; Duggal, A.; Bice, T.; Lederer, D. J.; Wilson, K. C.; Raghu, G. 2018 Clinical Practice Guideline Summary for Practicing Clinicians: Diagnosis of Idiopathic Pulmonary Fibrosis. *Ann. Am. Thorac. Soc.* **2018**, https://doi.org/10.1513/AnnalsATS.201809-604CME.

4. Schaefer, C. J.; Ruhrmund, D. W.; Pan, L.; Seiwert, S. D.; Kossen, K. Antifibrotic Activities of Pirfenidone in Animal Models. *Eur. Respir. Rev.* **2011**, *20* (120), 85–97. https://doi.org/10.1183/09059180.00001111.

5. Lin, X.; Yu, M.; Wu, K.; Yuan, H.; Zhong, H. Effects of Pirfenidone on Proliferation, Migration, and Collagen Contraction of Human Tenon's Fibroblasts in Vitro. *Invest. Ophthalmol. Vis. Sci.* **2009**, *50* (8), 3763–3770. https://doi.org/10.1167/iovs.08-2815.

6. Noble, P. W.; Albera, C.; Bradford, W. Z.; Costabel, U.; Glassberg, M. K.; Kardatzke, D.; King, T. E.; Lancaster, L.; Sahn, S. A.; Szwarcberg, J.; et al. Pirfenidone in Patients with Idiopathic Pulmonary Fibrosis (CAPACITY): Two Randomised Trials. *The Lancet* **2011**, *377* (9779), 1760–1769. https://doi.org/10.1016/S0140-6736(11)60405-4.

7. Costabel, U.; Albera, C.; Glassberg, M. K.; Lancaster, L. H.; Wuyts, W. A.; Petzinger, U.; Gilberg, F.; Kirchgaessler, K.-U.; Noble, P. W. Effect of Pirfenidone in Patients with More Advanced Idiopathic Pulmonary Fibrosis. *Respir. Res.* **2019**, *20* (1), 55. https://doi.org/10.1186/s12931-019-1021-2.

8. Mossotti, M.; Barozza, A.; Roletto, J.; Paissoni, P. Process for the Synthesis of Pirfenidone. US2018319747 (A1), November 8, 2018.

9. Gant, T. G.; Sarshar, S. Substituted N-Aryl Pyridinones as Fibrotic Inhibitors. WO2008157786 (A1), December 24, 2008.

10. Crifar, C.; Petiot, P.; Ahmad, T.; Gagnon, A. Synthesis of Highly Functionalized Diaryl Ethers by Copper-Mediated O-Arylation of Phenols Using Trivalent Arylbismuth Reagents. *Chem. - Eur. J.* **2014**, *20* (10), 2755–2760. https://doi.org/10.1002/chem.201303684.

11. Koyuncu, H.; Akgol, E.; Reis, O. An Improved Method for the Synthesis and Purification of Pirfenidone. WO2016122420 (A1), August 4, 2016.

12. Yang, S.; Yang, H.; Li, W.; Yang, L.; Yu, S. Anti-Fibrosis Drug Pirfenidone Crystal Forms and Preparation Method Thereof. CN105906558 (A), August 31, 2016.

13. Spek, A. L. Structure Validation in Chemical Crystallography. *Acta Crystallogr. D Biol. Crystallogr.* **2009**, *65* (2), 148–155. https://doi.org/10.1107/S090744490804362X.

14. Barbero, M.; Mossotti, M.; Sironi, A.; Giovenzana, G. B.; Colombo, V. Crystal Structure of Pirfenidone (5-Methyl-1-Phenyl-1H-Pyridin-2-One): An Active Pharmaceutical Ingredient (API). *Acta Crystallogr. Sect. E Crystallogr. Commun.* **2019**, *75* (7), 984–986. https://doi.org/10.1107/S2056989019006418.

15. Sheldrick, G. M. SHELXT – Integrated Space-Group and Crystal-Structure Determination. *Acta Crystallogr. Sect. Found. Adv.* **2015**, *71* (1), 3–8. https://doi.org/10.1107/S2053273314026370.

16. Sheldrick, G. M. Crystal Structure Refinement with SHELXL. *Acta Crystallogr. Sect. C Struct. Chem.* **2015**, *71* (1), 3–8. https://doi.org/10.1107/S2053229614024218.

17. Farrugia, L. J. WinGX and ORTEP for Windows: An Update. *J. Appl. Crystallogr.* **2012**, *45* (4), 849–854. https://doi.org/10.1107/S0021889812029111.

18. Macrae, C. F.; Bruno, I. J.; Chisholm, J. A.; Edgington, P. R.; McCabe, P.; Pidcock, E.; Rodriguez-Monge, L.; Taylor, R.; Streek, J. van de; Wood, P. A. Mercury CSD 2.0 – New Features for the Visualization and Investigation of Crystal Structures. *J. Appl. Crystallogr.* **2008**, *41* (2), 466–470. https://doi.org/10.1107/S0021889807067908.

19. Westrip, S. P. PublCIF: Software for Editing, Validating and Formatting Crystallographic Information Files. *J. Appl. Crystallogr.* **2010**, *43* (4), 920–925. https://doi.org/10.1107/S0021889810022120.

Chapter 8: Solid state characterization of Moxidectin solvates

8.1. Introduction

Human infections are considered a priority for the public health but at the same time, animal infections are important as they can represent an additional vehicle for the transmission to humans. In particular, infections that affect cattle, horses and domestic pets like cats and dogs[1,2] are especially dangerous as these animals live in close contact with peoples. Infections are caused by different type of macro or micro-organisms (parasites) able to attack all living species including humans and animals. Parasites can be broadly classified in two categories:

-   Endoparasites: living inside the body
-   Ectoparasites: living outside the body

Parasites affecting humans and animals may be ascribed to all kingdoms of biology, with the addition of viruses. Animal infections like filariasis[1], scabies[3], ocular thelaziosis[4], chagas, toxoplasmosis, leishmaniosis[5] are the most represented pathologies with a worldwide diffusion. As a consequence, the veterinary market for livestock and pets, will increase by 5.6% in next 5 years[6] leading to an increase of the global vaccines production.

Among human infections, a specific nematode, *Onchocerca volvulus*, is able to infect people leading to onchocerciasis, also known as "river blindness", a particular disease ultimately leading to blindness[7,8]. This pathology is mainly localised in Africa, especially in sub-Saharan states and in a few other countries like Brazil and Venezuela, as reported by the World Health Organization.

Ivermectin (Figure 8.1) and related molecules are the preferred treatment for onchocerciasis, as it is able to paralyse and kill the nematode.

Moreover, ivermectin is administered in a single dose, to be repeated after 6 months, has a well-established safety profile and does not need refrigeration, facilitating the treatment in undeveloped countries where these pathologies are particularly spread.

Ivermectin belongs to the avermectin class, 16-membered macrocyclic lactones with high potent anthelminthic activity. Avermectins were discovered by S. Omura, in collaboration with W.C. Campbell, in the mid-1970s and these types of compounds were obtained by fermentation culture broth of *Streptomyces avermectinius*[9]. For this important discovery they jointly received in 2015 the Nobel Prize for medicine[10].
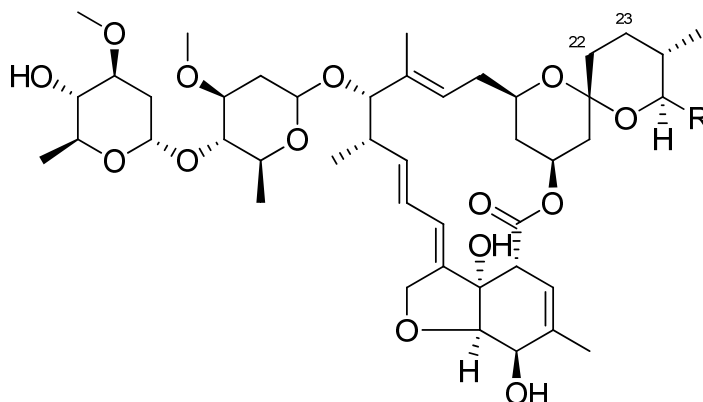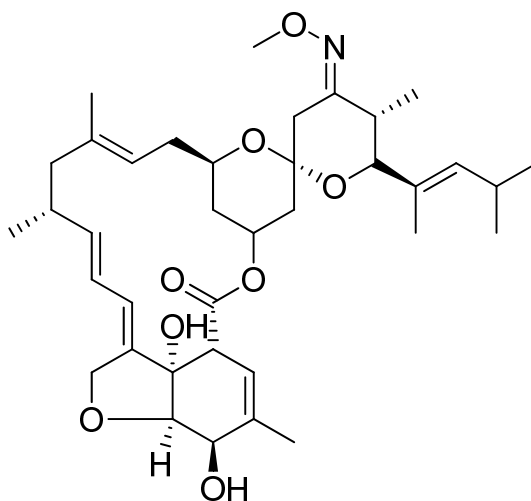

Figure 8.1: Ivermectin

Ivermectin is a semisynthetic compound composed by mixture of 22,23-dihydro derivatives of avermectins B_{1a} and B_{1b}, where –R is represented by –$CH(CH_3)CH_2CH_3$ or –$CH(CH_3)_2$, respectively[11]. These compounds are characterised by the presence of a glycoside on the macrocyclic lactone structure the latter embodying several unsaturated C=C bonds.

Moxidectin is a semisynthetic derivative of ivermectin, i.e. recently introduced for the treatment of onchocerciasis and of infections of cattle, horses and pets like dogs and cats.

Moxidectin (Figure 8.2, IUPAC name ((6*R*,23*E*,25*S*)-5-*O*-demethyl-28-deoxy-25-[(1*E*)-1,3-dimethyl-1-buten-1-yl]-6,28-epoxy-23-(methoxyimino) milbemycin B) is a semisynthetic 23-methoxime macrocyclic lactone, belonging to the milbemycin class[12,13]. The latter are produced by fermentation from *Streptomyces cyaneogriseus*.
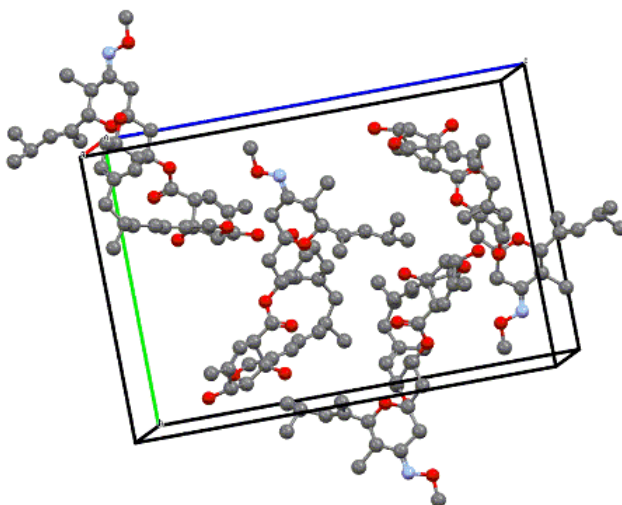

Figure 8.2: Moxidectin

Moxidectin has a high similarity with ivermectin, the only differences being limited to the presence of the *E*-methoxime group on C-23 and *E*-4-methylpent-2-enyl on C-25 and the absence of the disaccharide moiety on C-13.

Due to the high activity as anthelmintic drug, moxidectin is employed today for the treatment of parasitic infection in humans, in particular for the treatment of the "river blindness" disease, after approval by FDA in 2018. Its activity is related to the blocking of glutamate-gated chloride ion channel leading to flaccid paralysis of the neuromuscular system of the

nematode[14]. Moreover, due to the low toxicity, moxidectin is employed as ectoparasiticide agent in agriculture.

Thanks to the importance of moxidectin for human health, several articles have been reported in relation to its biological activity and its formulation.

On the other hand, a comprehensive knowledge of the solid-state behaviour of this compound is lacking, as information on the single crystal structure and the presence of polymorphs, solvates and hydrates, are currently scarce.

Beddall et al[15] first disclosed the single crystal structure of "dry" (unsolvated) moxidectin, characterized by the orthorhombic $P2_12_12_1$ space group. This form was named moxidectin form I and the details of the crystal structure are available in the CSD with the reference-code GETBOW (Figure 8.3).

Figure 8.3: Crystal structure of "dry" (unsolvated) moxidectin

Additional four forms, three solvates and amorphous forms, were claimed in a patent[16] and identified by PXRD and DSC, even if the structural details are not disclosed (Table 8.1).

Crystal form	Solvent	First report	Ref. for structure
Moxidectin	None	Beddall et al	GETBOW
Moxidectin·2EtOH	Ethanol	WO2013/082373A1	Not available
Moxidectin·2iPA	2-Propanol	WO2013/082373A1	Not available
Moxidectin·2BuOH	n-Butanol	WO2013/082373A1	Not available

Table 8.1: Summary of reported moxidectin crystal forms

During the PhD, we started a systematic investigation on moxidectin, by crystallising the API from many solvents and in different experimental conditions and techniques.

As a result of these efforts, we were able to obtain three distinct crystalline forms of moxidectin, suitable for single-crystal diffractometric analysis, all of them as solvates:

1) Moxidectin solvate with ethanol (1:2)
2) Moxidectin solvate with 2-propanol (1:2)
3) Moxidectin solvate with nitromethane (1:1.5)

The first two crystalline forms are useful to confirm the claim reported in the original patent[16], while the nitromethane solvate is completely unprecedented and represents a new solvate. We were not able to obtain any crystal of the alleged butanol solvate, nor of the "dry" unsolvated form. Experimental details and crystallographic data of the three forms are reported in Table 8.2.

|	Moxi·2EtOH	Moxi·2*i*PrOH	Moxi·1.5MeNO$_2$
Formula	C$_{41}$H$_{65}$NO$_{10}$ [C$_{37}$H$_{53}$NO$_8$) (EtOH)$_2$]	C$_{45}$H$_{69}$NO$_{10}$ [C$_{37}$H$_{53}$NO$_8$) (iPrOH)$_2$]	C$_{38.5}$H$_{57.5}$N$_{2.5}$O$_{11}$ [C$_{37}$H$_{53}$NO$_8$) (MeNO$_2$)$_{1.5}$]
Fw	731.96	760.01	730.56
System	Monoclinic	Monoclinic	Orthorombic
Space Group	*P*2$_1$	*P*2$_1$	*P*2$_1$2$_1$2
a, Å	11.1958(11)	11.5256(90)	19.793(2)
b, Å	8.8507(9)	9.1571(7)	13.9246(15)
c, Å	21.968(2)	21.8144(16)	15.2689(16)
α, °	90	90	90
β, °	93.7(2)	93.0690(10)	90
γ, °	90	90	90
V, Å^3	2172.3(4)	2299.0(3)	4208.3(8)
Z	2	2	4
Temperature (K)	120(2)	293(2)	100(2)
$\rho_{(calcd)}$, g cm^{-3}	1.116	1.054	1.203
μ, mm^{-1}	0.079	0.074	0.089
F(000)	792	792	1640
cryst size, mm	0.25 0.20 0.10	0.20 0.20 0.05	0.10 0.05 0.05
θ range for data collection, deg	0.929-30.791	0.935-24.903	1.334-24.944
limiting indices	-16 ≤ h ≤ 15 -12 ≤ k ≤ 12 -31 ≤ l ≤ 31	-13 ≤ h ≤ 13 -10 ≤ k ≤ 10 -25 ≤ l ≤ 25	-23 ≤ h ≤ 23, -16 ≤ k ≤ 16 -18 ≤ l ≤ 18
reflns collected/unique	25453/12892 [R$_{int}$ = 0.0218]	17822/7883 [R$_{int}$ = 0.0357]	32062/7327 [R$_{int}$ = 0.0325]
data/restraints/param	12892/1/473	7883/1/489	7327/0 /489
final R indices [*I* > 2σ(*I*)]	R1 = 0.0615 wR2 = 0.1429	R1 = 0.0553 wR2 = 0.1440	R1 = 0.086 wR2 = 0.2318
R indices (all data)	R1 = 0.0948 wR2 = 0.1591	R1 = 0.0736 wR2 = 0.1560	R1 = 0.0941 wR2 = 0.2390
GOF on F^2 [c]	1.039	1.056	1.059
largest diff peak and hole, e Å^{-3}	0.666 and -0.557	0.232 and -0.324	1.223 and -1.819

[a] $R_{int} = \Sigma|F_o^2 - F_o^2(mean)|/\Sigma F_o^2$, $R_\sigma = \Sigma\sigma(F_o^2)/\Sigma F_o^2$, $R1 = \Sigma||F_o| - |F_c||/\Sigma|F_o|$, $wR2 = \{\Sigma[w(F_o^2 - F_c^2)^2]/\Sigma[w(F_o^2)^2]\}^{1/2}$, $GOF = \{S/(n-p)\}^{1/2} = \{\Sigma[w(F_o^2 - F_c^2)^2]/(n-p)\}^{1/2}$.

Table 8.2: Crystallographic data

Moxidectin solvate with ethanol (hereinafter Moxi·2EtOH) and moxidectin solvate with 2-propanol (hereinafter Moxi·2iPrOH) are isostructural. Crystallographic description is here discussed only on the ethanol solvate, while the same considerations can be applied to the isopropanol solvate. Moxi·2EtOH (Figures 8.4 and 8.5) crystallizes in the monoclinic space group $P2_1$ with one molecule of moxidectin in general position. Two ethanol molecules are found in the unit cell (also in general position).
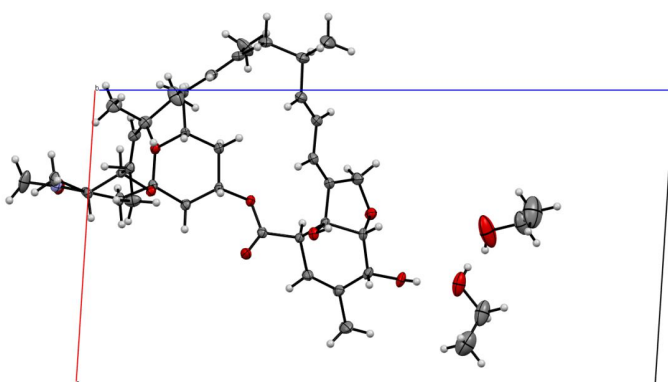

Figure 8.4. Asymmetric unit for Moxi·2EtOH crystal structure viewed down the [010] direction. Ellipsoids are depicted at 50% probability. Colour codes: gray, carbon; light gray, hydrogen; red, oxygen; blue, nitrogen.
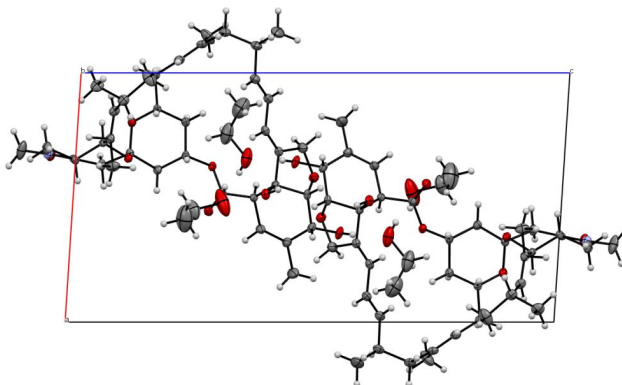
Figure 8.5. Moxi·2EtOH crystal packing viewed down to the [010] direction. Ellipsoids are depicted at 50% probability. Colour codes: gray, carbon; light gray, hydrogen; red, oxygen; blue, nitrogen.

An interesting H-bond pattern is found between solvent molecules and the OH groups of the hexahydrobenzofuran ring of the moxidectin molecule. Figure 8.6 (a and b) depicts the cyclic H-bond pattern found in the crystal packing. In these intermolecular H-bonds contacts, two ethanol molecules and two moxidectin molecules are involved; distances fall in the range 2.70-2.78 Å. All H-bonds contacts are of the type –O-H···O- and are between Moxi-EtOH; EtOH-EtOH; EtOH-Moxi and Moxi-Moxi, respectively. More in detail, between O(7)H···O(EtOH1), 2.703 Å; (EtOH1)O-H···O(EtOH2), 2.731 Å; (EtOH2)O-H…O(8), 2.783 Å and O(8)H…O(7), 2.764 Å. The latter H-bond also bifurcates through the O atom of the furane ring (3.172 Å). Figure 8.6b shows an enlargement of the two hexahydrobenzofuran rings of two different moxidectin molecules and the two ethanol molecules with highlighted, in dotted blue lines, the cyclic intermolecular H-bond pattern.
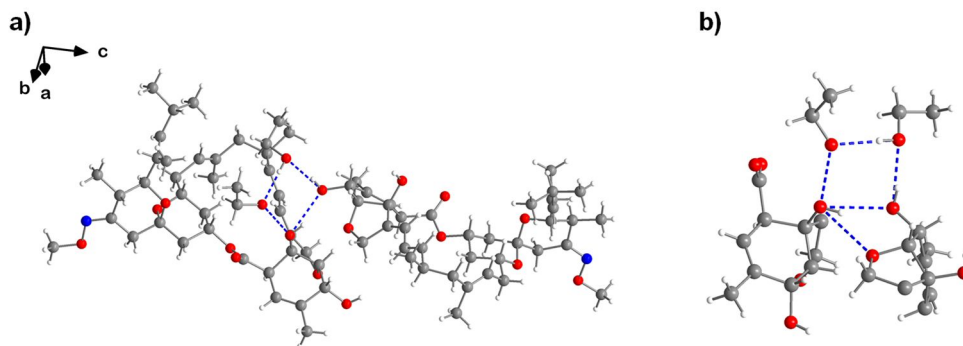
Figure 8.6. a) Crystal packing around the H-bond pattern found in Moxi·2EtOH solvate. B) Enlargement of the hexahydrobenzofuran rings which interact with the two ethanol molecules. Colour codes: C, gray; H, white; O, red; N, blue. H-bonds are highlighted in dotted lines.

Slow evaporation of a nitromethane solution of moxidectin gave transparent flat platelets, which has been analysed by single-crystal X-ray diffraction. Moxi·1.5MeNO$_2$ crystallizes in the orthorhombic space group, whit one molecule in general position. Quality of the crystals was found to be low (max resolution 0.85Å at 100K), this was later ascribed to the disordered nitromethane molecules, which are all confined in a portion of the unit cell and disordered around the twofold axis (Figure 8.7). During the solution process of the structure, all attempts done for a description of the solvent molecules failed, due to the high degree of disorder and to the fact that multiple molecules are present, all with different occupancy factor.

Indeed, we decided to use the SQUEEZE procedure, implemented in PLATON[17]. Squeeze gave rise to an 800 Å^3 void volume in the unit cell, which correspond to the 20 % of the total cell volume, and a total number of 180 electrons coming from the solvent molecules, which are in good agreement for a 1.5 nitromethane molecule in the asymmetric unit. In figure

8.7 and 8.8 are depicted the moxidectin molecules packed in the unit cell and, in yellow, the residual void volume obtained with PLATON-SQUEEZE procedure, where the nitromethane molecules are found.
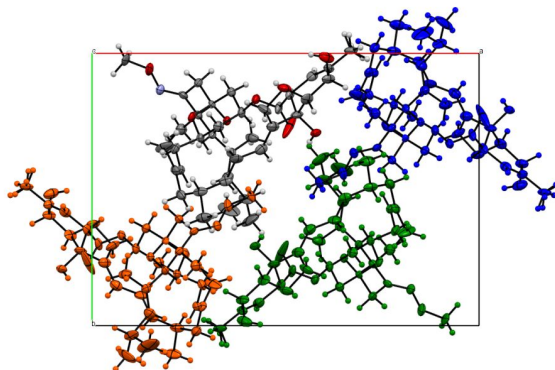
Figure 8.7: Crystal packing of Moxi·1.5MeNO$_2$ viewed along the [001] crystallographic direction. For clarity, solvent molecules are omitted and, because space group of this crystal structure is $P2_12_12$, three of the 4 molecules in the unit cell are coloured in orange, green and blue. Colour codes for the 4th molecule are C, gray; N, blue; O, red; H, white.
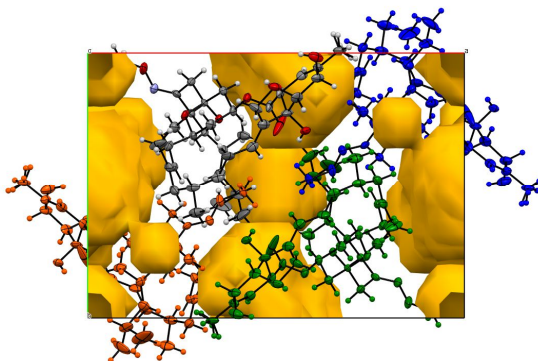
Figure 8.8: Void volume in the crystal packing after squeezing with PLATON. Voids account for 15% of the unit cell volume and about 660 Å^3, in good agreement with two MeNO$_2$ molecules per formula unit.

It is worth to highlight here two H-bond contacts found in this crystal structure, which are not present in the other two solvates. Indeed, an intramolecular H-bond is found between the tertiary alcohol located on the bridgehead position of the fused bicylic[4.3.0] residue and the carbonyl group of the O=C of the type O-H···O= with distance 2.716 Å (Figure 8.9). This intra-molecular bond is not present in the *i*PrOH and EtOH solvates, in which the bridgehead OH of moxidectin participates in the H-bond pattern involving the solvent molecules.
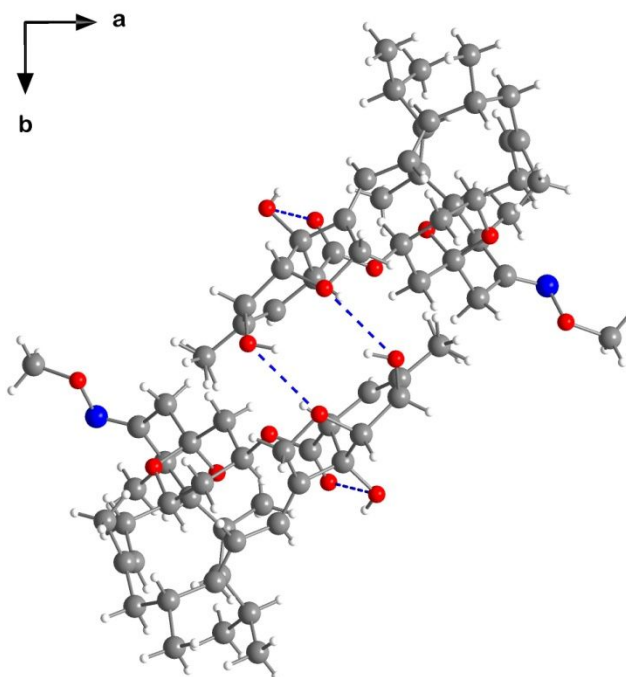

Figure 8.9: Intra- and inter-molecular H-bonds in Moxi·1.5MeNO$_2$

Moreover, intermolecular H-bonds are found between two moxidectin molecules, and are depicted in Figure 8.9. Here the H-bonds are both of the same nature and are exchanged between the oxygen atom of the furan ring (O6) and the –OH group of the secondary alcohol located on the six-membered carbocyclic ring of the hexahydrobenzofuran moiety. These are coupled between symmetry related (around the twofold axis) moxidectin molecules with distances 2.84 Å, in both cases.

An insight into the solid-state behavior of moxidectin solvates was then determined by means of variable temperature X-ray powder diffraction experiments.

As already discussed in the introduction, few information are reported in the literature regarding the formation of moxidectin crystals and moxidectin solvates. Even less information are reported in the possible mechanism of conversion between moxidectin and the corresponding solvates. In our study we analysed the behaviour of moxidectin solvates with *in situ* variable temperature powder X-ray diffraction analysis. With this technique, by using a custom-made conditioning chambers allowing to characterise the thermal behaviour of a sample under study, samples of moxidectin solvates were heated starting from room temperature up to decomposition.
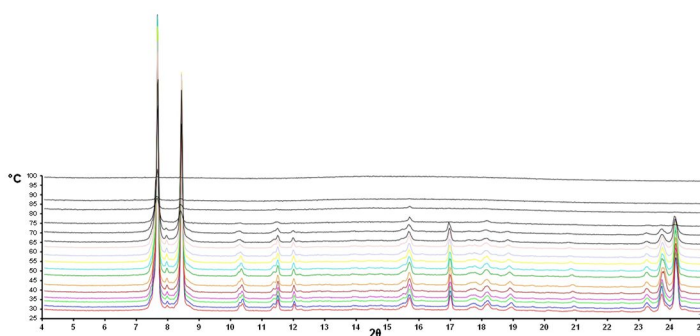
Figure 8.10: VT-PXRD plot, Moxi·2MeNO$_2$

Figure 8.10 reports the two-dimensional contour plot as a function of 2θ and temperature for the collection of powder X-ray diffraction patterns measured at increasing temperatures in the range 25-100 °C for Moxi·2iPrOH. The collection of PXRD patterns shows that, by rising the temperature, the sample loses crystallinity at about 70 °C, and become amorphous. An experiment repeated up to 210 °C showed no thermal events (*i.e.*: crystallization to a crystalline not-solvated form) other than decomposition of the molecule.
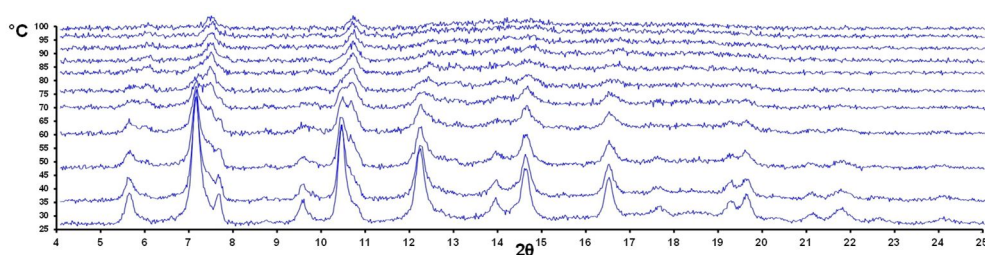
Figure 8.11: VT-PXRD plot, Moxi·2MeNO$_2$

Figure 8.11 reports the two-dimensional contour plot as a function of 2θ and temperature for the collection of powder X-ray diffraction patterns measured at increasing temperatures in the range 25-100°C for Moxi·2MeNO$_2$. The collection of PXRD patterns shows that, by rising the temperature, the sample loses crystallinity at about 60°C and gradually become amorphous.

As reported in Figure 8.10 and 8.11, following the loss of solvent molecules no evidence of the formation of a crystalline phase (*i.e.*: the expected unsolvated form previously reported[15]) is observed for Moxi·2iPrOH and Moxi·1.5MeNO$_2$, respectively.

Moreover, we tried to prove the accuracy of the purported mechanisms of interconversion between moxidectin forms (solvates and pure form),

reported in the patent WO2013/082373A1[16]. To this purpose, we heated *in situ* the amorphous moxidectin from 170 to 200 °C for several hours (ca. 5 h). No observation of a crystallization events was observed (see Figure 8.12).
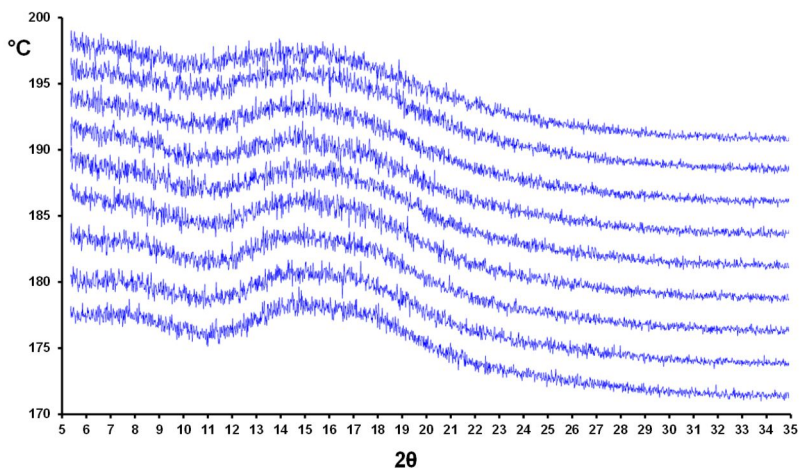
Figure 8.12: Collection of diffractograms for moxidectin (amorphous form) heated, in a range time of 5 hours, from 170 °C to 200 °C. This experiment shows that no conversion from amorphous form to pure crystalline form is observed at this temperature, in contrast to a previous patent[16]

8.2. Conclusion

The work on moxidectin was devoted to shed some light on the behaviour of this important API, for which the patent literature reports the formation of different solvates but, up to date, only one X-ray solved structure was deposited in the CCDC (unsolvated forms). A systematic screening of the crystallisation behaviour of moxidectin in different solvent was undertaken, leading to the preparation of three distinct solvates.

Single crystal X-ray diffractometric analysis of these solvates allowed to obtain important structural information on the location of the solvent molecules in the crystal, on the hydrogen bond networks formed intra- and intermolecularly and on the conformation of moxidectin.

These results will be useful not only in the manufacturing processes of moxidectin, where the solvates may form during the crystallisation step, but even for the formulation of this API in the pharmaceutical form (tablets) and for issues related to its conservation. Moreover, the structural information will be useful for future studies on the polymorphism of this API.

8.3. Experimental section

Moxidectin was generous gift by researcher group of Prof. Pattarino Franco, at Università del Piemonte Orientale "A. Avogardo"-Dipartimento di Scienze del Farmaco.

Diffraction experiments were performed using Cu-Kα radiation (λ = 1.5418 Å) on a vertical-scan Bruker AXS D8 Advance diffractometer in θ:θ mode, equipped with a Goebel Mirror and a Bruker Lynxeye linear Position Sensitive Detector (PSD), with the following optics: primary and secondary Soller slits, 2.3° and 2.5°, respectively; divergence slit, 0.1°; receiving slit, 2.82°. Generator setting: 40 kV, 40 mA. The nominal resolution for the present set-up is 0.08° 2θ (FWHM of the α1 component) for the LaB6 peak at about 21.3° (2θ). Variable-temperature X-ray powder diffraction (VT-PXRD) experiments were performed on Moxi·2iPrOH and Moxi·2MeNO$_2$. The experiments were carried out in a nitrogen atmosphere by coupling a custom-made sample heater, assembled by Officina Elettrotecnica di Tenno, Ponte Arche, Italy, to the instrumental set-up described above. A powdered microcrystalline sample was ground in an agate mortar and was deposited in the hollow of on a quartz zero-background plate framed by an aluminium skeleton. The data were acquired within a sensible, low-angle 2θ range, heating the samples in situ in the temperature range 30-150°C, with steps of 5 °C.

Moxidectin (approximately 100 mg) was heated until dissolution in appropriate solvent. The resulting solution was kept at 0 – 5 °C until crystals, suitable for X-ray analysis, were obtained.

8.4. References

1. Blagburn, B. L.; Arther, R. G.; Dillon, A. R.; Butler, J. M.; Bowles, J. V.; von Simson, C.; Zolynas, R. Efficacy of Four Commercially Available Heartworm Preventive Products against the JYD-34 Laboratory Strain of Dirofilaria Immitis. *Parasit. Vectors* **2016**, *9* (1). https://doi.org/10.1186/s13071-016-1476-7.

2. Ranjan, S.; Trudeau, C.; Prichard, R. K.; von Kutzleben, R.; Carrier, D. Efficacy of Moxidectin against Naturally Acquired Nematode Infections in Cattle. *Vet. Parasitol.* **1992**, *41* (3–4), 227–231. https://doi.org/10.1016/0304-4017(92)90082-K.

3. Chandler, D. J.; Fuller, L. C. A Review of Scabies: An Infestation More than Skin Deep. *Dermatology* **2019**, *235* (2), 79–90. https://doi.org/10.1159/000495290.

4. Otranto, D.; Solari Basano, F.; Pombi, M.; Capelli, G.; Nazzari, R.; Falsone, L.; Petry, G.; Pollmeier, M. G.; Lia, R. P. Effectiveness of the Spot-on Combination of Moxidectin and Imidacloprid (Advocate®) in the Treatment of Ocular Thelaziosis by Thelazia Callipaeda in Naturally Infected Cats. *Parasit. Vectors* **2019**, *12* (1). https://doi.org/10.1186/s13071-018-3262-1.

5. Esch, K. J.; Petersen, C. A. Transmission and Epidemiology of Zoonotic Protozoal Diseases of Companion Animals. *Clin. Microbiol. Rev.* **2013**, *26* (1), 58–85. https://doi.org/10.1128/CMR.00067-12.

6. Europe Veterinary Vaccine Market | Growth, Trends, Forecast (2019-24) https://www.mordorintelligence.com/industry-reports/europe-veterinary-vaccines-market.

7. Turner, H. C.; Walker, M.; Attah, S. K.; Opoku, N. O.; Awadzi, K.; Kuesel, A. C.; Basáñez, M.-G. The Potential Impact of Moxidectin on Onchocerciasis Elimination in Africa: An Economic Evaluation Based on the Phase II Clinical Trial Data. *Parasit. Vectors* **2015**, *8* (1). https://doi.org/10.1186/s13071-015-0779-4.

8. Koala, L.; Nikièma, A. S.; Paré, A. B.; Drabo, F.; Toé, L. D.; Belem, A. M. G.; Boakye, D. A.; Traoré, S.; Dabiré, R. K. Entomological Assessment of the Transmission Following Recrudescence of Onchocerciasis in the Comoé Valley, Burkina Faso. *Parasit. Vectors* **2019**, *12* (1). https://doi.org/10.1186/s13071-019-3290-5.

9. Ōmura, S.; Shiomi, K. Discovery, Chemistry, and Chemical Biology of Microbial Products. *Pure Appl. Chem.* **2007**, *79* (4), 581–591. https://doi.org/10.1351/pac200779040581.

10. Campbell, W. C. Ivermectin: A Reflection on Simplicity. 13.

11. Fisher, M. H.; Mrozik, H. The Chemistry and Pharmacology of Avermectins. *Annu. Rev. Pharmacol. Toxicol.* **1992**, *32* (1), 537–553. https://doi.org/10.1146/annurev.pa.32.040192.002541.

12. Awasthi, A.; Razzak, M.; Al-Kassas, R.; Greenwood, D. R.; Harvey, J.; Garg, S. Isolation and Characterization of Degradation Products of Moxidectin Using LC, LTQ FT-MS, H/D Exchange and NMR. *Anal. Bioanal. Chem.* **2012**, *404* (8), 2203–2222. https://doi.org/10.1007/s00216-012-6393-9.

13. Lumaret, J.-P.; Errouissi, F.; Floate, K.; Römbke, J.; Wardhaugh, K. A Review on the Toxicity and Non-Target Effects of Macrocyclic Lactones in Terrestrial and Aquatic Environments. *Curr. Pharm. Biotechnol.* **2012**, *13* (6), 1004–1060. https://doi.org/10.2174/138920112800399257.

14. Prichard, R. K.; Geary, T. G. Perspectives on the Utility of Moxidectin for the Control of Parasitic Nematodes in the Face of Developing Anthelmintic Resistance. *Int. J. Parasitol. Drugs Drug Resist.* **2019**, *10*, 69–83. https://doi.org/10.1016/j.ijpddr.2019.06.002.

15. Beddall, N. E.; Howes, P. D.; Ramsay, M. V. J.; Roberts, S. M.; Slawin, A. M. Z.; Sutherland, D. R.; Tiley, E. P.; Williams, D. J. Chemical Transformations of S541 Factors (A)-(D): Preparation and Reactions of the 23-Ketones. *Tetrahedron Lett.* **1988**, *29* (21), 2595–2598. https://doi.org/10.1016/S0040-4039(00)86121-3.

16. Cady, S.; Ma, B.; Chapman, R.; Yang, C.; Jain, U. Long-Acting Injectable Moxidectin Formulations and Novel Moxidectin Crystal Forms. WO2013082373 (A1), June 6, 2013.

17. Spek, A. L. *PLATON* SQUEEZE: A Tool for the Calculation of the Disordered Solvent Contribution to the Calculated Structure Factors. *Acta Crystallogr. Sect. C Struct. Chem.* **2015**, *71* (1), 9–18. https://doi.org/10.1107/S2053229614024929.

Chapter 9: General discussion

9.1. General discussion

APIs (Active Pharmaceutical Ingredients) play an important role in the control of public health. Pharmaceutical companies are directly involved in the synthesis, formulation and commercialisation of these fundamental compounds.

Pharma companies employ several synthetic and technological strategies, during the development of APIs, with the aim to satisfy the market request. The continued expansion of the industrial APIs portfolio stimulates the pharma companies to develop new, alternative and cheap manufacturing processes in order to decrease the production costs by reducing the number of synthetic steps and increasing the overall yield.

The manufacturing of APIs requires a consolidated and robust synthetic process suitable for the industrial productions. The process is selected after screening alternative synthetic routes, generally made in the R&D laboratory of the pharmaceutical industry. In this step several attempts are made in order to design and test the best synthetic route for the preparation of the API. The screening of reactions takes place by small scale experiments (1-10 g) giving useful information about the yield, the safety, the presence of byproducts and the overall costs. After the identification of the most efficient synthetic pathway, additional efforts are devoted to scrutiny the experimental conditions in order to increase the reaction scale, normally, to 50-200 grams. During this intermediate scale-up, reaction conditions such as the optimal concentration of reactants, reagents and catalysts, the correct temperature, and many other parameters, are optimised and used as necessary starting information for the future scale-up from the R&D laboratory to the industrial plant.

During the development of the manufacturing process, additional information about the solid-state properties are needed. The presence of different polymorphic forms can lead to problems during the formulation of the API. The presence of polymorphs, solvates, hydrates or the presence of amorphous forms are then thoroughly investigated.

During this PhD program, we studied a selection of APIs with the aim to discover new and alternative synthetic processes suitable for their industrial production. Exploration of synthetic methodologies led sometimes to identify unprecedented transformations, leading to interesting or unwanted compounds. Moreover, we explored the solid-state properties of APIs in order to identify the presence of polymorphic forms.

In particular, during the PhD program, I focused my attention on different APIs and molecules:

- Maropitant citrate hydrate (API)
- Vanillin (Starting material)
- DMAP molecule (Catalyst)
- Gepirone hydrochloride (API)
- Pirfenidone (API)
- Moxidectin (API)

In detail:

Maropitant

In this PhD work we analysed several different and alternative synthetic approaches for the synthesis of maropitant citrate monohydrate, API for the treatment of emesis induced by motion sickness in animals.

The optimization of the procedure for the synthesis of the key intermediate (2S)-2-benzhydryl-3-quinuclidinone allowed to synthesise maropitant in high yield and reducing of byproducts. An alternative approach based on an alternative scheme of reductive amination and the preparation of a staring material through the Tscherniac-Einhorn reaction, led to an additional synthesis of this API. Comparison of the efficiency and the cost of the two processes led to the selection of the first one for the scale up of the manufacturing of maropitant.

Vanillin oxidative fragmentation/amination

During the investigation of the reactions of vanillin with secondary alkylamines, we observed an unprecedented reaction in aerobic conditions, generating 2,5-diamino-1,4-benzoquinones. This complex reaction appears to involve several steps and intermediates. The importance of this reaction resides in the possibility of this reaction to take place more frequently than expected, due to the widespread use of vanillin in food and in general in flavouring. The obtained intensely coloured orange-to-red products may be interesting as new pigments for foods or colourants for pharmaceutical products especially on the base of safety studies that do not evidence significant toxic effects of 2,5-diamino-1,4-benzoquinones.

DMAP heterofunctionalisation

We reported the successful design and synthesis of a functionalised derivative of the well-known organocatalyst DMAP (4-(*N,N*-dimethylamino)pyridine). The preparation of the functionalised DMAP (*i.e.*:

3-aminomethyl-4-(*N,N*-dimethylamino)pyridine) was attained in two steps, taking advantage of the strong electrophile generated in the Tscherniac-Einhorn reaction to introduce an aminomethyl group on the DMAP molecule. The desired product is obtained in high yield and avoiding chromatographic separations, optimal prerequisites for a future large-scale preparation. The additional aminomethyl functional group has been exploited for the preparation of a silylated derivative, useful for grafting DMAP to an heterogenous inorganic support.

Future development of this work will deal with the grafting of the functionalised DMAP to silica-based inorganic supports for the preparation of organic-inorganic hybrid catalysts and with the evaluation of their properties in heterogeneously catalysed acylation reactions.

Gepirone Hydrochloride

Gepirone hydrochloride belongs to the class of APIs known as azapirones and is used for the treatment of the major depressive disorder. In the literature, three polymorphs were detected by DSC but no structural information were reported, nor were information about the presence of additional polymorphs. Thermal analysis confirmed the presence of three forms of this API and we succeeded in isolating crystals of two of these forms, along with crystals of the free base. Single crystal X-ray diffraction analysis of these forms allowed to obtain detailed structural information. In addition, variable temperature PXRD studies defined the stability range of these forms.

Pirfenidone

In this work we investigated the solid-state properties of pirfenidone, API employed for the treatment of idiopathic pulmonary fibrosis. After a screening of solvents and mixtures thereof, a single crystal of this specific API, suitable for X-ray analysis, was obtained and the solid-state structure solved. Neither additional polymorphs were isolated, nor were adducts, solvates or inclusion compounds. The limited number of functional groups and degrees of rotational freedom are probably the reason for the lack of additional polymorphs.

Moxidectin

Moxidectin is an important API for the treatment of onchocerciasis, but limited informations are available on the solid-state forms of this compound. The patent literature claims the presence of different solvates, but to date only one (unsolvated) solid state structure has been deposited in international databases. In this PhD, we investigated the presence of additional polymorphs and, through a screening of solvents and mixture thereof, we were able to isolate three solvates (with ethanol, 2-propanol and nitromethane), then subjected to X-ray diffractometric analysis.

During the PhD period, my personal contribution to these topics may be summarised as follows:

- Proposal of different synthetic strategies for the synthesis of target compounds and selected intermediates thereof.
- Starting material and reagents: I focused my attention on the choose of the correct starting material in relation with the

corresponding synthetic approach. Particular attention was dedicated to the cost, the availability and to safety issues related to the starting materials and reagents.

- I run all test experiments, initially in small scale (1 – 10 g), with the aim to gain information about the reactions: yield, presence of by-products, purity and safety.

- I isolated the desired product and by-products in order to characterise them by different analytical instruments such as NMR, MS, HPLC.

- I was directly involved in the optimisation of the reaction conditions in order to improve the efficiency of each step.

- I increased the synthetic scale from 10 to over 500 grams. In this step I identified issues and problems related to the scale-up procedure such as temperature control, stirring and work-up conditions.

- I completed the purification of the target compound through crystallisation processes in order to increase the purity of the final compound and to reach the purity required by regulatory agencies.

- Moreover, I screened many conditions for the crystallization of APIs with the aim to obtain suitable crystals for the X-ray analysis and to identify the presence of polymorphic forms of a specific API.

- Finally, I was directly involved in the writing of internal reports, articles and patent applications.

In conclusion, in the PhD period I was able to expand my knowledge in the vast world of APIs. The identification of the synthetic process and costs are only two of the different driving forces leading to the identifications of a suitable synthetic process for the manufacturing of APIs. Moreover, the solid-state properties play a central role during the production of the API. The presence of different crystalline forms can raise problems during the purification of the API and the formulation and conservation of the final pharmaceutical form.

9.2. Publications

7- Colombano G., **Barbero M.**, Giovenzana G.B., Roletto J., Paissoni P. PCT submission n° 102019000000657

6- Colombano G., **Barbero M.,** Bogogna L., Roletto J., Paissoni P. PCT submission n° 102019000013941

5- **Barbero M.,** Colombano G., Bogogna L., Roletto J., Colombo V., Giovenzana G.B. Polymorphism of Gepirone Hydrochloride, Crystal Growth & Design, submission in progress.

4- **Barbero M**., Pattarino F., Giovenzana G.B., Colombo V. Moxidectin: Discovery and Description of Three Novel Solvates, CrystEngComm, submission in progress.

3- **Barbero M**., Papillo V., Grolla A., Negri R., Travaglia F., Bordiga M., Condorelli F., Arlorio M., Giovenzana G.B. Unprecedented Formation of 2,5-Diaminoquinones from the Reaction of Vanillin with Secondary Amines in Aerobic Conditions, European Journal of Organic Chemistry, **2020**, 136-139. DOI: 10.1002/ejoc.201901553.

2- Donnola M., Mossotti M., **Barbero M**., Roletto J. Paissoni P. Process for the Synthesis of 2-Benzhydryl-3-Quinuclidinone, WO2019086434(A1).

1- **Barbero M**., Mossotti M., Sironi A., Giovenzana G.B., Colombo V. Crystal structure of pirfenidone (5-methyl-1-phenyl-1*H*-pyridin-2-one): an active pharmaceutical ingredient (API), Acta Crystallographica Section E Crystallographic Communications, **2019**, *E75*, 984-986 DOI: 10.1107/S2056989019006418.

Chapter 10: Acknowledgments